THE INFLUENCE OF PROCESS ROUTE ON MECHANICAL PROPERTY DEVELOPMENT IN SINTERED COMMERCIALLY PURE AND BLENDED ELEMENTAL TITANIUM

A dissertation submitted in fulfillment of the requirements for degree of Masters in Engineering

UNIVERSITY OF CAPE TOWN

Centre for Materials Engineering

Student: Lwazi Qangule
Supervisor: Prof. R.D. Knutsen

September 2015

Abstract

This work focuses on optimizing the sintering process of Ti-6Al-4V using Al-V master alloy powder to achieve a cost efficient product with acceptable mechanical properties. Reference was also made to Ti-6Al-4V products produced by Clinning (University of Cape Town 2012) using elemental Al and V instead of the master alloy addition proposed in this work. Commercially pure titanium (CP-Ti, Alfa Aesar) was used in this study as a reference, since its behavior during processing is more predictable. Relative density and the microstructural feature were studied in-depth in order to understand their impact on mechanical properties.

The two starting materials were sintered under vacuum (approximately 10^{-5} mbar) at 1000^0C (6hrs), 1100^0C (2, 4, 6hrs), 1200^0C (1, 2, 4hrs) and 1300^0C (1, 2hrs). Relative density, microstructure analysis and mechanical property measurements characterized on the as-sintered material before specimens were hot deformed at 800^0C to 0.69 strain and subsequently annealed at 870^0C for 1hr. Similar measurements and analyses were conducted on the samples post deformation and annealing.

In the as-sintered material relative density was directly proportional to the mechanical properties as expected. Deformation as a final step significantly improves relative density of both CP-Ti and Ti-6Al-4V, resulting in an associated hardness increase. In Ti-6Al-4V specimens grain refinement by thermomechanical processing (TMP) could not be directly associated with increased mechanical properties; even though TMP played a crucial role in improving mechanical properties this was strongly associated with pore reduction instead.

Care needs to be taken in selecting sintering temperatures, as treatment at 1000^0C and 1100^0C have detrimental impact on TMP processed material due to the inherent non-diffused Al-V particles that exist in the metal matrix. These non-diffused Al-V particles are associated with pores which consequently induce crack propagation upon loading, ultimately leading to failure.

Specimens treated with master alloy show much improved mechanical properties compared to degraded mechanical properties observed in elemental Al and V investigated by Clinning .

Dedications:

I would like to dedicate this dissertation to my daughter Inam'iNkosi Lathitha Qangule, born on the 9 November 2013. I have sacrificed spending time with her in order to make my contribution to the "Body of Knowledge". I would also like to make a special dedication to my mother Phumla Elizabeth Qangule who made numerous sacrifices to ensure I am where I am today.

Acknowledgements:

- Department of Mechanical Engineering (UCT) – Centre for Materials Engineering and National Research Fund (NRF) for Financial Support.
- Professor Robert Knutsen: Supervisor & Academic Coach.
- Dr. D Blaine of Stellenbosch University (SUN) for making available their equipment and providing technical assistance.
- Mr. Hendrik Bosman of SUN for lab assistance and comparing of data.
- Dr. Sarah George and Mr. Chase Hyde for their help with the Gleeble 3800 TMP machine.
- Ms Liezl Matthews & Penny Park-Ross for their technical assistance.
- Mr Glen Newins and the workshop stuff for assisting with the preparation of some of my samples.
- Candice Mias for her help with light microscope imaging.
- All students and stuff at the Centre for Materials Engineering for their support, assistance and friendship.
- Inga Macakati and Lungile Malinga for their help.

Last but not least I would like to thank God, my family and friends, who stood by me and were patient with my absence during my studies.

Declaration

I, Lwazi Qangule, know the meaning of plagiarism and declare that all the work in this document, save for that which is properly acknowledged, is my own.

Signature: 

Date: Sept 2015

Table of Contents

List of Acronyms and Abbreviations

- MA- Master Alloy
- BE – Blended Elemental
- CP – Commercially Pure
- PM – Powder Metallurgy
- PA - Pre- Alloyed
- NNS – Near-Net-Shape
- HCP- Hexagonal Close Packed
- BCC- Body Centred Cubic
- TMP- Thermo-Mechanical Processing
- CIP- Cold Isostatic Pressing
- HIP- Hot Isostatic Pressing
- DRC- Dynamic Recovery
- DRX- Dynamic Recrystallisation
- LM – Light Microscopy
- TRB – Transverse Rapture Bar
- PSC – Plane Strain Compression
- CP.11.2 – Commercially Pure Titanium Sintered at 1100^{0}C for 2hrs.
- Ti.10.6. – Ti-6Al-4V sintered at 1000^{0}C for 6hrs
- Ti.12.2D- Ti-6Al-4V sintered at 1200^{0}C for 2hrs and TMP

1. INTRODUCTION

1.1 Subject of the thesis

The subject of this thesis is to compare the mechanical property development between two different process routes: (a) Cold compaction + Sintering and (b) Partial Sintering + Hot Deformation processing of CP-Ti and Ti-6Al-4V material.

1.2 Background to thesis

The motivation for interest in producing titanium and titanium alloy flat products by direct powder rolling is described in US Patent 7,311,873 B2 which is an invention that relates to the manufacturing of fully dense strips, plates, sheets and foils from titanium alloys, titanium metal matrix composites, titanium aluminides and flat multilayer composites of said material by direct powder rolling followed by sintering. This method essentially proposes progressive powder compaction by cold rolling to near theoretical density followed by high temperature (approximately 1200 °C for 4hrs) sintering. The sintering process aims to reduce porosity, elicit diffusion bonding of individual powder particles and homogenization of the powder blend. Unfortunately, sintering as a final process step means that the grain size of the product will tend to be large to the detriment of certain mechanical properties such as elongation and toughness.

High temperature heat treatment may be mandatory when using the blended elemental approach due to the need to homogenize the composition. Thus the deformation process must be designed to produce grain refinement; which is currently not the case in the conventional method. So the following question arises: How does grain size compare if one follows the conventional sintering process versus the partial sinter + hot deformation route?

1.3 Objectives of thesis

The objectives of this research are;

1. To compare the mechanical property development in two different process routes:
    a) Cold compaction + Sintering
    b) Partial Sintering + Hot Deformation processing

2. To further confirm that the use of master alloy powder produces better mechanical properties than the elemental Al and V powders investigated by Nicholas Clinning, MSc Dissertation, University of Cape Town, September 2012.

This research is focused primarily on optimizing the sintering process of powdered Ti-6Al-4V to achieve the best mechanical properties. Relative density and the microstructural features were studied to understand their impact on mechanical properties.

1.4 Scope and limitations

This research only refers to commercially pure and blended elemental compacts which are made from the titanium hydride-dehydride powder process. No test parameters regarding the manufacturing of the BE preforms to be tested as part of this research were altered during the study.

The strain and strain rate of TMP was kept constant throughout.

The ideal ratios of specimen thickness to platen width (from 2 to 4) and specimen width to platen width (>6) to ensure plane strain deformation during plane strain compression was not able to be achieved in this research due to the limited size of the sintered preforms that was able to be created.

Due to material size limitations, mechanical testing was not able to be carried out using standard specimens, as would be desirable, and was conducted by three-point-bending.

1.5 Plan of development

The dissertation begins with a literature review of important topics related to the manufacture of titanium powder and powder metallurgy. It provides details of the compaction and sintering of the samples and hot deformation. This is then followed by a detailed account of the testing methodology used. The results of the testing are then analyzed and discussed. The microstructural properties are assessed. The changes in mechanical properties of the sintered samples are compared to the samples which had been hot compressed. The comparison of the master alloy results to those with elemental powders follows. The report will be concluded with recommendations and future work.

2. Literature Review

2.1 Titanium

2.1.1 Introduction

Titanium was first discovered as a new and unknown metallic element by William Gregor (clergyman and mineralogist) in England (1791), and was given the name Titanium a few years later (1795) by Martin Heinrich Klaproth (a chemist) in Germany after the Titan of the Greek mythology [1]. Titanium is plentiful in the earth's crust making up approximately 0.62%. Vast deposits of it make it the ninth most abundant element and the fourth most abundant structural metal after aluminium, iron, and magnesium. Its two most common sources are ilmenite, $FeTiO_3$, which is present in igneous rocks, and rutile,TiO_2, which is found in beach sands, especially near coastlines where erosion and wave action have elevated its concentrations [2]. The ore that is turned into a metal is used on wide range of applications, such as for a jet turbine or for the replacement of a human knee. The whole process from ore to final product is time-consuming and expensive; however titanium is well worth the effort because it offers a superior combination of metallurgical and physical characteristics, which allows an application to perform at its maximum potential [2].

2.2. Titanium Powder Metallurgy.

Titanium alloys are amongst the most essential of the advanced materials which are profound in improving performance in aerospace and terrestrial systems [3]. This is because of the excellent combinations of specific mechanical properties (normalized by density), outstanding corrosion behaviour, good elevated temperature performance and allowance for damage tolerant design, exhibited by titanium alloys. However, negating widespread use is the high cost of titanium alloys compared to competing materials.

This has led to numerous investigations of various potentially lower cost processes, including powder metallurgy (PM) techniques [4]. Titanium powders that are currently available are listed in Table 2.1 below.

Powder metallurgy (PM) can be described as a process where the starting stock material for parts is elemental or pre-alloyed powders. This technology greatly limits material waste, especially compared to traditional titanium part manufacturing processes.

Table 2.1: Categories of Titanium PM [3].

Category	Feature	Status
Laser forming	Powder feed melted with laser	Pilot Production
Powder Injection Molding	Use of a binder to produce complex small parts	Production
Spraying	Solid or potentially liquid	Research Base
Near Net Shapes	Pre-alloyed and blended elemental	Commercial
Far from Equilibrium Process	Rapid solidification, mechanical alloying and vapour deposition	Research Base

2.2.1 Production of titanium powders

The titanium powders that are currently available are formed via four standard processing methods, namely[3]:

- Hydride-dehydride powders, which are generally pre-alloyed and are angular in nature.
- Sponge fines are "sponge-like" in nature and contain remnant salts which prevent the achievement of full density and negatively affect weldability.
- Atomised powders, which are generally pre-alloyed and spherical in shape [5].
- Reverse Electrolytic process.

Sponge fines

At present all titanium ingot and wrought products start off from titanium sponge produced by the chemical reduction of titanium tetrachloride, either by pure Hunter process or pure magnesium (Kroll process) [6]. The Kroll process starts with the reduction of $TiCl_4$ by magnesium at a temperature above 800 °C [5].

$$TiCl_4 + 2Mg \rightarrow Ti + 2MgCl_2$$

$MgCl_2$ is periodically tapped off as the reduction proceeds. This by-product is leached out to obtain sponge titanium with chloride contamination levels of 1,500ppm or less. The cost of titanium production is high because of the large consumption of energy, problems associated with the elevated temperatures involved and difficulties associated with the removal of $MgCl_2$ [5].

A scanning electron micrograph (SEM) of titanium sponge powder is shown in figure 2.1. This by-product has been utilized as coarse titanium powder suitable for conventional bulk PM processes such as press-and-sinter (P/S), and cold isostatic pressing/sintering (CIP/Sinter). These solid performs, such as plates and billet, are suitable for conversion by conventional manufacturing techniques into sheet, bars and tubes [6].

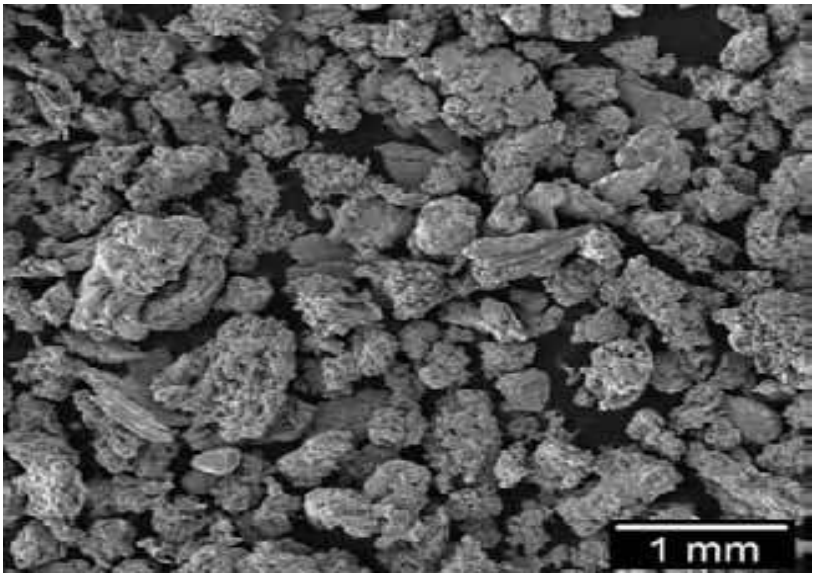

Figure 2.1: Representative micrograph of 180–850µm titanium sponge [6].

Hydride-Dehydride Processes

Titanium sponge cannot be crushed into powder < 850µm due to its high ductility. If, however the titanium sponge was embrittled, it could readily be crushed and milled into a finer powder. Cryogenic crushing has been successfully used on a limited scale to produce titanium sponge powders. The HDH process has been successfully scaled up to produce high volumes of crushed titanium sponge powder, as shown in Figure 2.2 [6].

The hydride processing route enables very fine and highly reactive powders to be produced from metals which are capable of forming solid hydrides. The hydride is obtained by the reaction of metal with molecular hydrogen at elevated temperatures under a suitable partial pressure. The powder becomes embrittled and are easily crushed or ground into finer powders and dissociated in a vacuum at similar or higher temperatures than that at which they were formed [5]. The metal powders produced from hydrides are highly reactive and often pyrophoric; depending on the dissociation conditions. Special precautions, such as inert gas absorption on powder surfaces, are needed in order to avoid instantaneous ignition on exposure to air [6].

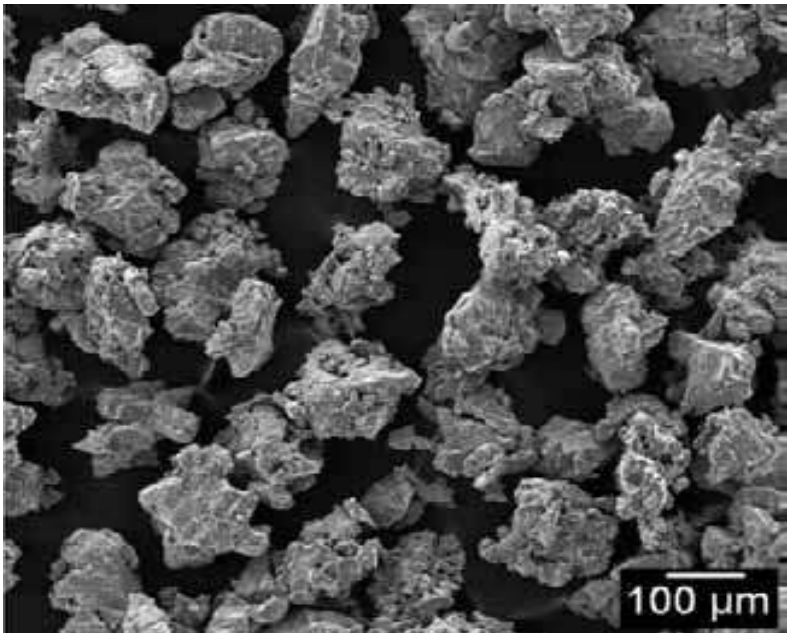

Figure 2.2: Representative micrograph of 75-150µm HDH titanium sponge powder produced by the Kroll process. SEM [6].

2.2.2. Powder Characterization

The properties of the powders used in the PM process have a great influence on the properties of the final parts, and as such, it is important to have a good understanding of various powder properties and the effect they have on the process [7]. Below is a discussion on some powder characteristics:

Particle Shape and Size

Depending on the process route employed during powder production, individual powder particles can have very different shapes and sizes. Figure 2.3 below shows a collection of

possible particle shapes and their qualitative descriptors. The larger variety of particle shapes makes it almost impractical to compare sizes of particles of different shapes. The easiest particle shape to quantify in size is the spherical kind because it requires only a single dimension (diameter) to completely define the particle. As the particle shape becomes more irregular, it becomes very difficult to define size.

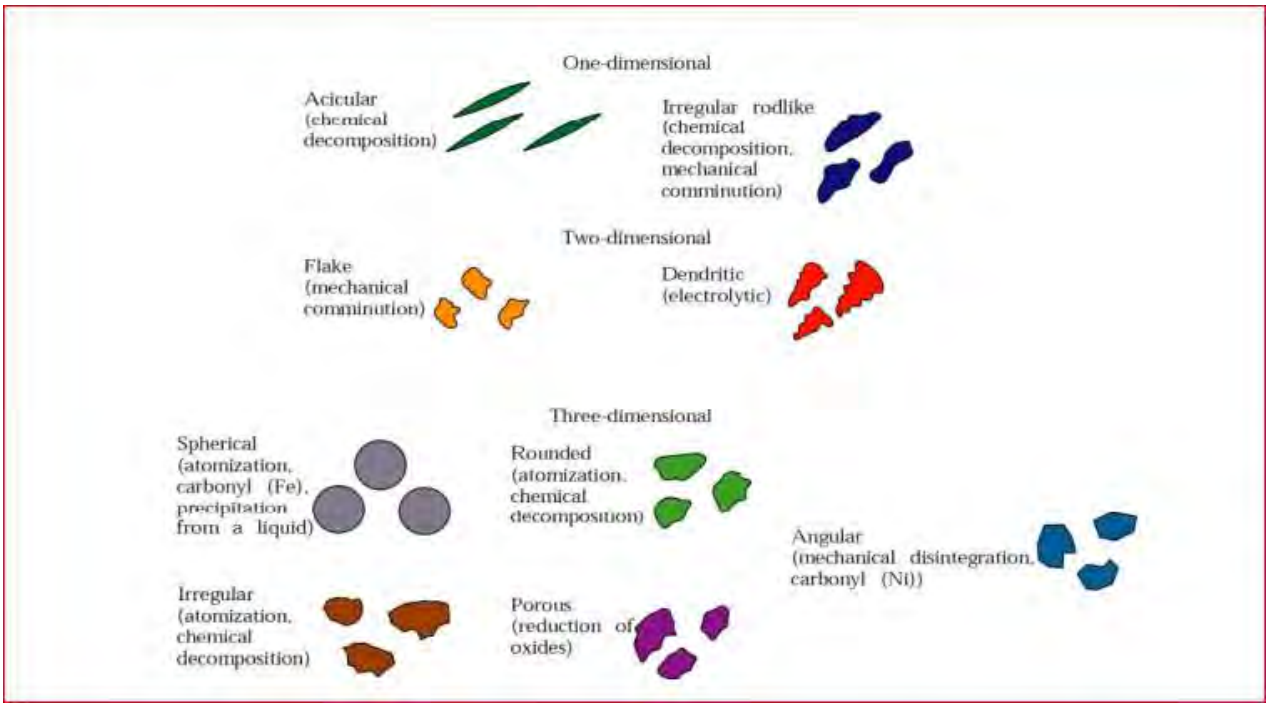

Figure 2.3: Various particle shapes and the descriptors used to identify them [8]**.**

Screening is the most common technique for describing the particle size of a powder and works by passing the powder through a series of screens or sieves. The screens consist of square openings created by orthogonal wires of a standard thickness (52 μm) and are described by a "mesh" number, which is the number of openings per linear inch. As such, an increasing mesh number results in smaller openings. The powder that passes through a specific mesh designated by a (–) sign and a powder that fails to pass through a mesh is designated (+) sign, for example a powder described as -200mesh will pass through a mesh of 200mesh screen, a powder described as +200 will not pass through the same screen, a powder described as -100+200mesh will pass 100mesh screen but will not through a 200mesh screen. This technique is carried out by stacking screen with increasing mesh opening on top of one another and placing a sample of powder in the top screen and then agitating the screens stack for roughly 15minutes; this is depicted in Figure 2.4 on the

facing page. It is possible to create conventional screens to a maximum of 325mesh and as a result, powders of size -325mesh are termed "subsieve powders". Figure 2.5 shows the apparent micron size corresponding to different mesh sizes [7].

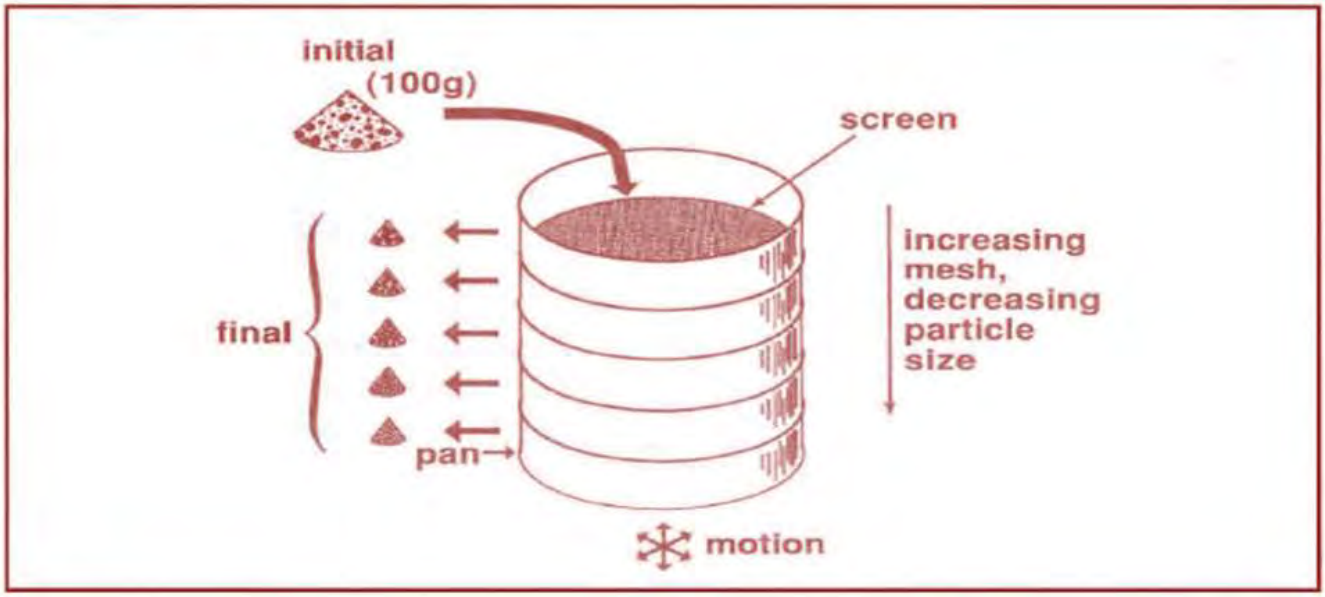

Figure 2.4: Schematic representation of the screening process to categorize particle size by way of a stack of mesh screens of progressively smaller openings [8].

Mesh Size	Openings (µm)	Mesh Size	Openings (µm)
18	1000	100	150
20	850	120	125
25	710	140	106
30	600	170	90
35	500	200	75
40	425	230	63
45	355	270	53
50	300	325	45
60	250		
70	212		
80	180		

Figure 2.5: The size of the square openings in the mesh screens for different standard mesh sizes [8].

To attain high density in the compact stage, factors like packing density of the powder need to be considered. Packing density is dependent on the characteristics of the powder particles. The main factors affecting the packing density for single component powder packing are particle size, particle shape and the ratio of the diameter of the container to the particle [3].

McGeary (1962)[9] studied the effect of the ratio of the diameter of the container to the particle D/d (D is the diameter of container and d is the particle diameter) and concluded that if the ratio D/d is greater than 50 the packing density tends to reach maximum value.

Particle shape varies significantly depending on the manufacturing process used and influences the particle packing, flow and compression properties. The greater the particle surface roughness or the more irregular the particle shapes, the lower the packing density [3, 11, 12].

Powder Impurities

Chemical impurities are problems in all industrial material and material processes. Impurities can be a perilous aspect in PM processes, because of the high specific surface area of the powder. A large amount of the material is exposed to the atmosphere and possible impurities during both production and processing. Impurities are very easily picked up through absorption, which concentrate on the surface of the particles and thus become included in the final PM part and are detrimental to the achievement of very high density aspect. Oxygen is the most deleterious impurity to all metal and non-oxide ceramics [8].

2.3 Production of Sintered Parts

Parts are produced from CP titanium (CP-Ti) powder by various consolidation and forming processes, including press-and-sinter, powder injection moulding (PIM), hot isostatic pressing (HIP), cold isostatic pressing (CIP) and powder rolling.

The press-and-sinter method is the most widely used PM manufacturing process and the most economical production technique for mass production of parts of desired density, strength and dimensional accuracy. It is not suitable for complex shaped parts. PIM is used

for the production of high volumes of small, complex shaped metal parts. CIP is an economical, low volume production path for complex-shaped, highly uniform density compacts. It has the advantage of the short production times coupled with the ability to produce long and slender parts. The compacts must be sintered to bond the particles together after CIPing. HIP is similar to CIP except that it involves the simultaneous application of pressure and heat. HIP is used for powder that is difficult to sinter and parts that require excellent properties. Currently, most titanium parts that are commercially manufactured require HIPping to obtain the material properties required. Powder rolling is a method where powders are rolled to produce coherent strips. Parts with fine grains, high mechanical strength and close to theoretical density can be produced with this method [12].

Titanium alloy powder metallurgy fabrication methods are divided into two major categories based on the initial powder mixtures: blended elemental (BE) and pre-alloyed (PA) powders.

For pre-alloyed (PA) titanium, titanium alloy powders are made from their molten state. The wrought form of the material, for instance wrought Ti-6Al-4V, is vacuum melted and atomized using gas. High purity, spherical powders are produced from this method due to purity level of the starting raw materials. The powders are also consolidated and sintered to produce titanium alloys. These powders are not suitable for die compaction unless mixed with sponge fines due to their spherical shape. They are suitable for PIM and laser sintering or direct metal deposition. The PA powders produced by gas atomization and plasma rotating methods undergo hot isostatic pressing (HIP) to produce more fully dense compacts. PA titanium parts have superior properties as compared to BE produced part but are much more costly. PA parts are more in demand in aerospace industry because of their mechanical properties [14, 7].

In the BE technique, different (for example, titanium, aluminium and vanadium) powders are blended together, consolidated and sintered to produce the alloyed material. Sponge fines used in this technique contain 0.12-0.15 wt % chloride which prevents full density being reached, resulting to inferior mechanical properties [14]. This approach produces titanium PM at lower costs; however, parts produced by this method are limited in size and

complexity. Blended Elemental material can be improved by undergoing a secondary process of hot forging to increase density.

The general sequence of operations involved in the powder metallurgy process is shown schematically in Figure 2.6. The component powders are mixed together with lubricant until a homogeneous mix is obtained. The mix is then loaded into a die and compacted under pressure, after which the compact is sintered [15].

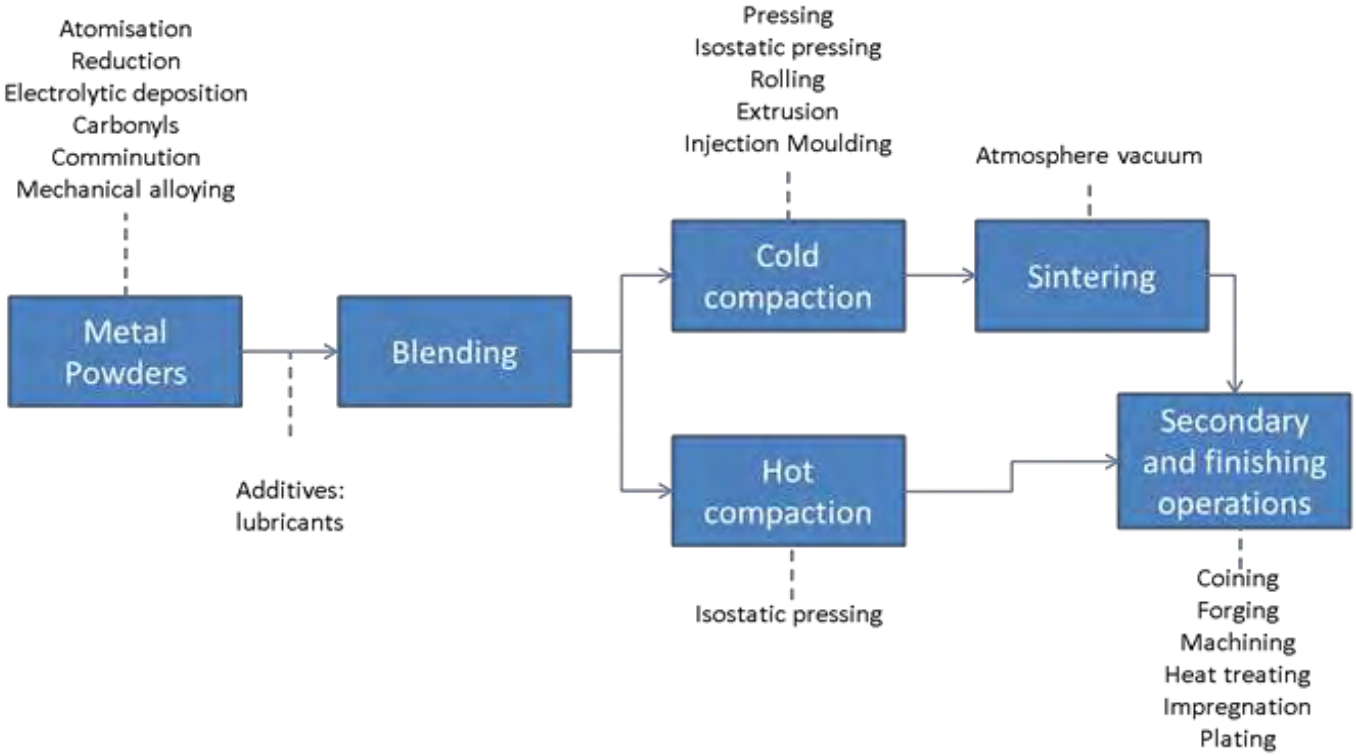

Figure 2.6: Powder metallurgy flow chart [15].

The pre-compaction steps include classification, blending, mixing, agglomeration, de-agglomeration and lubrication [16].

Blending and mixing are done to combine powders into a homogeneous mass prior to pressing. Agglomeration provides a coarser particle size, which flows easily in automatic forming equipment. Attrition and de-agglomeration are useful in those instances when a fine, discrete powder is needed [16]. Finally, lubricant of a powder using organic molecules provides for easier part ejection from compaction tooling and longer die life. It is essential to reduce friction between the pressed compact and the rigid tool components when compacting metal powder in steel or carbide tooling. The lubricants are usually mixed with

the metal powder as a final step before pressing. For metal powders, stearates based on, Al, Zn, Li, Mg, or Ca are commonly used lubricants. Besides these stearates, other lubricants include waxes and cellulose additives [16]. Lubricants assist in achieving the desired uniformity of density from top to bottom of the compact. Of equal importance is the fact that the reduction of friction also makes it easier to eject the compact and so minimizes the tendency to form cracks [15]. It has been suggested that an additional function of the lubricant is to help the particles to slide over each other, but it seems doubtful whether this factor is of much significance: - good compacts can be obtained without any admixed lubricant, e.g. using die wall lubrication or isostatic pressing. Care in the selection of lubricant is necessary, since it may adversely affect both the green body and sintered strengths especially if any residue is left after the organic part has decomposed [15], [17], [18].

2.3.1 Pressing (or Compaction)

The mixed powders are pressed to shape in a rigid steel or carbide die under pressures of 150 – 900 MPa. At this stage, the compacts maintain their shape by virtue if cold-welding of the powder grains within the mass. The compacts must be sufficiently strong to withstand ejection from the die and subsequent handling before sintering. Compaction is a critical operation in the process, since the final shape and mechanical properties are essentially determined by the level and uniformity of the as-pressed density [15]. The point contacts deform as the pressure increases. Plastic flow is localized to particle contacts at low pressures, whereas it occurs homogeneously throughout the compacts as the pressure increases. Eventual fragmentation causes densification and an increase in the compacts surface area, but the strength of the compact shows little improvement [16].

In the compaction of metal powders when the pressure is transmitted from only the top punch, the process is termed single action pressing as compared to double action pressing. The type of pressure applications determines the density gradients in the compact and hence its strength. The density is highest at the top of the compact and decreases towards the bottom as shown in Figure 2.7. However, in a double-ended pressing the minimum density is achieved at the center of the compact and the density distribution is more homogeneous than that of the single ended pressing [16].

The height to diameter ratio of the compact also plays an important role in the densification. With an increasing height to diameter ratio, density gradients in a compact will increase and this causes a decrease in the overall compact density, as shown in Figure 2.7 below. However, pressure transmissions can be improved by reducing the friction, which affects the use of suitable lubricants such as paraffin wax, stearic acid and various stearates on die walls [16].

SINGLE ACTION

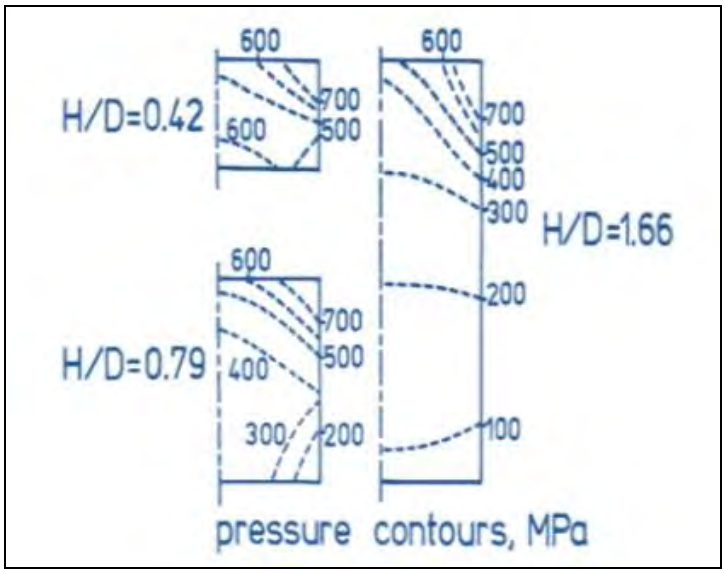

Figure 2.7: Pressure distribution in single action pressing compression [16].

Densification by compaction process involves particle deformation [18]. The powder has a density approximately equal to the apparent density (mass of the powder divided by the volume occupied by it under specified conditions of packing) at the beginning of the compaction cycle. Voids result between the particles, even with vibration the highest obtainable density is only the tap density. With loose powder there usually exist an excess of void space, with no strength and low coordination number (number of touching particles). When rapid pressure is applied, rearrangement of particles occurs such that they fill the large pores, giving a higher packing coordination. This is analogous with vibrating the powder. Rearrangement is assisted by hard, smooth particle surfaces [18].

When the pressure is increased, better packing results and this leads to a decreasing porosity and the formation of new particle contacts. The point contacts undergo elastic deformation and at all the points in the compaction cycles a residual elastic energy is stored in the compact. High pressures increase density by contact enlargement through plastic deformation as shown in figure 2.8 below. Pressure causes localized deformation at

the contacts giving work/strain hardening and thus allowing new contacts to form as gaps between the particles collapses [18].

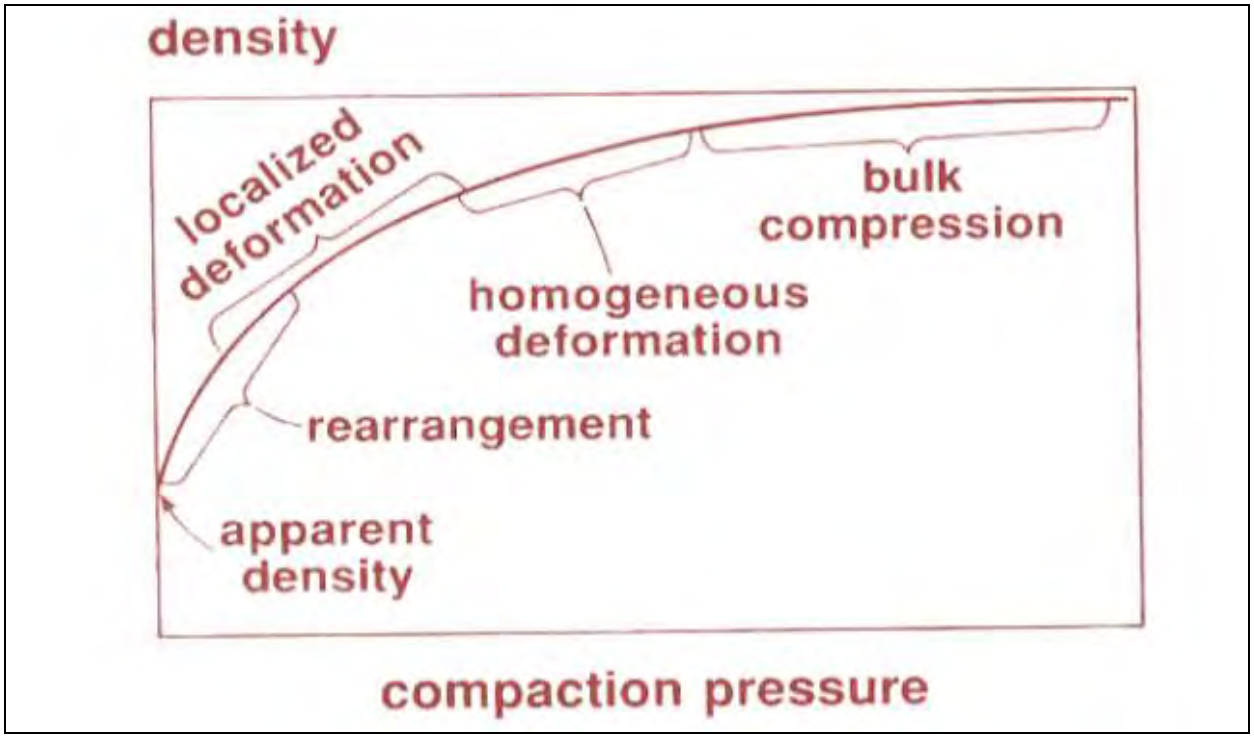

Figure 2.8: A sketch of the density versus compaction pressure during metal powder compaction, showing key stages and declining compressibility as the density increases [9].

Compaction involves, 1) flow of powder particles past one another interacting with each other and with die-punch, 2) deformation of particles. In the case of homogeneous compaction, two stages are observed (see Figure 2.9):

- First stage: rapid densification occurs when pressure is applied due to particle movement and rearrangement resulting in improved packing.
- Second stage: increase in applied pressure leads to elastic and plastic deformation resulting in locking and cold welding of particles. In this second stage, large increments in pressure are seen to affect a small increase in density [17].

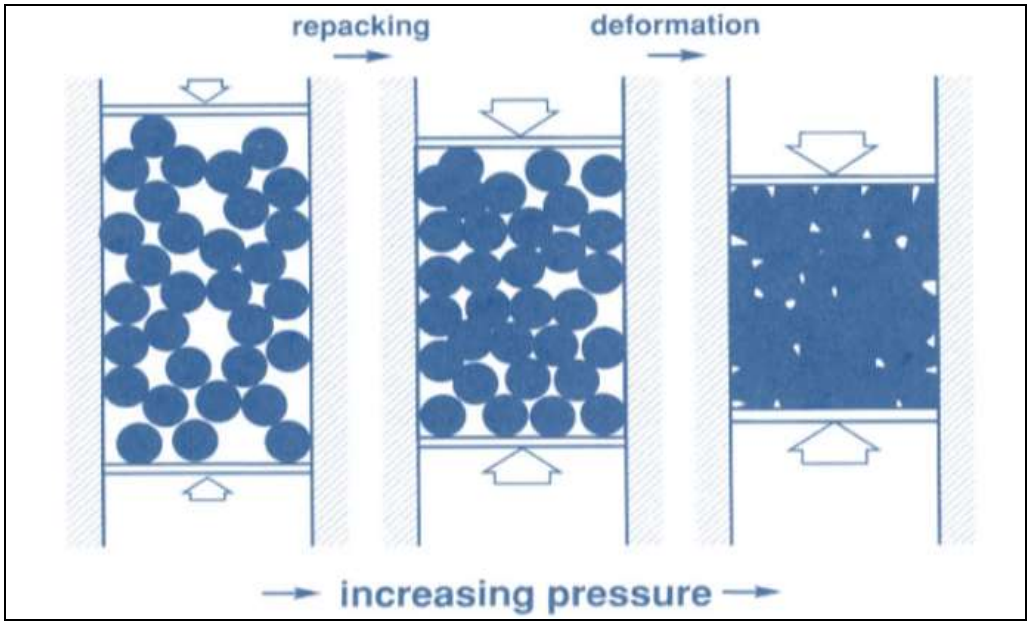

Figure 2.9: A simplified view of the stages of metal powder compaction. Initially repacking occurs with the elimination of particles of bridges. With higher compaction pressures particle deformation is the dominant mode of densification [9].

The green compact produced can be considered as a two-phase aggregate consisting of powder particles and porosity each having its own shape and size. Compaction can be performed at low and high temperatures. Room temperature compaction employs pressures in the range of 100-700MPa and produces density in the range of 60-90% of the theoretical density [18]. At high temperatures, pressures are kept low within the limits of preventing die damage [17], [18].

Work done by Gronostajski *et al*. [19] showed that, when titanium alloy powder was pre-compacted under different pressures (1019MPa, 700MPa, 550MPa and 400MPa) where the compaction time under the maximum pressure was constant and amounted to 2 minutes, each specimen was made of 26.7g of powder and it was 25mm in diameter. In the case of the spheroidal powder produced by gas atomization, no compact with permanently bonded powder particles was obtained. All specimens broke while being removed from the die (Figure 2.10) [19].

Figure 2.10: Compact made of Ti6Al4V titanium alloy powder produced by gas atomization (GA) after compaction under pressure of 1019MPa [19].

Gronostajski *et al.* also investigated the case of the irregular powder produced by HDH, and determined that 500 MPa was sufficient to obtain permanent bonding of titanium alloy powder grains. This pressure was adopted as the pressure limit for the powder produced by HDH. Several different pressures were applied in order to determine the effect of pressure on the porosity of the compacts before and after sintering. The specimens were sintered in a vacuum furnace because of the high chemical activity of titanium alloy (particularly at high temperatures) and the risk of spontaneous ignition at temperatures above 237.5°C. During sintering there was a vacuum of 1.1 x 10^{-4}mbar in the furnace. The specimens were heated up at a rate of 15°C /min to 1200°C. This heating operation lasted about 80 min while sintering at a temperature of 1200°C lasted 40 min. Figure 2.11 shows the relation between porosity and compaction pressure, and its changes caused by sintering [19].

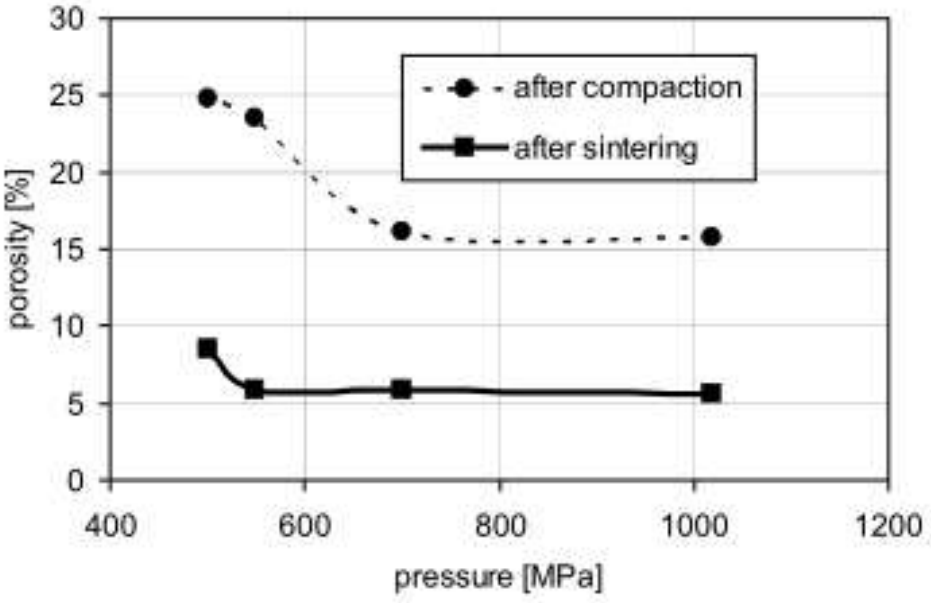

Figure 2.11: Porosity versus pressure for Ti6Al4V titanium alloy produced by HDH [19].

According to the diagram, before sintering, porosity rapidly decreases from 24.8% at 500MPa to 16.2% at 700MPa. For pressure greater than 700MPa, it seems porosity remains at an almost constant level of 15.7%. After sintering, at pressure below 550MPa, porosity quickly decreased while above 550MPa the porosity remains almost constant at a value of 5.7%. This means that in the case of Ti6Al4V titanium produced by HDH, it is not necessary to use too high pressures since after the limit of 550MPa is exceeded, the porosity of the material after sintering changes only slightly.

Work done by Ivasishin *et al.* showed that, in order to attain maximum density in the final product, it is desirable to obtain high density in the compacts at the cold pressing stage, and then further increase the density by sintering [4]. Table 2.2 shows the powder compositions and powder sizes used by Ivasishin *et al.* The different combinations of powder properties give insight into the influence different alloying elements and powder sizes with respect to improving the density of the sintered product. The dependence of the density of green compacts on applied pressure is shown in Figure 2.12 [4].

Table 2.2: Properties of Powder Mixtures [4].

Mixture Number	Major Constituent	Alloying elements and method of addition
1	Ti, –100 µm, concentration of impurities ≈1%, including 0.29% O	Elemental powders Al, 98%, –100 µm V, 99%, –100 µm
2	Ti, +100–200 µm, concentration of impurities ≈0.7%, including 0.21% O	Elemental powders Al, 98%, –100 µm V, 99%, –100 µm
3	TiH_2, –100 µm, concentration of impurities ≈1%, including 0.30% O	Elemental powders Al, 98%, –100 µm V, 99%, –100 µm
4	Ti, –100 µm, concentration of impurities ≈1%, including 0.29% O	Elemental powders Al, 95%, –20 µm V, 98%, –40 µm
5	TiH_2, –100 µm, concentration of impurities ≈1%, including 0.30% O	Elemental powders Al, 95%, –20 µm V, 98%, –40 µm
6	Ti, –100 µm, concentration of impurities ≈1%, including 0.29% O	Master alloys 65 Ti – 35 Al, 98.5%, –100 µm, 25 Al – 75 V, 98.3%, –100 µm
7	TiH_2, –100 µm, concentration of impurities ≈1%, including 0.30% O	Master alloys 65 Ti – 35 Al, 98.5%, –100 µm, 25 Al – 75 V, 98.3%, –100 µm

The mixtures are divided into two groups according to their compactibility: 1, 2, 4 and 6 based on titanium powders, compacted to much higher densities than 3, 5, and 7 based on titanium hydride powders, as listed in the above table 2.2. Figure 2.12 below shows that the highest relative density upon cold pressing was attained in the mixture based on coarse titanium powder (mixture 2) which is the most ductile due to low contamination by impurities. Specimens of mixture 3, 5 and 7, based on titanium hydride powder, had substantially lower densities because of practical zero ductility of titanium hydride [4].

The compaction mechanisms of the titanium and hydride mixtures are different. Ductile particles of titanium are highly deformable, the higher the applied pressures the greater the area of contact between particles. The brittle hydride particles have a strength limit of 250MPa [20], consequently their compaction at all investigated pressures occurs by fracturing and mechanical locking of projections on the particles with each other. In the spite of their low densities, the compacts based on titanium hydride had sufficient strength for further sintering [4].

As per Figure 2.12, the variation of method of addition and particle size of alloying element powders at a given base metal particle size did not have a noticeable effect on the density of titanium mixtures 1, 4 and 6. The density of mixtures 3, 5 and 7, based on titanium hydride, remained practically at same level for all methods of alloying element addition [4].

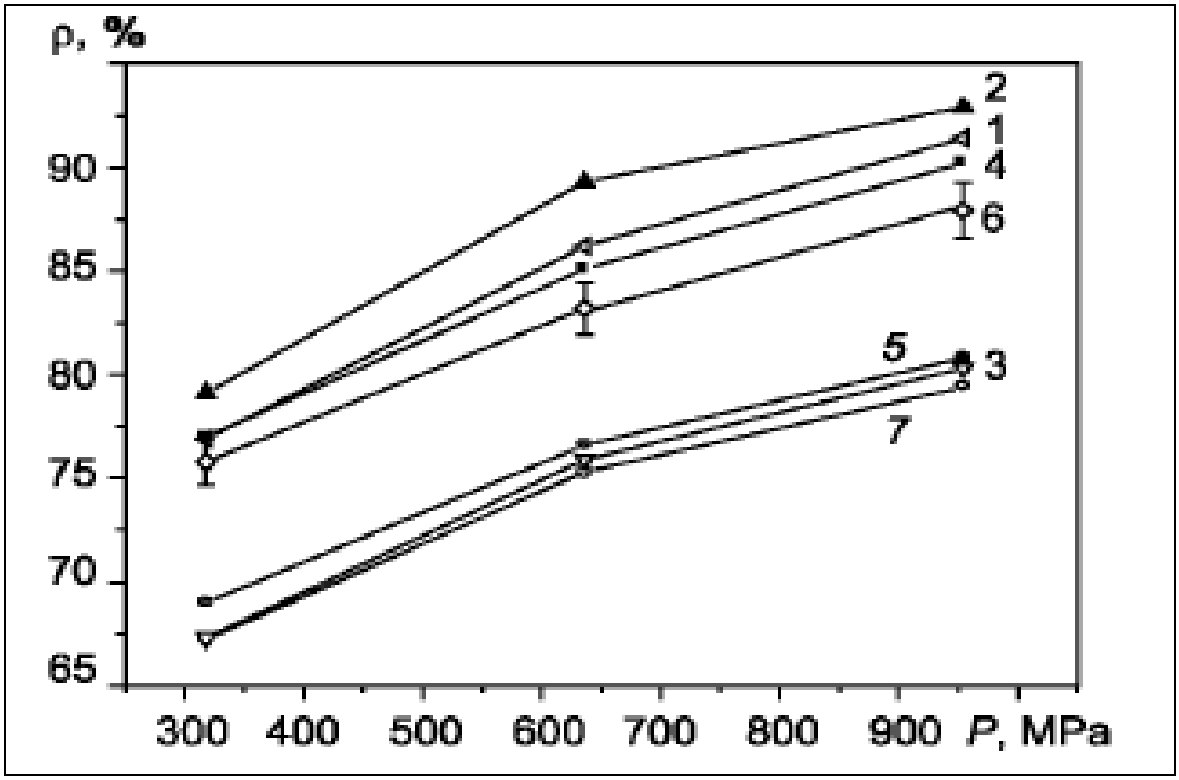

Figure 2.12: Shows dependence of compact density on pressing pressure for various powder mixtures. The density measurement error is given for mixture 6. It is similar to the other mixtures [4].

2.3.2 Sintering

Sintering is the process of consolidation of either loose aggregate of powder or a green compact of the desired composition under controlled conditions of temperature and time [17]. On a microstructural scale consolidation occurs as cohesive necks grow at the particle contacts. Such neck growth causes the property changes [18].

Particles sinter by atomic motions that eliminate the high energy surface associated with powder. The surface energy per unit volume depends on the inverse of the particle diameter. Typically the surface energy is assessed by the surface area. Thus, smaller particles with high specific surface areas have more energy and sinter faster. However, not all surface energy is available for sintering. For a crystalline solid, nearly every particle contact will evolve a grain boundary with associated grain boundary energy. The grain boundaries, important to atomic motion, are defective regions with high atomic mobility. The sintering mechanism describes the path of atomic motion which produces the mass flow. For metal powders, the mechanisms are usually diffusion processes over the surfaces, along the grain boundaries, or through the crystal lattice. The stages of sintering follow a geometric progression that they relate to the driving force and kinetics, and mathematically describe the process [18].

There are four types of sintering procedures:

- solid state sintering,
- liquid phase,
- activated sintering and
- reaction sintering.

For the purpose of this dissertation more focus will be placed on solid state sintering [17]. This is the commonly occurring consolidation of metal and alloy powders. This type of densification occurs mainly because of atomic diffusion in solid state [17].

Sintering Theory

Sintering may involve, 1) *single component system* – here self-diffusion is the major material transport mechanism and the driving force results from a chemical potential gradient due to surface tension and capillary forces between particles. 2) *Multi-component system* (involve more than one phase) – inter-diffusion occurs with the concentration gradient being the major driving force for the sintering in addition to self-diffusion caused by surface tension and capillary forces. In this sintering, liquid phase formation and solid solution formation also occurs with densification [17].

In single component systems, when two particles are placed in contact, inter atomic forces act between them, driving them together. They deform elastically, forming a neck. The neck formed with small particles is relatively large compared to larger particles [21]. At temperatures above $0.25T_m$, adhesion is followed by diffusion-controlled neck growth. The diffusion quickly removes the contact stresses generated; from then on the diffusive fluxes are driven by difference in surface curvature [21]. The chemical potential of atoms at the neck where two particles meet is determined by the principal curvature there. Matter flows into this region from all other parts of the system where the chemical potential is higher. The neck growth-rate is determined by the total flux of matter arriving at the neck; and this is simply the sum of contributions from the several independent paths [21].
The diffusion paths for single component systems are; surface diffusion (surface), lattice diffusion-substitutional (surface), vapour/pore transport (surface), boundary diffusion (grain boundary), lattice diffusion (grain boundary), and lattice diffusion (dislocations) [21].

During intermediate stages of sintering all dislocation segments in the neck region climb becoming curved, until they reach a configuration such that they are in static equilibrium. In climbing, the dislocations release matter which joins the neck. However dislocation-dominated sintering rarely appears as an important driving force simply because other mechanisms always go faster. As the neck grows, the curvature differences, which drive most of these mechanisms, slowly dwindle. During the final stage only two mechanisms are important; grain boundary diffusion from sources on the boundary, and lattice diffusion from the same sources [21].

In multi component systems, diffusion mechanism differs in the intermediate stage to a significant degree compared to that of the single component system. This is because in multicomponent system concentration gradient (lattice diffusion – interstitial) is the driving force.

Work done by X. Xu *et al*. [22] on pre-alloyed Ti-6Al-4V powder produced by the Armstrong process and HDH Ti-6Al-4V powders, (showed that for solid state sintering) there are several possible sintering mechanisms. Surface diffusion acts in concert with grain boundary diffusion to give cooperative mass flow, but the densification is still controlled by transport along the grain boundary. Surface diffusion results in no densification, only neck growth. They showed that lattice diffusion dominates the densification process at high temperature (1100^0C -1300^0C). At 900^0C, grain boundary diffusion contributes more to densification of the powder compact than lattice diffusion. Grain boundary diffusion rather than lattice diffusion controls the sintering at lower temperature, as a result of several orders (four to six) of magnitude faster diffusivity than lattice diffusion [23]. The dominant sintering mechanism according to Xu *et al.* strongly depends on the grain size of the powder. It has been found that grain boundary diffusion dominates the densification up to $0.9T_m$ and up to 90% sintering density for sintering of 10 μm particles size silver powder[24] and sintering of 15 μm stainless steel powder [25]. Grain boundary diffusion controls the densification below 90% sintered density and $0.7T_m$-$0.8T_m$ for sintering of 40μm copper particles. For 100 μm silver particles, the densification is all controlled by lattice diffusion in the range from $0.4T_m$-T_m. This means that the transition temperature from grain boundary diffusion to lattice diffusion control shifts to lower temperature with increasing particle size. Xu *et al.* concluded that, as for the sintering of Armstrong Ti-6Al-4V powder compact with 3μm grain size, boundary diffusion controls the densification below 91% sintered density and 900^0C, which is $0.6T_m$. This value is reasonable considering the fine grains and lower relative density. Above 1000^0C ($0.7T_m$) when the relative density is higher than 90%; densification mostly results from lattice diffusion. The particle size of HDH Ti-6Al-4V powder was 45 μm to 150 μm, and so it is reasonable that the whole sintering process is dominated by lattice diffusion. However, because in this work a master alloy addition is used the result could possibly be different.

Solid state sintering process

Condition for sintering [17]:

1. Densification occurs during sintering and solid state sintering is carried out at temperatures where material transport due to diffusion is appreciable. Surface diffusion is not sufficient, atomic diffusion is required.

2. Atomic diffusion occurs by replacing high energy solid-vapour interfaces (with free energy γ_{sv}) with the low energy solid-solid interface (particle-particle) of free energy γ_{ss}. This reduction in surface energy causes densification.

3. Initial free energy of solid-solid interface must be lower than free energy of solid-vapour interface. The process of sintering will stop if the overall change in free energy of the system ($d\mathbf{E}$) becomes zero, i.e., $d\mathbf{E} = \gamma_{SS}d\mathbf{A}_{SS} + \gamma_{SV}d\mathbf{A}_{SV} \leq 0$. Where dA_{SS} and dA_{SV} are the interfacial area of the solid-solid and solid-vapour interfaces.

4. Initially, the surface area of compact represent the free surface area, since no grain boundaries have developed and hence $A_{SV} = A_{SV0} + A_{SS} = 0$. As sintering proceeds, A_{SV} decreases and A_{SS} increases. The sintering process will stop when $dE = 0$,

   i.e. $\gamma_{SS}d\mathbf{A}_{SS} + \gamma_{SV}d\mathbf{A}_{SV} = 0 \Rightarrow \gamma_{SS}/\gamma_{SV} = -d\mathbf{A}_{SV}/\ d\mathbf{A}_{SS}$

5. Densification stops when $-d\mathbf{A}_{SV}/\ d\mathbf{A}_{SS}$ is close to zero. To achieve densification without grain growth, the solid-solid interface must be maximized. Such conditions can be achieved by doping or by using suitable sintering conditions for surface free energy maximization.

Stages in solid state sintering

In general, solid state sintering can be divided into four stages(see Figure 2.13)[17]:

- 1st stage: particles arrange themselves such that adequate contact is established.

- 2nd stage: necks are formed at the contact points between the particles, which continue to grow. During this stage, rapid neck growth takes place. The pores

become interconnected creating pore channels (pore networks) and the pores shapes remain irregular.

- 3rd stage: In this stage, with sufficient neck growth, the pore channels (see also Figure 2.14) become more cylindrical in nature. With continued sintering, a network of pores and a skeleton of solid particles are formed. The pores continue to become connected throughout the compact. The curvature gradient is high for small neck size leading to faster sintering and grain boundary formation. The pore channels start to form along the grain boundaries of diffused particles. With sufficient time at the sintering temperature, the pores eventually start rounding. As the neck grow, the curvature gradient decreases and sintering rate decreases. This means that there is no change in pore volume but with gradual change in pore shape although pores may become spherical and isolated.

- 4th stage: In this stage, pore channel closure occurs and the pores become isolated, rounded and no longer interconnected. Porosity does not change and small pores remain even after long sintering times.

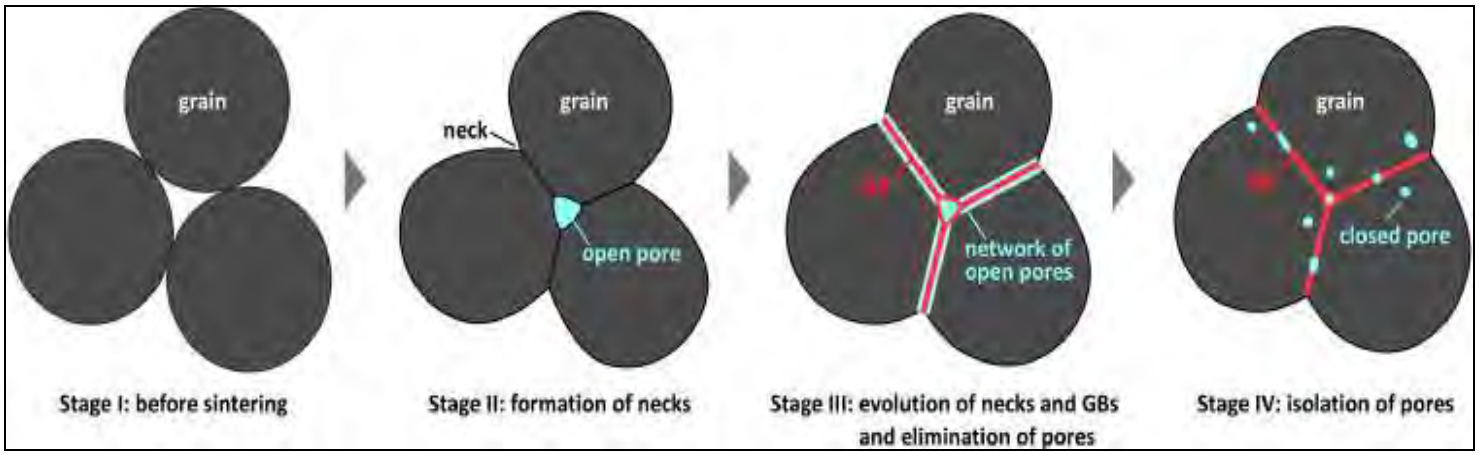

Figure 2.13: Stages of Sintering: particles in contact, formation of (necks, grain boundaries and pores), final sintering geometry [17]. ***The lines marked in red are grain boundaries (GB).***

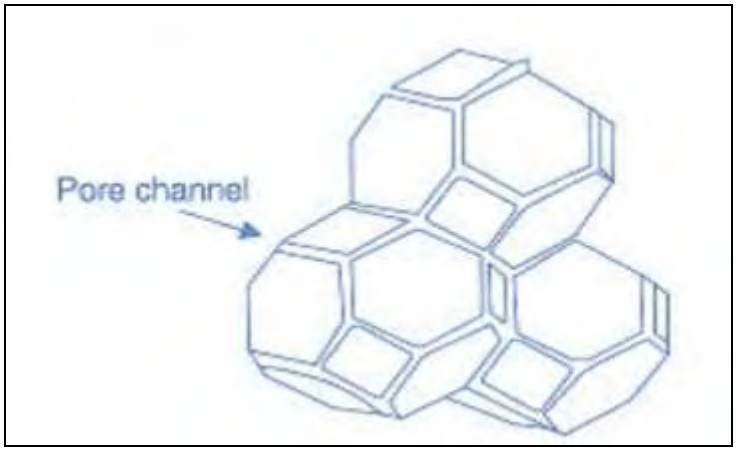

Figure 2.14: Showing pore channel formation [17].

Driving force for sintering

The main driving force for sintering is excess surface free energy in solid sintering. The surface energy can be reduced by transporting material from different areas by various material transport mechanisms so as to eliminate pores. Material transport during solid state sintering occurs mainly by surface transport and grain boundary transportation. This surface transport can be done through adhesion or surface diffusion [17].

Property changes during sintering

Densification is proportional to the shrinkage or the amount of pores removed in the case of single component system. In multi-component system, expansion rather than shrinkage will result in densification and hence densification cannot be treated as equal to amount of porosity removed. Densification results in mechanical property change like hardness, strength and toughness as well as physical property changes like electrical and thermal conductivity, magnetic properties etc. Also change in composition is expected due to the formation of solid solution [17].

Ivasishin *et al*. shows that chemically and microstructurally homogeneous alloy Ti-6Al-4V was obtained from all mixtures shown in Table 2.2 that were sintered under identical conditions at 1350 °C. However, the relative densities of the various powder mixtures post sintering were substantially different, as seen in Figure 2.15 below compared to those observed in Figure 2.12 for green compacts [4]. It should be noted that the same numbering system is used as in Figure 2.12.

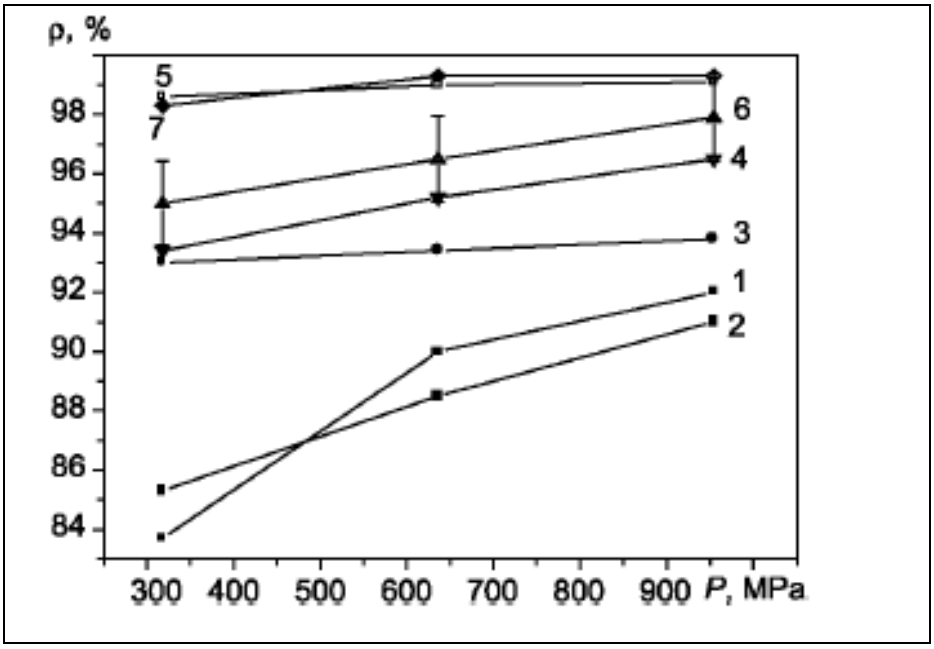

Figure 2.15: Shows the dependence of relative density of alloy Ti-6Al-4V obtained by sintering different powder mixtures on compaction pressure [4].

Mixtures to which the alloying additions were added in the form of elemental powders were compared. The density of compacts of mixture 1 was only slightly increased by sintering, and when coarse titanium powder was used (mixture 2) a decrease was observed (Figure 2.12). The low final density in these cases is a consequence of substantial swelling of the compacts upon heating due to reaction of titanium with molten aluminium. The subsequent "healing" of pores upon further annealing at high temperatures is not fully able to compensate for swelling effects, partly because healing is impeded by a layer of intermetallics which form at contacting surfaces. As a result, relative densities above 92% were not attained in mixture 1 and 2. Lower density values are obtained in mixtures based on titanium (mixtures 1, 2, 4 & 6) even at the highest preliminary compacting pressures (fig. 2.16) [4]. This can be clearly observed in figure 2.16 where both compacted and sintered specimens compared side to side.

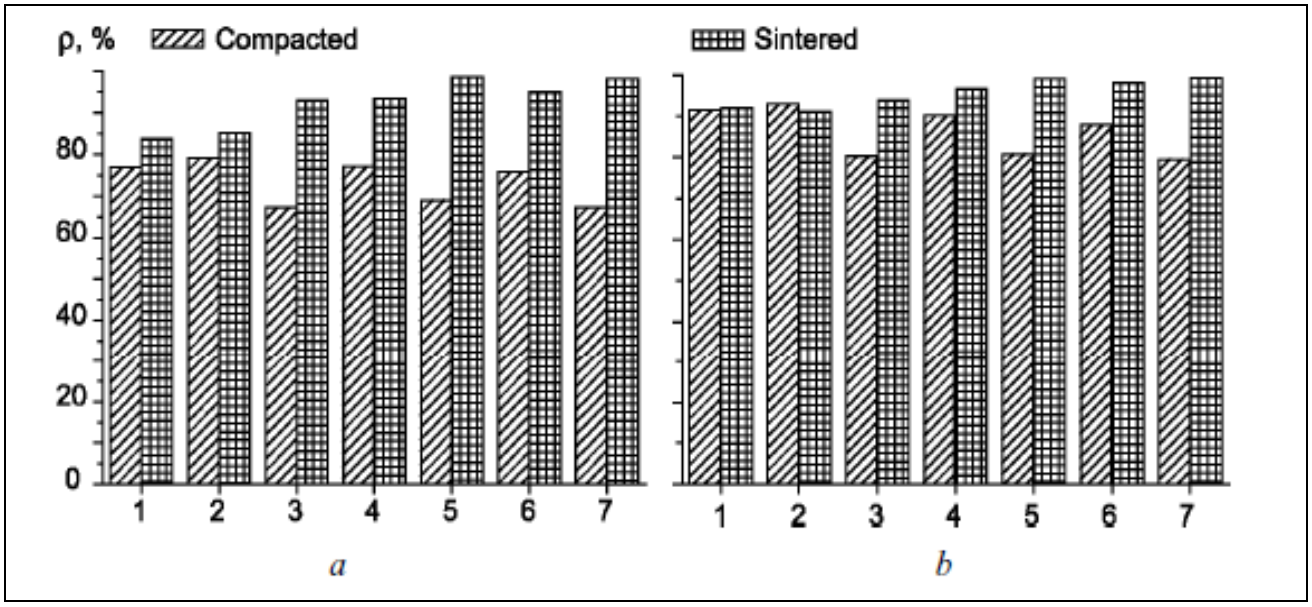

Figure 2.16*: Relative *Density of compacts of various mixtures upon sintering. Compacting pressure (a) 320MPa; (b) 960 MPa [4].

The density increase of mixture 3 based on titanium hydride with elementary powders was more substantial than that of mixtures 1 and 2 based on titanium, which is particularly noticeable at low compacting pressures (figure 2.16a) [4]. The decomposition of titanium hydride upon heating leads to the appearance of titanium in the mixture, activated by high concentration of crystal-structure defects produced by the given phase transformation. As a result, the reaction of aluminium with titanium occurs at low temperatures (570-560 °C), below the melting temperature of aluminium. The possibility of complete or partial reduction of oxides on contacting surface hydrogen atoms formed during hydride decomposition is also important. Subsequent heating in a vacuum at high temperatures completely removes the hydrogen so that it cannot impair the properties of the final material. It should be noted, however, that the final density of mixtures 3 is approximately 93% which is far from the required level [4].

The research of Xu *et al*. [26] research on cost effective press and sinter of titanium and Ti-6Al-4V powder for low cost components in vehicle applications studied the use of powder metallurgy technology. Xu *et al*. investigated CP-Ti and Ti-6Al-4V samples which were fabricated using different powders, different lubricant methods and sintered under different conditions to obtain optimal properties. CP-Ti and pre-alloyed Ti-6Al-4V were fabricated by the hydride-dehydride process, and a master alloy of 60% Al and 40% V (admixed) were used. Powders were lubricated in two different ways, die wall lube (DWL)

and admixed lube (ENST). Sintering target temperatures were 1371^{0}C and 1450^{0}C for 30 min and 90 min holding time respectively to determine the optimum sintering parameters.

Xu *et al*. also showed that the ADMX (blended CP-Ti and master alloy) obtained higher green and sintered density both in DWL and ENST, and this phenomenon is also observed in the hydride specimens, especially the ADMX-ENST specimen sintered for 90min which obtained 95.5% relative density. On the other hand, the pre-alloyed specimen showed 10% lower sintered density for the same condition (see Figure 2.17 below). The mechanical properties also revealed the same tendency that the flexural strength of blended specimens can reach an average of 1813 MPa, while the pre-alloyed specimen only achieved 1145MPa. Fracture strain showed that the best ductility achieved from the ADMX specimen was 7% when the samples are held for 90 min at 1371^{0}C.

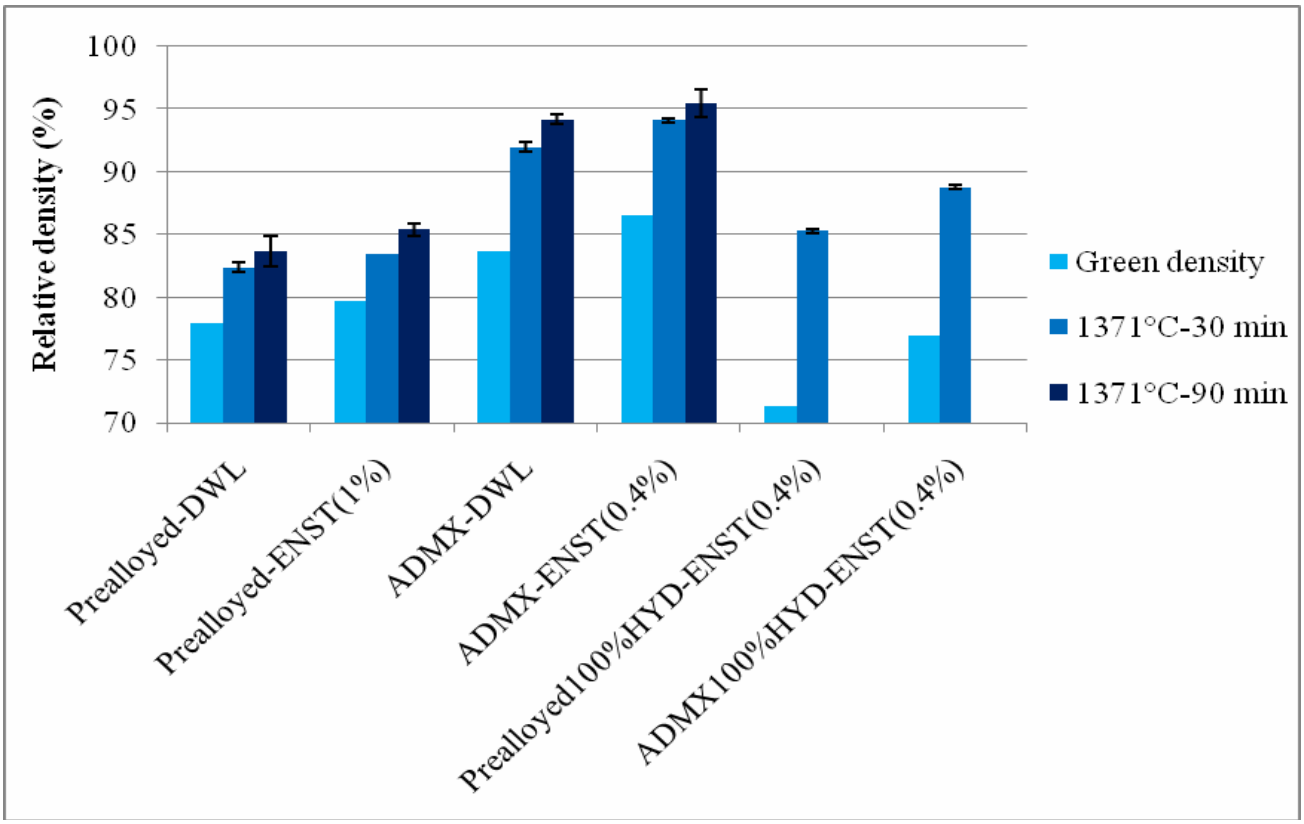

***Figure 2.17*: Green and sintered relative density for different specimens sintered at 1371^{0}C for 30min or 90min** [26].

It was also observed that the 90 min sintered specimen has significantly greater ductility than the 30 min specimen (see figure 2.18a). It was further concluded that blended powder

performed better than the pre-alloyed specimens. Flexural strength of ADMX-DWL sample reached 1813 MPa after 1371^{0}C-90min, and 7% flexural strain to fracture. Higher temperature (1450 ^{0}C versus 1371^{0}C) and longer sintering time (90 min versus 30 min) enhances the mechanical properties. However, due to the consideration of furnace limitations and expense, 1371 ^{0}C -90 min seems the best choice. 100% hydride powders did not show improved properties over the non-hydride powders. Internal lubrication and die wall lubrication show similar mechanical properties except for low fracture stain in ADMX-ENST samples (Figure 2.18b).

Bolzoni *et al*. [27] studied the mechanical behaviour of pressed and sintered titanium alloys obtained from pre-alloyed and blended elemental powders. The microstructural evolution of the pre-alloyed Ti-6Al-4V showed that specimens sintered at 900^{0}C -2hrs (see Figure 2.19) show that the sintering of the powder particles was already initiated, because the inter-particle boundaries were observed to disappear and the residual porosity was mostly irregular in shape [27]. The microstructural analysis also indicated that the main microconstituent is the alpha phase was isolated two-phase α+β islands homogeneously distributed throughout the microstructure [27]. A sintering temperature of 1000^{0}C leads to a pore structure constituted mainly of isolated pores, though the presence of highly irregular pores measuring approximately 30/40μm, which are derived from the joining of diverse neighbouring pores, can also be observed. In general, the composition of the Ti-6Al-4V pre-alloyed samples sintered at 1000^{0}C is much more homogenous, but there are still some darker zones dispersed throughout the matrix, which are characterized by slightly higher aluminium content [27].

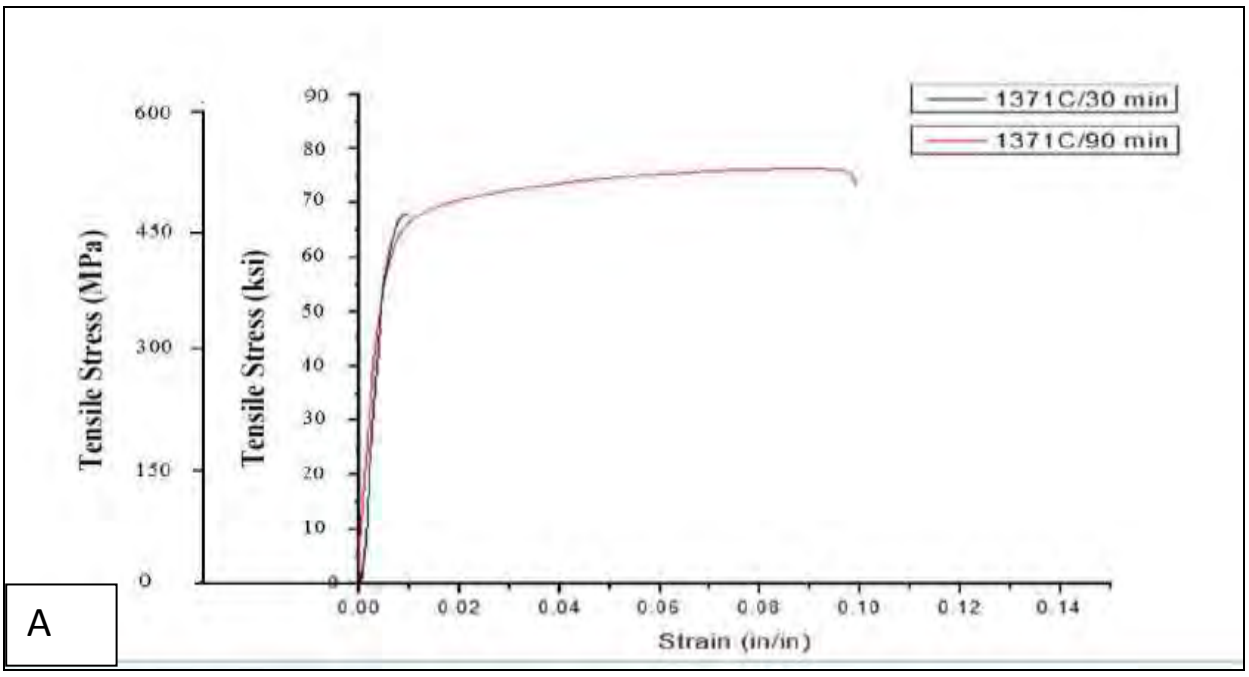

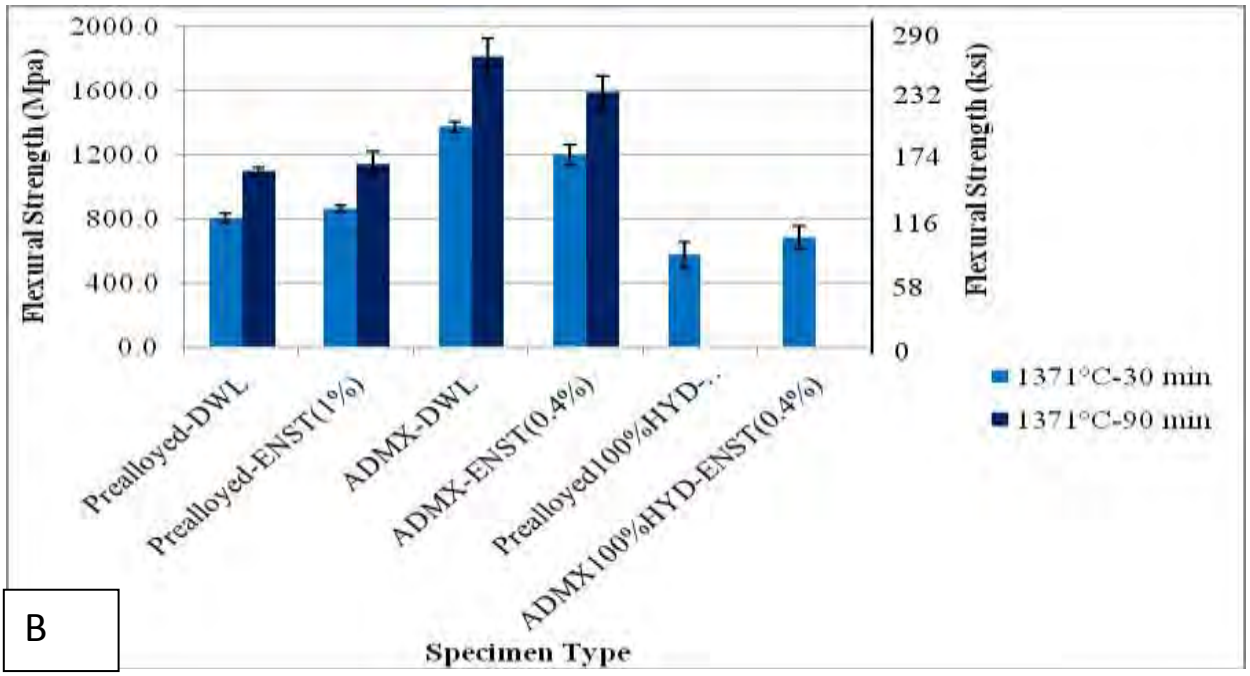

Figure 2.18*: *(a) Fracture stress-strain curves of B Type –ENST CP Ti for different sintering times at 1371°C. (b) Flexural strength of different kinds of Ti-6Al-4v specimens for sintering holding times of 30 min and 90 min at 1371°C, obtained from three point bending tests [26].

Starting from a sintering temperature 1100^0C, the percentage of residual porosity is reduced, the shapes of the pores become more spherical and the pore structure is

constituted by isolated pores. Moreover, the diffusion of the alloying elements seems to be complete, and the distribution of the elements is homogeneous [27].

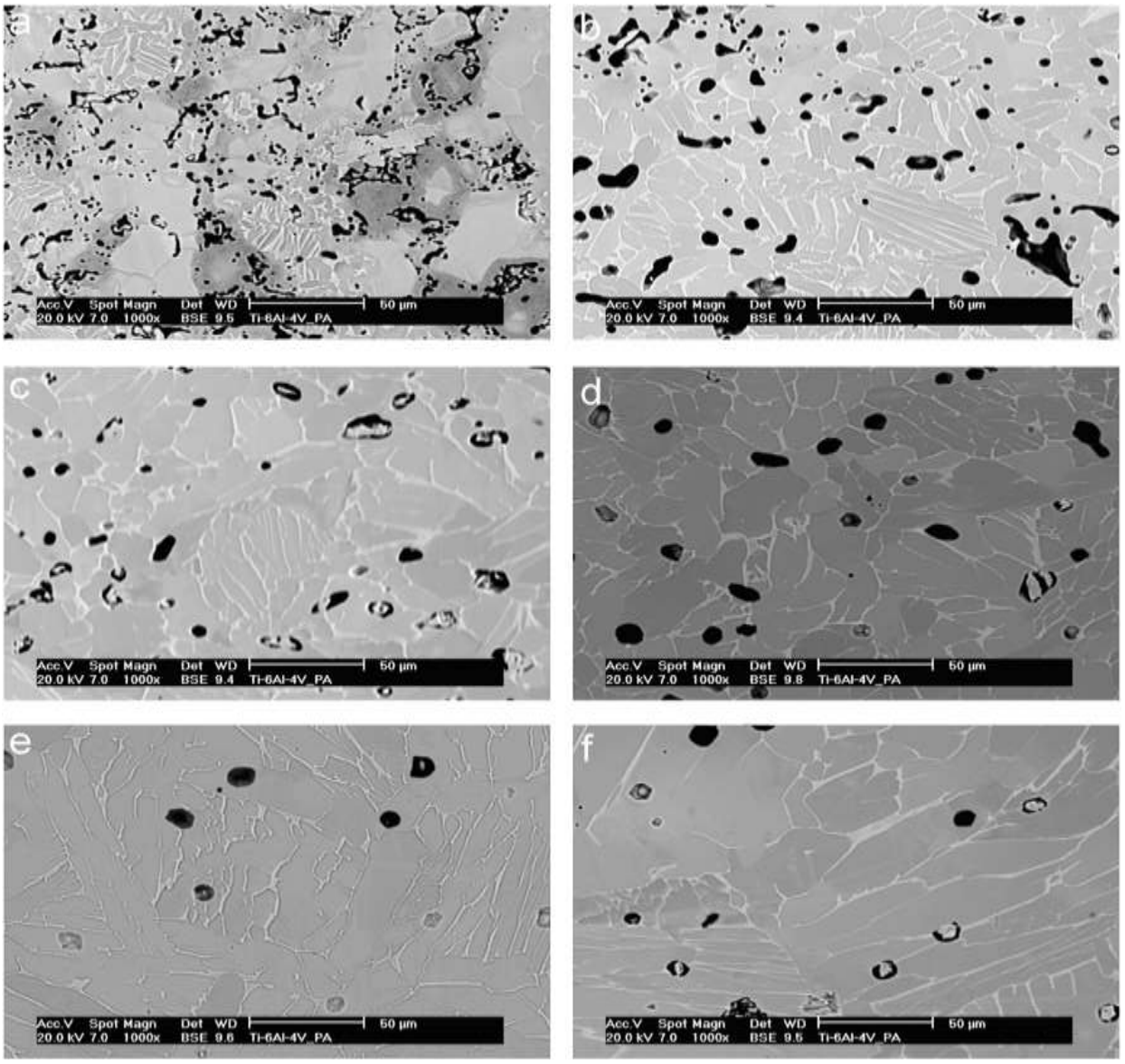

Figure 2.19*: *Microstructural evolution of the pre-alloyed Ti-6Al-4V powder sintered under high vacuum: (a) 900^{0}C, (b) 1000^{0}C, (c) 1100^{0}C, (b) 1200^{0}C, (e) 1300^{0}C and (f) 1400^{0}C [28].

Guo Shi-bo *et al*. [28] studied the mechanical properties and microstructure of Ti-6Al-4V compacts produced by metal injection molding. Ti-6Al-4V pre-alloyed powders made from HDH pre-alloy (A1) and mixed pre-alloy powder (A2) containing 90% gas-atomized powder and 10% HDH powder were used. This work showed that when sintering time is increased, porosity decreases and the microstructure of sintered products changes from equiaxed to typical Widmanstatten. The average grain size of prior β grains, α colonies and

α phase thickness in the β grains increase accordingly. The A1 powder specimens sintered at 1260^{0}C for 3-6hrs show high density but lower tensile strength and worse ductility[28]. When mixed pre-alloy powder (A2) containing 90% gas-atomized powder and 10% HDH powder is used, the sintered compacts show better properties such as higher density (95.8% - 96.9%) and tensile strength (800-848 MPa). Porosity decreases and pores become smooth and uniformly-distributed as sintering increased. When sintering time is increased, the microstructure of sintered products changes from equiaxed to typical Widmanstatten, and the average size of prior β grains, α colonies and α phase thickness in the β grains increase accordingly [28].

2.4 Hot Deformation of Metals

2.4.1. Introduction

The process that is involved in hot working of a metal such as hot rolling, hot forging and isothermal forging has great industrial importance.

This is the case because at high temperatures most metals exhibit a lower resistance to deformation and a higher ductility. A high rate of working is often necessary to improve the strength of the material but leads to an increase in the resistance to deformation and also to decrease ductility.

When conducting hot compression testing the sensitivity of the material to the rate of straining and the deformation temperature need to be taken into consideration. These conditions should be carefully controlled especially when the test results are intended to mimic industrial processing parameters [29].

Two phase titanium alloys most often are hot deformed, mainly by open-die or close-die forging. Desired mechanical properties can be achieved in these alloys by development of appropriate microstructure through plastic working and heat treatment processes. Irreversible microstructural changes caused by deformation at the temperature in $\alpha + \beta \leftrightarrow \beta$ phase transformation range quite often cannot be eliminated or reduced by heat treatment and therefore required properties cannot be achieved [30], [6]. Some of the properties of titanium alloys, such as: high chemical affinity for oxygen, low thermal conductivity, high heat capacity and significant dependence of plastic flow resistance on strain rate, make it very difficult to obtain finished products having the desired microstructure and properties as a result of hot working. Differences in temperature across the material volume, which result from variations in deformation conditions (local strain and strain rate) lead to formation of zones having various phase compositions (equilibrium α and β phases, martensite phases ($\alpha'(\alpha'')$), morphology (equiaxial, lamellar, bimodal) and distribution (fine-or coarse-grained) and therefore various mechanical properties [31], [32].

Obtaining the desired microstructure of Ti6Al4V titanium alloy using plastic deformation in the $\alpha + \beta \leftrightarrow \beta$ phase transformation range is related to appropriate conditions selection taking into account plastic deformation, phase transformation, dynamic recovery and recrystallization effects [31], [33], [32]. Grain refinement can be achieved by including

preliminary heat treatment in the thermomechanical process. Final heat treatment operations are usually used for stabilization of the microstructure as they restrict grain growth [34].

Titanium alloys together with aluminium alloys belong to the largest group of superplastic materials used in industrially. Their main advantages are good superplasticity combined with relatively high susceptibility to diffusion bonding. Among them, the two-phase in α + β Ti6Al4V alloy has been the most popular for many years as it exhibits superplasticity even after application of conventional plastic working methods [33].

2.4.2. Uniaxial Compression

Uniaxial compression specimens are cylindrical in cross-section and have a height to diameter ratio of less than 2, to avoid buckling during compression. During uniaxial compression, the samples are loaded axially and plastically deform such that the height of the cylindrical specimens is reduced [35].

When a cylindrical sample is compressed Poisson expansion occurs [6]. Unless lubrication at the ends of the specimen is very good, friction between the compression platen and the sample occurs. The friction acts as a restraint retarding the outward motion of the end faces during compression. The friction that exists between the specimen and the platens at their interface impedes the plastic flow of the specimen near to this interface and this result in "barreling" of the compresses sample. As seen in Figure 2.20 on the next page, the end faces which are in contact with the compression platen are actually created by the folding over of the sides that make up the original cylinder. The barreling that results from the frictional restraint introduces a complex state of stress and strain in the entire specimen [29].

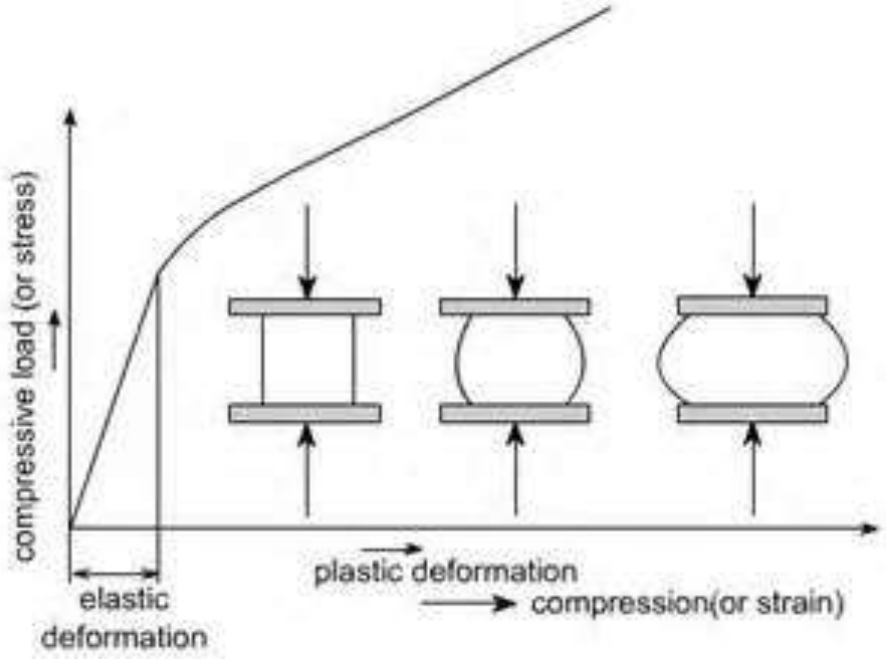

Figure 2.20- Schematic drawing showing the barreling of a uniaxial compression specimen as deformation increases. [29]

Low deformation zones develop adjacent to the compression platens, whereas severely deformed zones are connected more or less diagonally to the platens between the opposing edges the specimen. In figure 2.21 hot deformation of a cylinder under poor lubrication, and where the platens are cooler than the specimen is shown schematically.

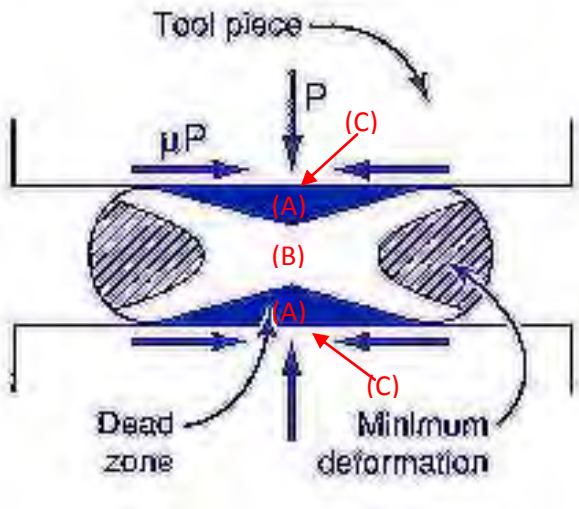

Figure 2.21: Deformation in a cylindrical wrought titanium sample which has been hot been hot compressed. A) Dead Zone. B) Maximum deformation zone. C) End Faces. [29]

The cooling that occurs on the faces that are in contact with the platens restricts the flow of the material resulting in the concentration of deformation being located in a central zone (labelled B) with dead-metal zones (labelled A) forming adjacent to the surface (labelled C) of the platens, As further deformation occurs, severe inhomogeneity develops and the growth of the end faces is almost entirely due to the folding over of the sides. The initial diameter of the specimen before deformation is known as D_0 and the initial height of the specimen is known as l_0. The final diameter of the specimen after compression is known as D_f and the final height is known as l_f. When the value of D_0/l_0 exceeds 3, expansion of the faces occurs and this should be avoided during hot compression testing.

Efforts to reduce this friction can be taken by utilizing lubricants between the specimen-platen interfaces but the friction cannot be completely eradicated. The flow stress measured using compression can be corrected for friction by means of the following equation.

$$\sigma = (4F_2/\pi d^2)\,(1+ ud_i/3l_i)^2$$

Where u is the coefficient of friction at the specimen-platen interface and F, d and l are force, diameter and length(height) respectively and for all equations presented here the subscripts o, f and i denote original, final and instantaneous measurements respectively [29], [36].

It is not considered necessary to correct for friction when calculating the flow stresses if the barreling coefficient (B) is not less than 0.9, where B is given by:

$$B = (4F_i l_i/\pi l_i d_0^2)$$

Whereas if friction can be neglected, stress is given by:

$$\sigma = (4F_i l_i/\pi l_i d_0^2)$$

And strain by:

$$\varepsilon = \ln\left(\frac{l_0}{l_i}\right)$$

The effect of friction can be minimized by using long thin specimens. This would result in most of the specimen volume being unaffected by the dead metal zones at the platens. This approach is restricted because the specimens will buckle if l/d exceeds approximately 2. In our testing facility friction is present and results in barreling of the specimen.

2.4.3 Plane Strain Compression

2.4.3.1 Plane Strain Compression Tests

Plane strain compression (PSC) tests are predominantly used to simulate deformation conditions experienced in industrial rolling operations, either at ambient or elevated temperatures, as the mode of deformation are very similar[37], [38], [39].

The basic PSC testing setup is shown in figure 2.22. Of great significance in a PSC test is the ratio of platen width to specimen thickness (w/h) ratio. The requirements for PSC test as prescribed by the ASM handbook [35] requires that the width of the specimen be at least 6 times the breath of the platens (i.e. b/w > 6) and that the w/h ratio should at all times be between 2 and 4.

The true stress and true strain in a PSC test can be given by the following equations respectively:

$$\sigma_{psc} = 4F_i / wb$$

$$\varepsilon_{psc} = \ln (h_0/h_i)$$

Where F is the deformation force and the subscripts o and i represent original instantaneous conditions respectively [35].

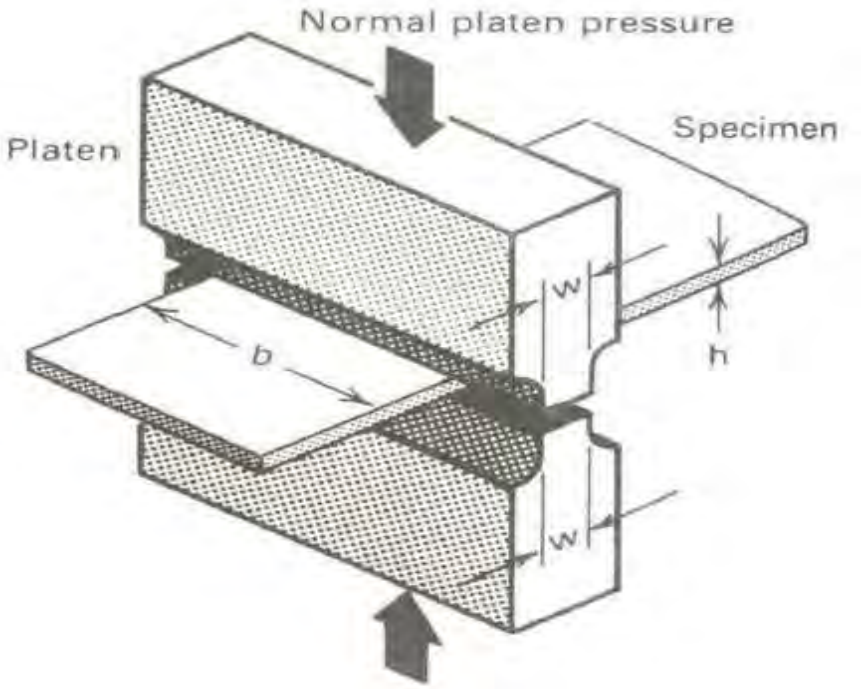

Figure 2.22: PSC testing setup [35].

When comparing the true stress associated with PSC conditions to those occurring during uniaxial compression, the PSC conditions result in the mean pressure on the platens being 15.5% greater than those associated with uniaxial compression. Because of this, the true stress-strain curve in uniaxial compression can be obtained from the corresponding PSC compression curve through the following equation [35].

$$\sigma = \sqrt{3}/2\ (F_i / wb)$$

$$\varepsilon = 2/\sqrt{3}\ \ln\ (h_0/h_i)$$

2.4.3.2 Characteristics of Deformation by PSC

For frictionless conditions the slip line field patterns for PSC typically appear as 45° lines originating from the platen-edge- specimen contact and the influence of the w/h on these field patterns are shown in Figure 2.23 [40].

Beynon and Sellars [40], working on aluminium, showed that the field patterns shown in Figure 2.23 were mostly clearly visible in the test specimen when the compression was carried out to low strain values. This is due to that fact at high strain values, ever changing w/h ratio due the reducing of h as a result of the compression, distorts these field patterns.

It was found that when high strain values were applied, a strain profile as shown in Figure 2.24 resulted within the sample.

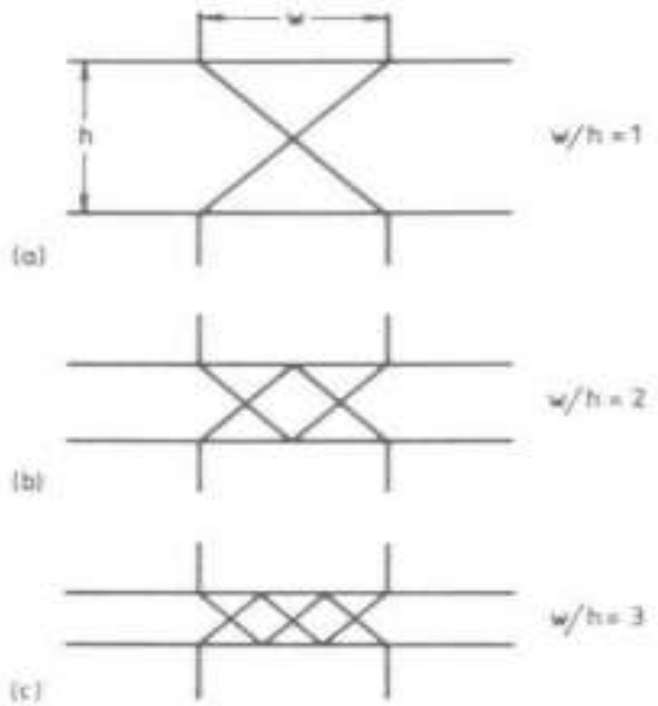

Figure 2.23: Influence of w/h ratio on slip line field patterns during PSC testing [40].

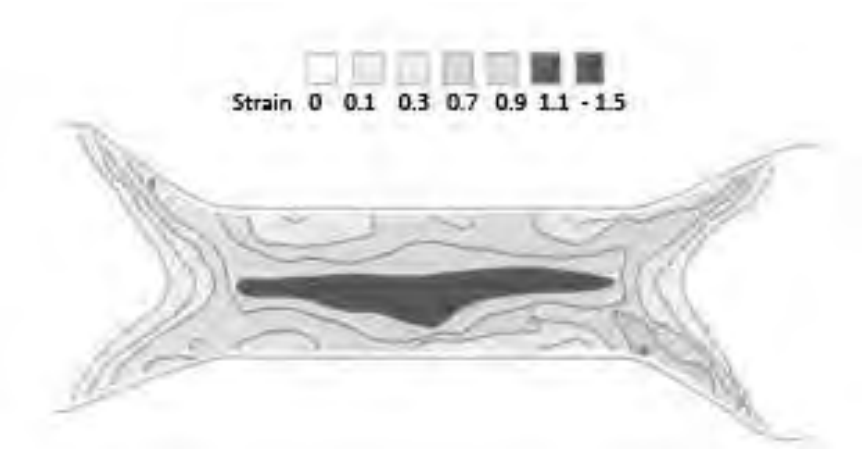

Figure 2.24: Strain distribution in aluminium after undergoing PSC to a nominal strain of 0.742 [40].

2.4.4 Recrystallization caused by hot deformation

2.4.4.1 Introduction

The softening process of recovery and recrystallization may occur during deformation at high temperatures. These phenomena are called dynamic recovery and dynamic recrystallization in order to distinguish them from static annealing process which occurs during post-deformation heat treatments. The static and dynamic processes have many processes in common, although the simultaneous operation of deformation and softening mechanisms lead to some important differences [41].

Dynamic recovery and dynamic recrystallization (DRX) occur during metal working operations such as hot rolling, extrusion or forging. They are important because they lower the flow stress of the material, thus enabling it to be deformed more easily and they also influence the texture and grain size of the worked material. Dynamic recrystallization may also occur during creep deformation with the main difference between hot working and creep being the strain rate. Hot working is generally carried out at a strain rate ranging between 1-100s^{-1}, whereas typical creep rates are below 10^{-5} s^{-1}. In many cases similar atomistic mechanisms occur during both types of deformation. Dynamic recrystallization also occurs during natural deformation of minerals in the earth's crust and mantle [41], [42], [43].

2.4.4.2 Recrystallization of titanium under hot deformation

While there has been much written about texture and deformation twins related to plastic anisotropy of titanium and on the general microstructure of titanium, relatively few studies have been made about the metallurgical importance of the recrystallization behaviour of commercially pure titanium during hot deformation [44]. Thus, this chapter summarizes three key paper/journal articles which have formed the bases for outlining the parameters and expected outcomes from which comparison can be made to the hot compression of sintered CP-Ti compacts.

2.4.4.3 Recrystallization Behaviour of CP-Ti during Hot Rolling

CP-Ti is manufactured generally by hot deformation processes such as forging and hot rolling. Problems however arise due to the reactivity and anisotropy of plasticity of titanium. These problems are most conspicuous during hot rolling. Therefore it becomes necessary to experimentally investigate the restoration processes i.e. recovery and recrystallization that occur during the hot rolling of ingots into slabs and then from slabs

into sheets. CP-Ti ingots in the as cast condition were heated to between 400°C and 1200°C. As soon as the slab was hot rolled the specimen was water quenched for 2-3 seconds [44]. The study concluded that when the hot rolling temperature is low (600°C-700°C), hardness slightly increases with increasing reduction. At the lower temperature side (600°C), a recovered structure appears where deformation bands containing lenticular deformation twins are formed. The recovery and recrystallization processes do not readily precede when the microstructure of the titanium material is coarse grained. The recrystallization recrystallized structure observed in the study is considered to have resulted from static recrystallization immediately after hot rolling, and is influenced by strain, temperature and strain rate [44].

2.4.4.4 Microstructure evolution of CP-Ti during high temperature deformation

Superplastic forming (SPF) is cost effective process for the manufacturing of complex shaped structural component and SPF of CP-Ti is very attractive in many areas due to the inert nature of this alloy. Investigation of superplasticity, mechanisms, related phenomena and microstructural evolution are important for achieving the desired mechanical properties [45]. In a study by Furnhura *et al.* CP-Ti sheets were used to create tensile specimens with a gauge of 11mm long, 4mm wide and 1.5mm thick. The specimens were machined with the tensile axis oriented parallel to the final rolling direction. The specimens were deformed at 600°C, 750°C and 800°C with differential initial strain rates. After testing the deformed specimens were cooled rapidly to room temperature by forced cooling in order to preserve the microstructure. Specimens were sectioned along the gauge and grip part of the deformed specimen. The volume fraction of fine grain ratio was measured using an optical microscope. SEM and EBSD are used to produce grain maps based on the orientation measurements [47, 39]. This study concluded that CP-Ti alloy does not show good superplasticity at 600°C-800°C due to rapid grain growth. The maximum elongation to failure value that can be obtained is 88% at an initial strain rate of $0.001s^{-1}$. Dynamic recrystallization happens when the alloy was deformed between 600°C and 800°C. The optimum DRX conditions are found to be at 600°C with an initial strain rate of $0.01s^{-1}$, attaining the highest volume fraction of fine grains whose average grain size is ±9.7μm at a strain of 80%. The distribution of fine grains is not homogeneous. The processes not only decrease the average grain size of the alloy, but also increase the misorientation angle [46].

2.4.4.5 Dynamic recovery and recrystallization in Ti alloys by hot deformation

In (α+β) alloys and metastable β titanium alloys, hot deformation by rolling or forging is conventionally performed in the β single-phase and (α+β) two-phase regions. During hot deformation dynamic recovery and dynamic recrystallization take place. The refinement of β grain size is beneficial for the improvement of the strength-ductility balance [45]. Dynamic recrystallization is quite effective in grain refinement when deformation is performed at high strain rate and lower temperature condition. Work done by Furuhura *et al*. [45] examined hot deformation microstructure of β titanium alloys in the β single-phase and (α+β) two-phase regions using a SEM and transmission electron microscope (TEM). A variety of alloys were solution treated so that equiaxed β structures were obtained. Solution treatment was followed by furnace cooling or air cooling to produce a lamellar (α+β) structure and by water quenching to obtain a martensite structure. After β solution treatment was performed the specimens were isothermally held at various temperatures in the β phase region or the (α+β) two phase region and subsequently compressed at the same temperature at strain rates of between $4.2x10^{-1}\ s^{-1}$ and $4.2x10^{-5}s^{-1}$ and strains of up to 55% to reduction 75% reduction [45]. This study concluded that when local orientation measurement techniques in SEM and TEM were applied to study the dynamic restoration mechanisms in hot deformation of titanium alloys, DRC was found to be the most dominating restoration process in β single-phase alloys. However, DRX also occurred partly along the β grain boundaries. When the (α+β) two-phase alloys with larger volume fractions of the 2^{nd} phase are deformed, continuous DRX occurs and (α+β) microduplex structures containing high angle boundaries were formed after certain amounts of deformation. Such application of DRX and manipulation of the grain boundary structures are important and useful in titanium alloys as well as other duplex alloys for lowering flow stresses improving superplasticity and obtaining ultra-fine grained structures.

2.4.5 Grain Refinement of α/β phase Ti-6Al-4V alloy by thermomechanical treatment

Thermomechanical treatment methods of α/β phase Ti-6Al-4V alloy usually involves a series of hot rolling and heat treatment steps where the ultimate objective is to produce a uniform, fine, globularized α grain [47]. The mechanical properties of Ti-6Al-4V are strongly influenced by the grain size and the well-known Hall-Petch equation with a decrease in grain size (d) [48].

$$\sigma = \sigma_0 + K/\sqrt{d}$$

Sirilar and Srichandr [49] investigated grain refinement of α/β phase Ti-6Al-4V alloy by thermomechanical treatment showed that when Ti-6Al-4V specimens are hot rolled with a starting equiaxed α, grain size of 20 micron, at a temperature range of 850-950^{0}C and reduction per pass of 16 and 64% followed by air cooling, 950^{0}C deformation with 64% reduction per pass produced 8 micron refined equiaxed α (See Figure 2.25). Grain refinement occurred at the temperature of α/β phase equilibrium below the β-transus temperature with large reduction percentage results in dynamic recrystallization (DRX). The annealing structure at 950^{0}C for 4 hours showed globularized α which grain-aspect-ratio was 1.2 [49].

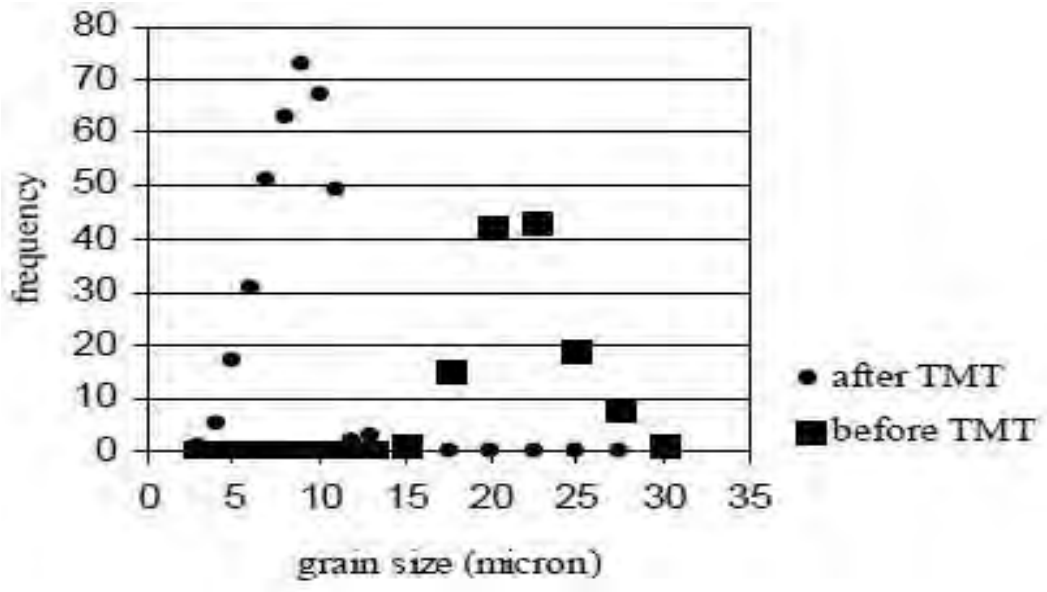

Figure 2. 25: Alfa grain distribution of Ti-6Al-4V before and TMT with 20 micron mean grain size and after TMT with 8 micron mean grain size [49].

Sirilar and Srichandar further showed that the tensile properties of Ti-6Al-4V were depended on microstructure and tensile and yield strength increased with decrease in α grain size, from Hall-Petch equation [49]. Figure 2.26 below indicate the increase of tensile strength from 957.38 to 989.85 MPa and yield strength from 918.18 to 942.12 MPa with decrease of α grain size from 20 to 8 micron. However, the different grain shapes may affect the different properties. Tensile and yield strength are 1604.20 and 1543.82 MPa respectively for Widmanstatten structure, and are 1741.56 and 1704.10 MPa respectively for martensite structure. It is surmised that the differences are a result of dislocation and grain orientation changes as there was no evidence that could confirm the difference are a result of the mentioned changes.

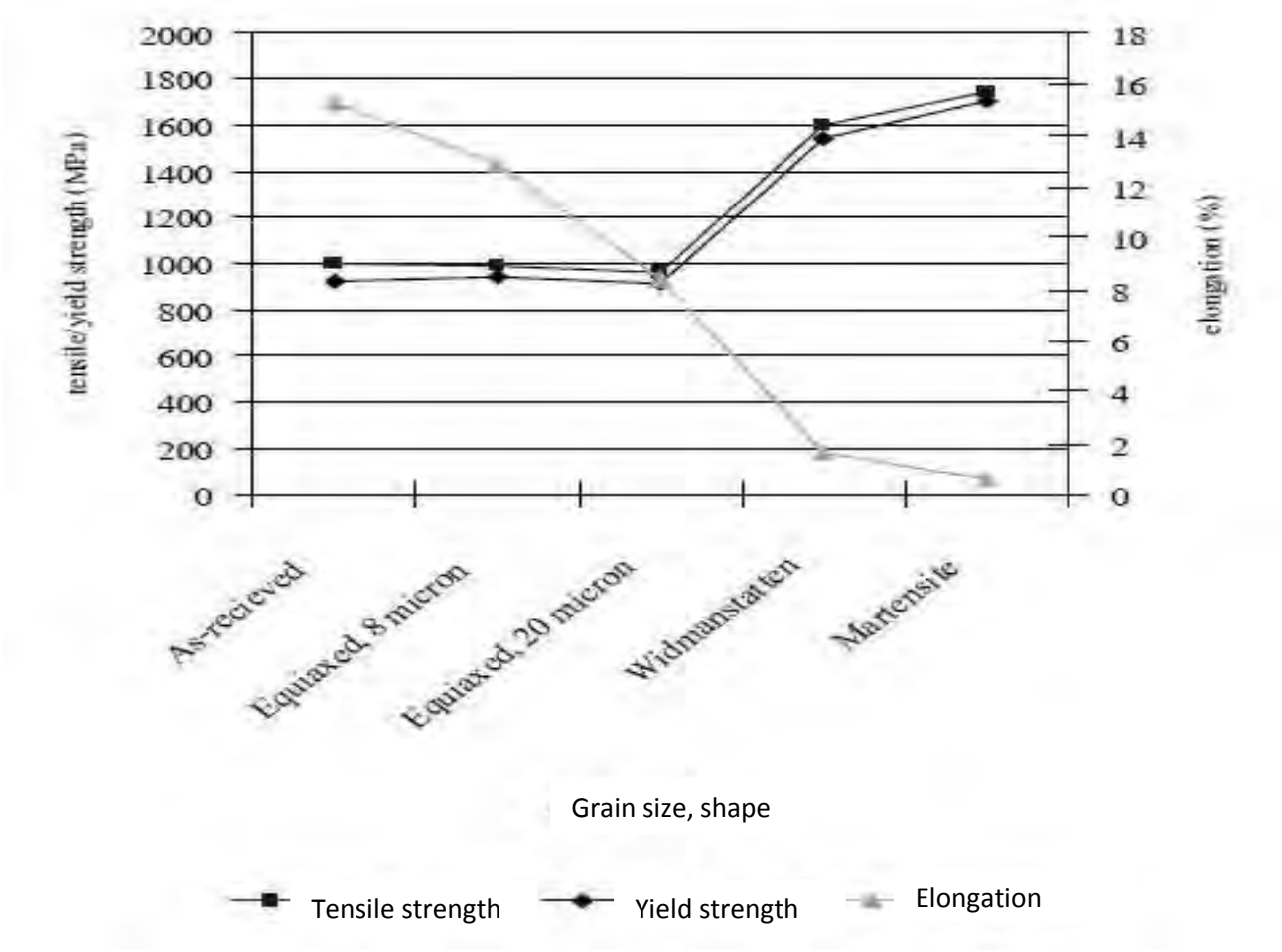

Figure 2.26: Tensile properties of Ti-6Al-4V [49].

The two processes for grain refinement by TMP are dynamic recrystallization and globularization. Dynamic recrystallization occurs during hot rolling below transus temperature of α/β phase equilibrium, with higher reduction per pass. The dynamically recrystallized grains were equiaxed and refined. Globularization occurred after annealing below transus temperature, the material was hot rolled with lower reduction per pass. The primary-α grain was produced at the edge, kinking, of low α structure. The tensile properties of Ti-6Al-4V are strongly influenced by the α grains and shape, because of the difference in dislocation density and grain orientation [49].

3. EXPERIMENTAL PROCEDURE

3.1 (a) General Experimental Overview

This study consists of two test materials (systems), one being commercially pure titanium (CP-Ti) and the other being CP-Ti blended with an Al-V master alloy. Test specimens of both systems were prepared using a cold compression and sintering process. The test specimens were designed to be cylindrical and rectangular in shape. Cylindrical specimens with 10mm diameter were used to test for density, microstructure and hardness behavior and the rectangular specimens were used to conduct strength tests as these specimens had the ideal shape for three point bend test conditions. The study then investigates thermo-technical processes (TMP) sequences for cylindrical and rectangular specimens. The TMP process comprises a hot deformation and an annealing process. The cylindrical specimens were uniaxially deformed and the rectangular specimens underwent plane strain compression (PSC). A flow chart summarizing the whole process is shown in Figure 3.2 seen on page 60.

The University of Cape Town and Stellenbosch University had a sharing agreement of resources such as the die-press, vacuum furnace and Gleeble 3800. Data was also shared between these two institutions in instances where there was an investigation overlap to avoid duplication of work and to limit waste.

3.1 (b) CP-Ti Powder Selection

Green Specimens

Recent work done by the University of Stellenbosch (Bosman [50]) investigating the influence of powder particle size distribution on the properties of press and sintered titanium and Ti-6Al-4V preforms yielded data that was used in this work which compared Alfa Aesar and Global Titanium powders that were compressed at 300MPa, 350 MPa, 400 MPa, 450 MPa and 500 MPa respectively are shown in Table 3. 1(a) and (b). Figure 3(i) shows the green density profile for the specimens compressed at these pressures.

Table 3.1(a): Alfa Aesar Green Density [50]

Alfa Aesar (AA)		Relative green density		
Compaction pressure [MPa]	**300**	65.32%	65.02%	64.57%
	350	67.53%	67.13%	67.53%
	400	69.18%	69.55%	69.13%
	450	70.48%	71.30%	71.40%
	500	73.05%	73.23%	73.51%

Table 3.1(b): Global Titanium Green Density [50]

Global Titanium (GT)		Relative green density		
Compaction pressure [MPa]	**300**	71.19%	70.91%	70.99%
	350	73.43%	73.39%	73.29%
	400	75.69%	75.24%	75.64%
	450	77.29%	77.01%	76.99%
	500	78.67%	78.67%	78.82%

It can be observed from figure 3(i) below that as compaction pressure is increased the relative green density also increases. It can also be seen that in all cases the Global Titanium has higher a relative green density than the Alfa Aesar. The highest green density attained when using Global Titanium powder at 500MPa, which is the highest pressure tested, averages 79% and the yield for Alfa Aesar at this pressure is only 71%.

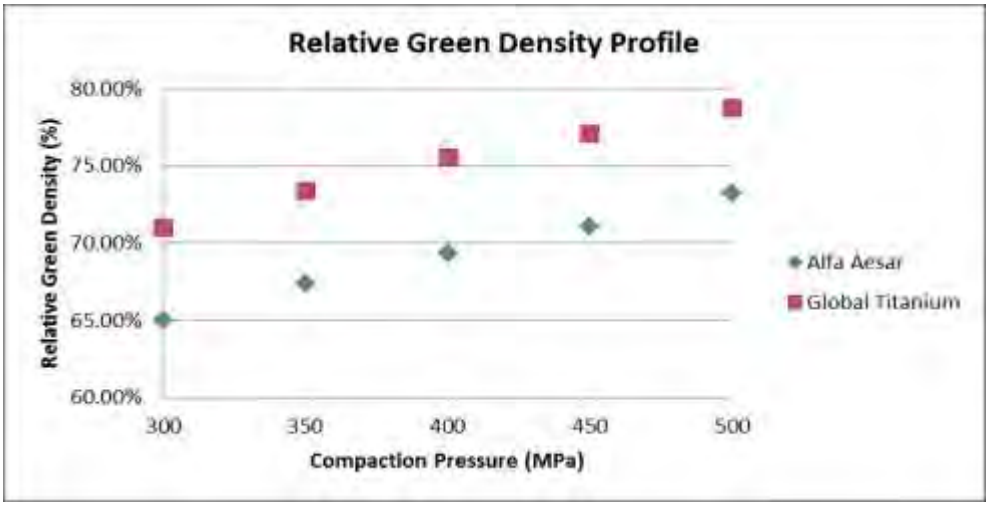

Figure 3(i): Relative Green Density Profiles of Alfa Aesar and Global Titanium compacted at 300MPa, 350MPa, 400MPa, 450MPa and 500MPa

Sintered Specimens

Further testing was performed by Bosman [50] where Alfa Aesar and Global Titanium powders were sintered at 1100^0C, 1200^0C and 1300^0C for 2hrs respectively. The densities obtained are shown in Tables 3.1 (c) and (d) and a sintered density profile was generated, shown as Figure 3(ii).

Table 3.1 (c): Alfa Aesar Sintered Density[50]

Relative sintered density Archimedes		Sintering temperature [°C]		
		1100	1200	1300
Compaction pressure [MPa]	300	78.77%	85.51%	89.68%
	350	87.26%	90.29%	94.13%
	400	93.14%	93.39%	97.24%
	450	92.17%	93.94%	97.68%
	500	92.41%	93.61%	97.53%

Table 3.1(d): Global Titanium Sintered Density [50]

Relative sintered density Archimedes		Sintering temperature [°C]		
		1100	1200	1300
Compaction pressure [MPa]	300	80.28%	84.56%	86.90%
	350	82.75%	86.38%	89.15%
	400	84.25%	87.19%	90.85%
	450	85.60%	88.01%	90.85%
	500	86.62%	87.95%	90.92%

The profile in figure 3(ii) shows that between 350MPa and 500MPa Alfa Aesar (AA) has higher relative density than Global Titanium (GT). At 300MPa the AA specimens have slightly lower relative density than GT specimens, however at 1300^0C AA the specimen have the highest relative density. AA at 1300^0C also has the highest density across all compaction pressures.

The difference between the relative density of AA and GT increases as the compaction pressure increases. It can be observed that both the relative density for AA and GT stabilizes after 400MPa. AA specimens have a steeper gradient than GT between 300MPa and 400MPa, showing that the rate of densification for AA is greater than that of GT with increasing compaction pressures.

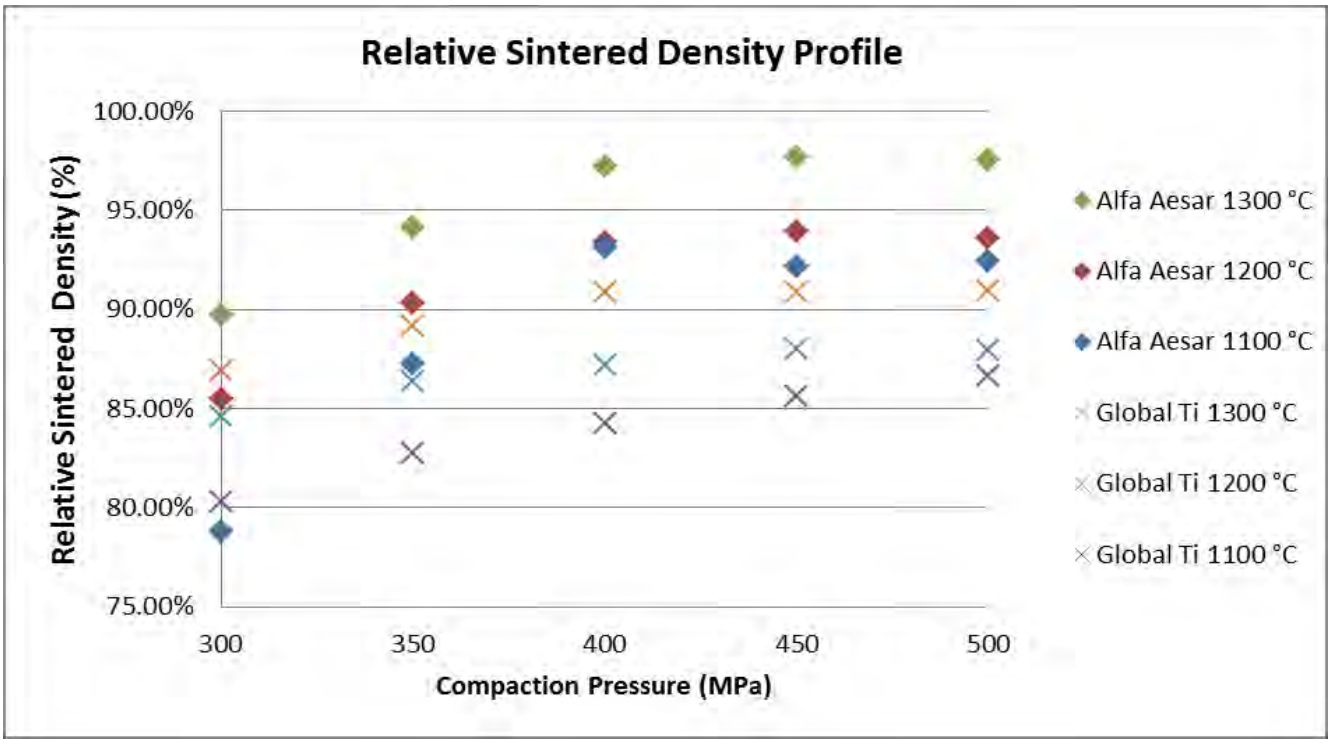

Figure 3(ii): Relative Sintered Density Profiles of Alfa Aeser and Global Titanium sintered at 1100^{0}C, 1200^{0}C, 1300^{0}C for 2hrs.

Discussion of Alfa Aesar and Global Titanium Specimens

Global Titanium powder used in Bosman [50] had an average particle size of 60µm which is relatively lower than the 74 µm of the Alfa Aesar powder.

The results evidently show that Global Titanium green specimen' yield better relative green density results than Alfa Aesar. Global Titanium powder having slightly lower particles size allows for better packing than the larger Alfa Aesar particles in the green compacts, leading to higher density yields.

Post sintering, the results show that Alfa Aesar has higher relative densities than the Global Titanium which improves with an increase in compaction pressure. However the increase in density slows down as compaction pressures exceeds 400MPa and it stabilizes at 450MPa in both Alfa Aesar and Global Titanium. This means that at compaction pressures beyond 450MPa there is no significant improvement in relative density of the specimens and this result is in line with the observations made by Ivasishin *et al*. [51].

The results also suggest that Alfa Aesar has far greater rate of densification than Global Titanium with increasing compaction pressure. It was anticipated that Global Titanium

would have higher relative density post sintering than Alfa Aesar as it had higher green densities and smaller powder particle size. This suggests that the rate of diffusion differs in the different powders and it would be interesting to understand the thermodynamics involved. However the scope of this work is limiting to only determining the powder that yields the best density results.

Based on the obtained green and sintered density results attained from Bosman [50] it is evident that Alfa Aesar is the best CP-Ti powder to use that will yield the best possible density outcomes. Therefore Alfa Aesar powder is used for this current investigation.

3.2 Powder Blending

A 500g mixture (see figure 3.1(a)) of Ti-6Al-4V was blended for 10 minutes in the following composition:

- 450g CP-Ti (Alfa Aesar) 99.5% (metal basis)
    - Average particle size: -200 mesh (74µm),
- 50g Master alloy (Reading Alloys) 99.5% (metal basis)
    - Average particle size: -230 mesh (63µm).

The blending equipment (figure 3.1(b)) had to be thoroughly cleaned with ethanol to avoid any contamination that could occur during the blending process. Blending for longer periods was avoided as this could result in reduction of powder size and modified shape which might affect the properties of the final product as discussed in the literature review chapter. Work done by Xu *et al*. showed that admix lubrication does not yield better mechanical properties than die wall lubricants. As a result lubrication was only to clean the die wall to avoid powder clogging which has been seen to cause die punch to be stuck during ejection of green part[26]. Therefore in this work zinc stearate was used as a die lubricant for the purpose of keeping the die clean and also reducing friction caused by the powder on the die wall.

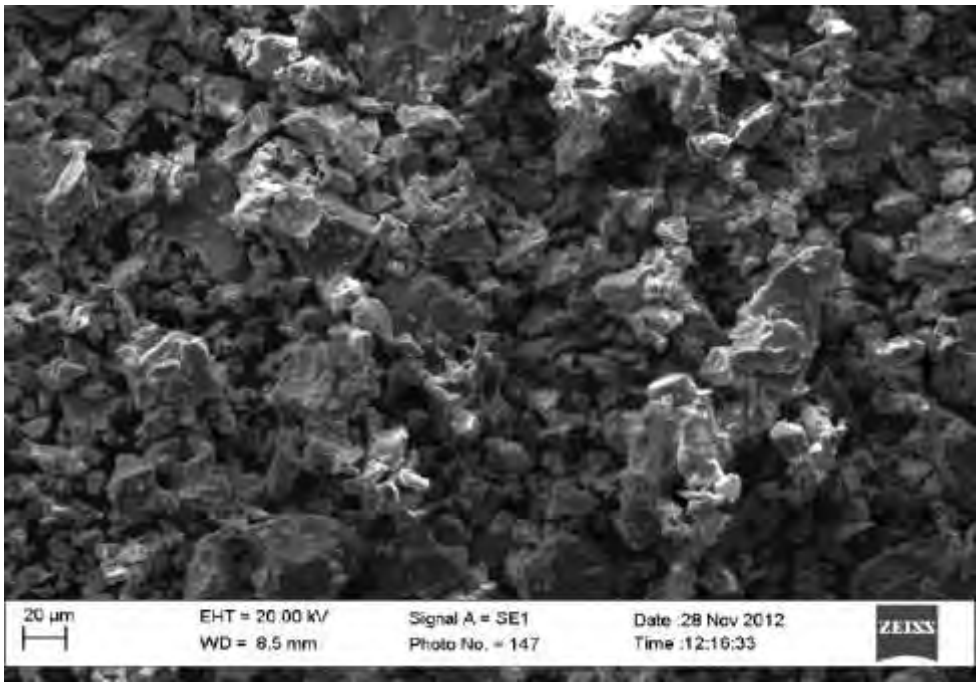

Figure 3.1(a): SEM image of Ti-6Al-4V alloyed powder, showing irregular shaped powder particles* [50]. *(Courtesy of Stellenbosch University)

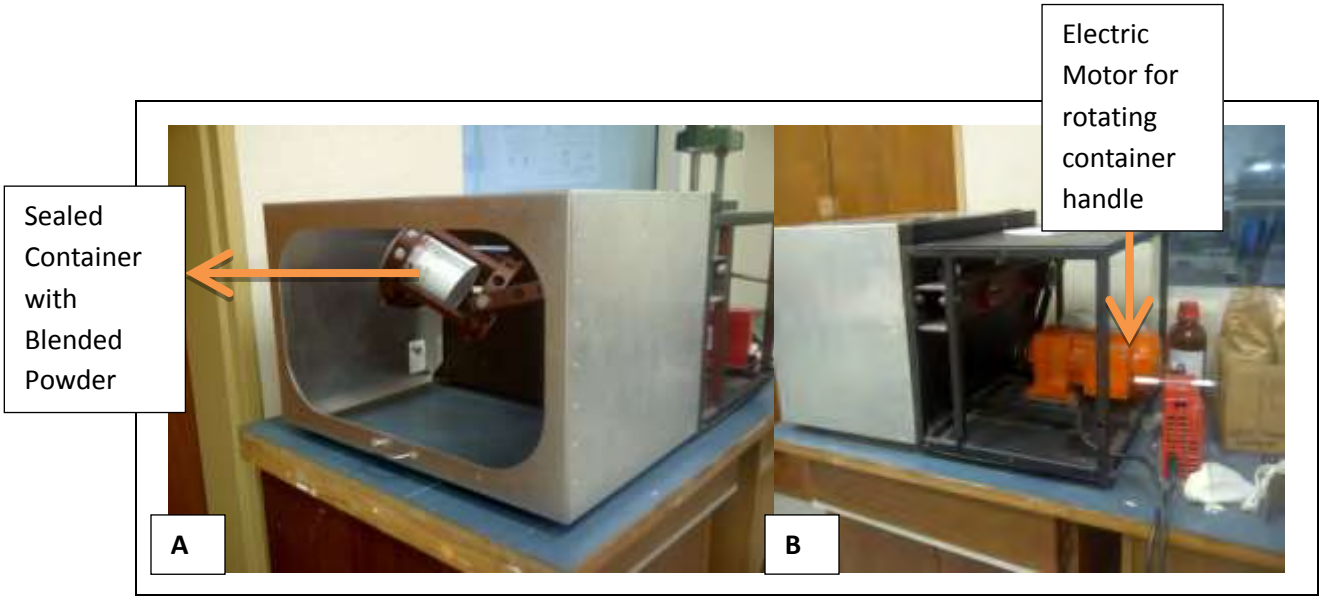

Figure 3.1(b): Apparatus used to blend CP-Ti with master alloy (courtesy of Stellenbosch University). Front view (A) and back view (B) with electric motor.

Figure 3.2: Flow Chart Summarizing the Methodology used in this Project

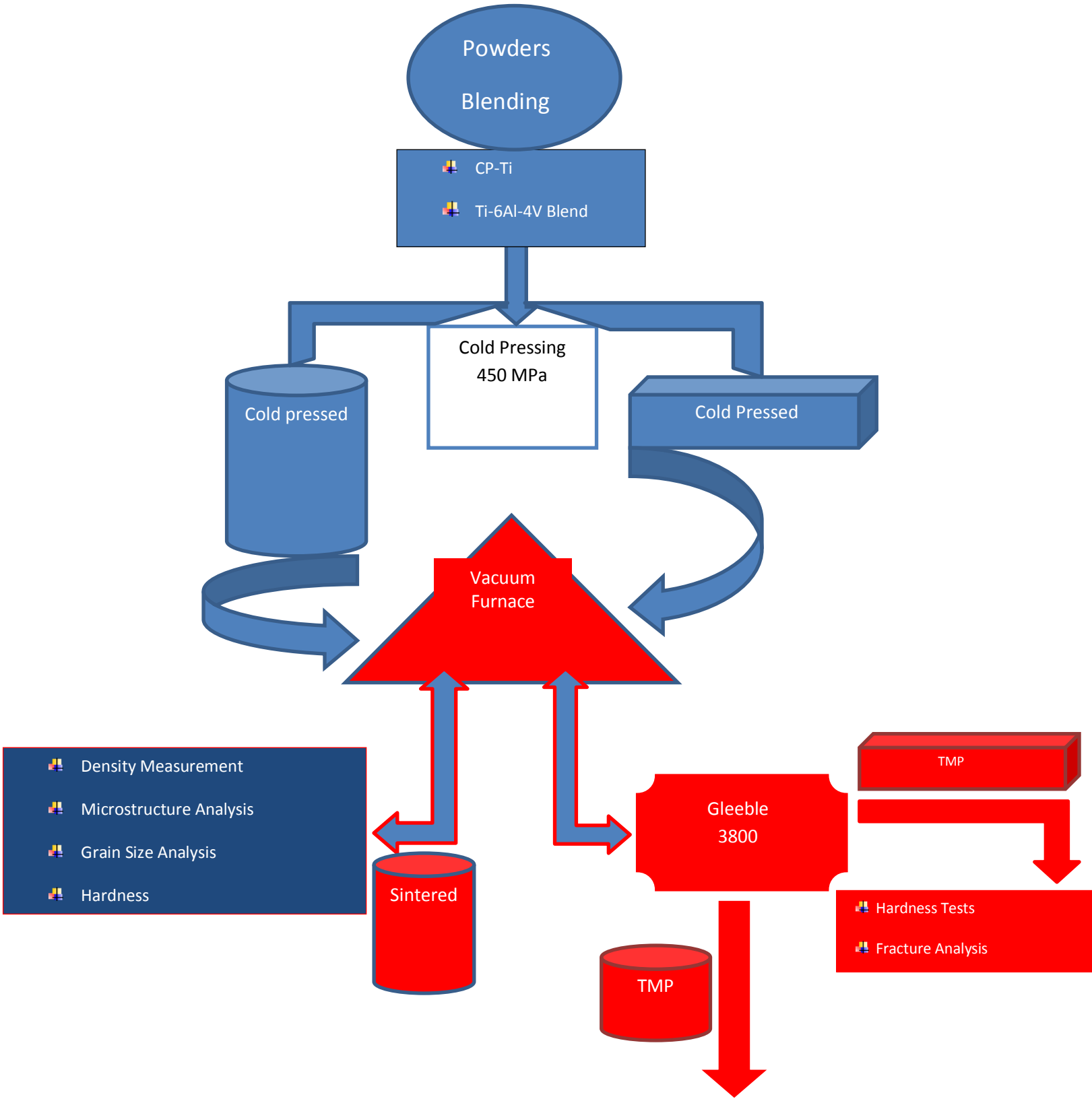

3.3. Compaction and Sintering

3.3.1 Cylindrical Specimens

Figure 3.3 (a, b) show the general pressing process in a float die press. Cylindrical specimens with 10mm ϕ, 16.3 ± 0.3mm in height were pressed using a manual jack press at Stellenbosch University (see Figure 3.3b). The compaction procedures were conducted at a pressure of 450MPa. This pressure was within the acceptable compaction pressure proposed by Ivasishin *et al*. [4].

The compacted specimens were subjected to pressureless sintering under varying temperature and time conditions (see Table 3.2) in a vacuum environment at pressures lower than 10^{-5} mbar. The heating rate to the sinter temperature was 300^0C/hr and the specimens were allowed to furnace cool after sintering.

Note: For nomenclature in the remaining document as an example, Ti-6Al-4V and CP-Ti specimens sintered at 1100^0C for 2hrs and later TMP is identified as Ti.11.2D and CP.11.2D respectively.

Table 3.2: Shows sintering conditions used in this study

Temperature	*Sintering Time (hours)*	*Specimen Nomenclature*
1000°C	6	CP/Ti.**10**.6
1100°C	2, 4, 6	CP/Ti.**11**.2/4/6
1200°C	1, 2, 4	CP/Ti.**12**.1/2/4
1300°C	1, 2	CP/Ti.**13.** 1/2

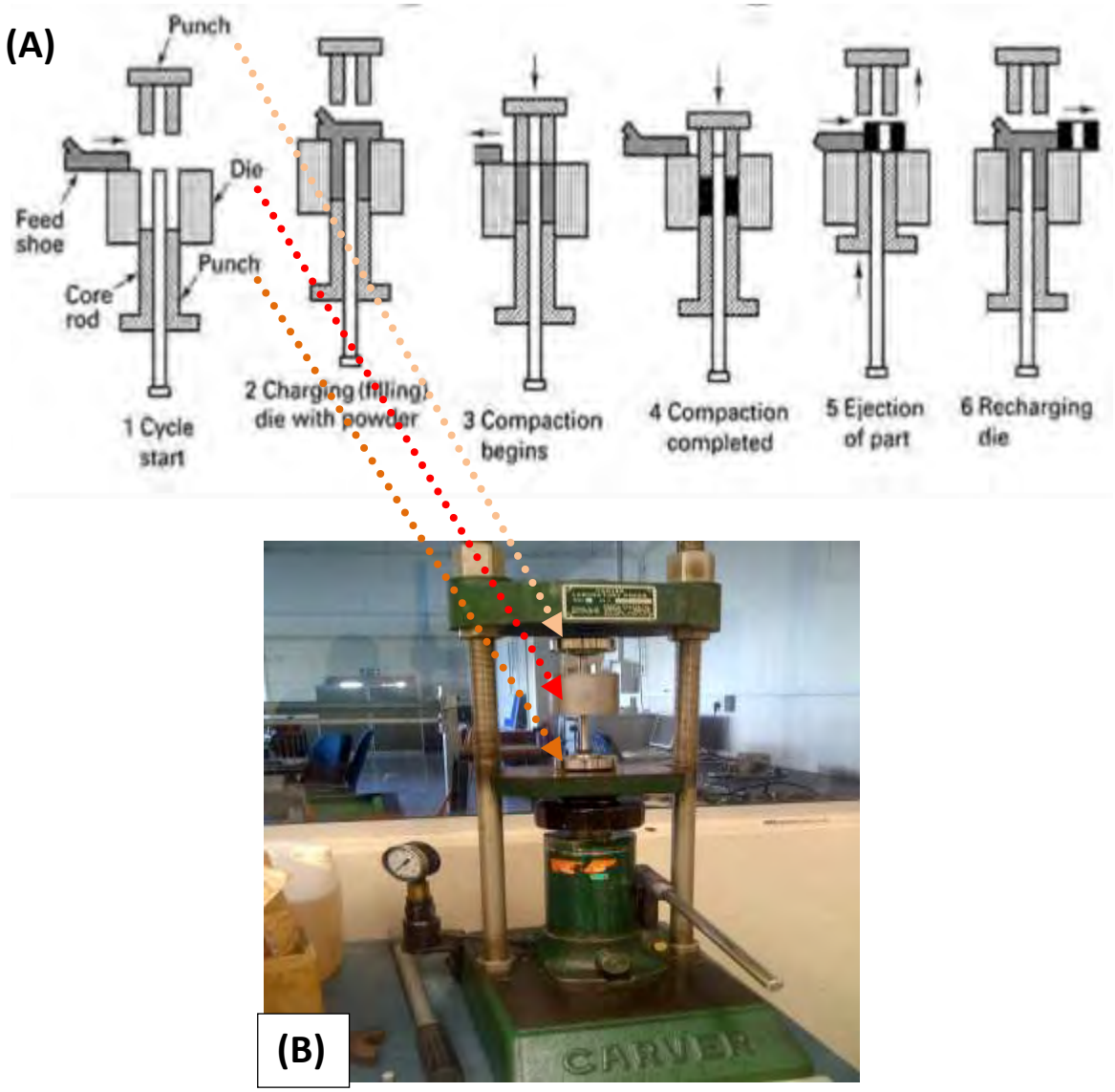

Figure 3.3 : (a)Compaction Process of Ti-6Al4V alloy powder in float die [19]***, (b) Jack laboratory press [Stellenbosch University Metallurgy Lab]***

3.3.2 Rectangular Specimens

Due to the limitations on cylindrical specimens in meeting the required geometry for determining mechanical properties, rectangular specimens were used (see Figure 3.4). The pressing of the BE powder for these specimens was carried out using the tooling prescribed in standard 41 of the MPIF standards (2010 edition) [18] for creating transverse rapture bars. MPIF standard 41 is presented in the appendix along with the details of the TRB tooling. The die cavity is rectangular with dimensions of 31.75mm x 12.70mm and the "thickness" of the specimen is controlled by the amount of powder used. For the creation of the rectangular specimens used in this work, the thickness of the green compacts was 7 ±

0.1mm. The press and sinter procedure used for these rectangular specimens was exactly the same as that used for cylindrical specimens.

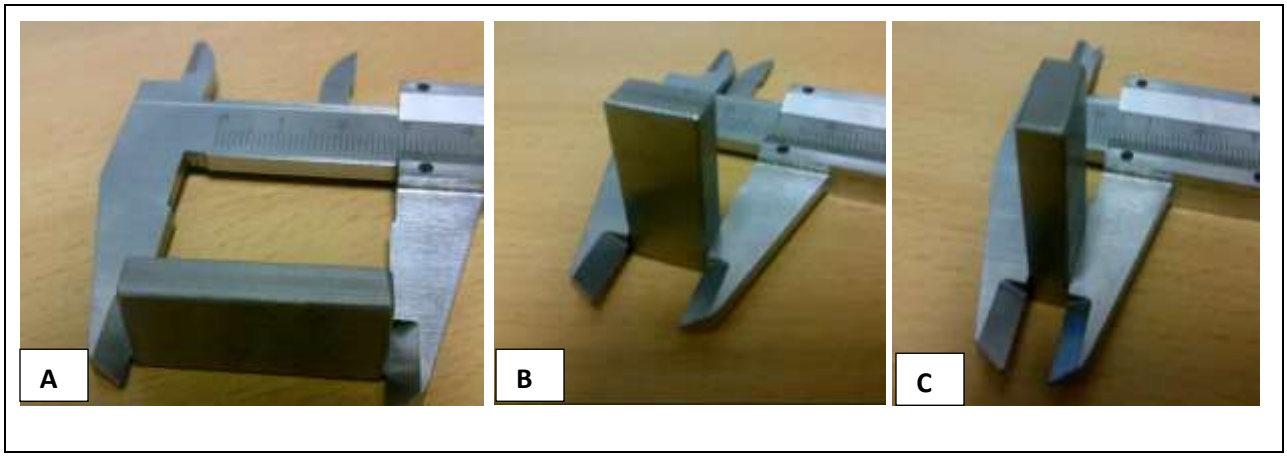

Figure 3.4: As-sintered transverse rupture bar specimen created according to MPIF standard 41.

3.4 Density Measurements (Water Displacement Method)

The density tests were performed according to Standard 54 of the MPIF standards 2010 edition[18]. This method determines the density of PM (Powder Metallurgy) material using the Archimedes principle of water displacement. The equipment required is shown in figure 3.5 on the subsequent page. The rig consists of a mass balance, a "bridge" and a specimen support structure. The bridge is used to support the beaker above the balance pan and the specimen support is connected to the balance pan. A wire basket, connected to the specimen support, hangs into the water and contains the specimen. The technique involves taking three measurements:

- Weigh test specimen in air, this value is labelled mass A (Figure 3.5a).
- Fix support stand and test specimen to a beaker filled with distilled water and place apparatus on the scale as shown in Figure 3.5b. This mass is labelled B.
- Mass of the specimen support in water without the specimen. Record the weight as mass C.

Measure the water temperature and record the density as provided in the tables in Standard 54 of the MPIF standards 2010 edition. The specimen density is calculated according to the following expression:

$$D = A\,[A-(B-C)]/\,\rho_w$$

Where ρ_w is the density of water at the measured temperature in g/cm^3. Also added to the distilled water was 0.07 volume % dish-washing liquid to act as a wetting agent. Relative density was calculated as a percentage of the theoretical full density of Ti-6Al-4V and a figure of 4.43g/cm^3 was used for this density.

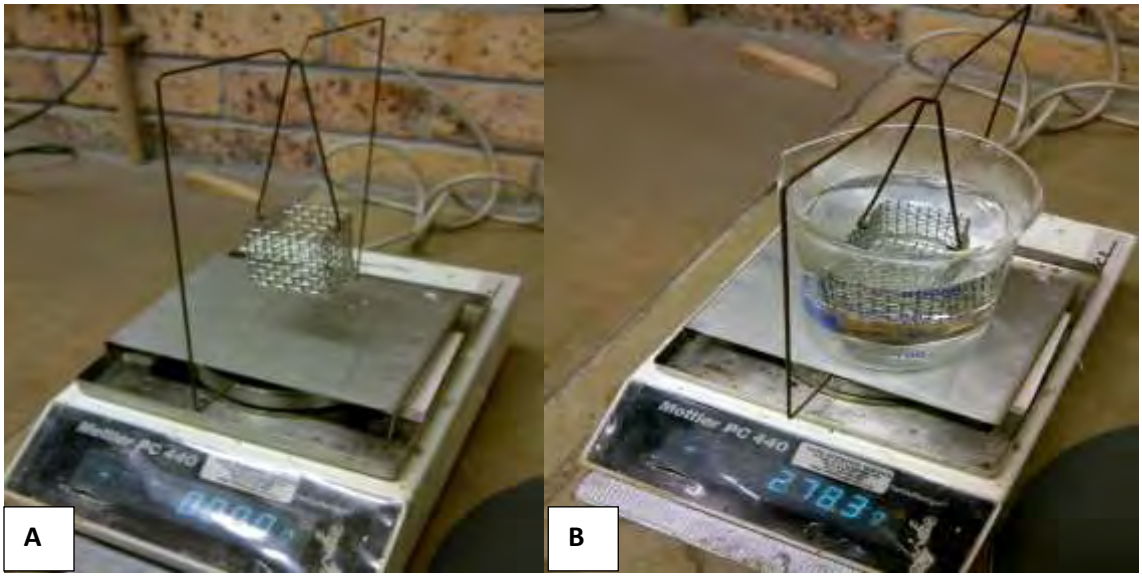

Figure 3.5: a) Specimen support immersed in distilled water b) Density testing rig on scale.

3.5 Microstructural Analysis

3.5.1 Specimen Preparation for Microstructural Analysis

Specimens were ground and polished by conventional techniques for Ti-6Al-4V as detailed in Table 3.3. Figure 3.6 below shows the general method of how specimens were sectioned and microstructure was viewed in the as-sintered (AS) and thermo-mechanically processed (TMP) specimens.

Table 3.3: Specimen grinding and polishing steps for specimen preparation.

Step	Grit/Pad	Speed	Force	Time (mins)	Lubricant
1	800 SiC	150 rpm	30N	2:00	Water
2	1200 SiC	150 rpm	30N	2:00	Water
3	MD Dac	150 rpm	30N	10:00	9 µm diamond suspension
4	MD Chem	150 rpm	30N	10:00	OP-Nap colloidal Silica
5	MD Chem	150 rpm	30N	5:00	Water

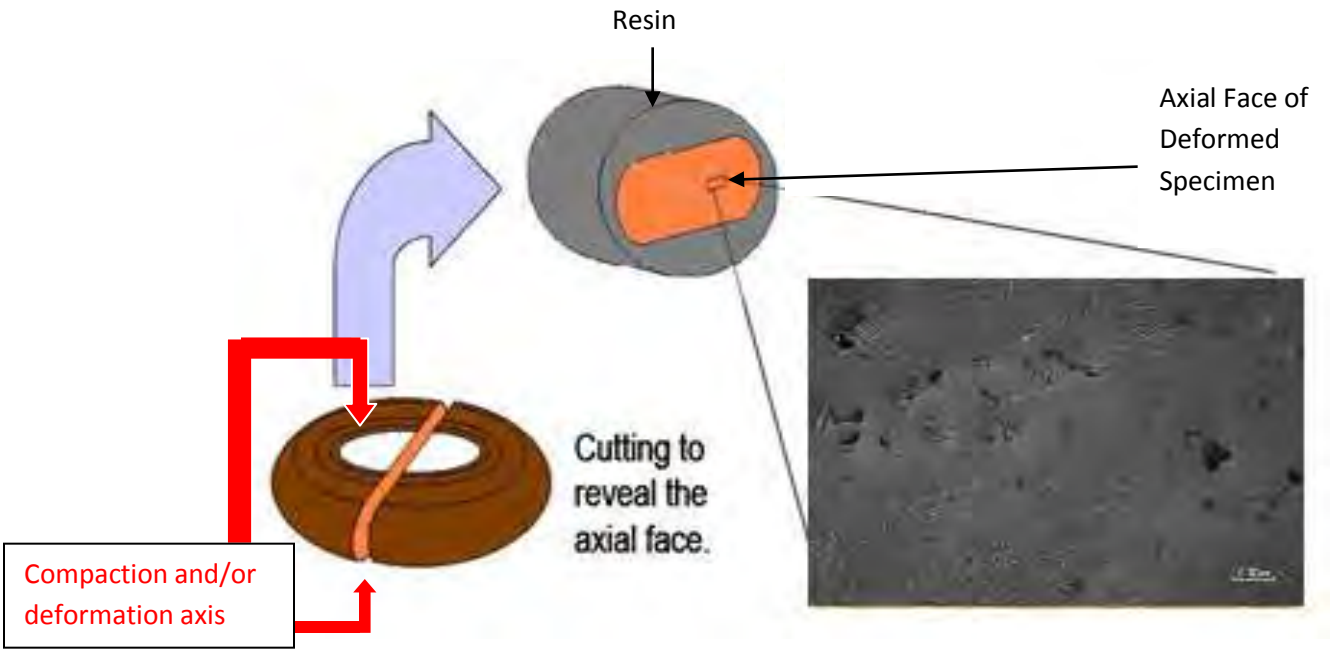

Figure 3.6: Showing sample compaction and/or deformation axis, cut on axial surface mounted, polished and viewing of microstructure[52].

3.5.2 Microscopy

Light Microscopy (LM) was used to analyze the microstructure of the samples. The specimens for which LM was used to analyze the grain morphology were etched using Kroll's Reagent (100ml distilled water, 4ml HNO_3 and 2ml HF) after being polished according to the method detailed in table 3.3. LM was carried out on a Reichert MeF3A inverted light microscope fitted with a Leica DCF 320 camera and Leica acquisition software. The images were acquired using Nomarski interference contrast imaging.

Work done by Miller [53] showed a comparison of optical and SEM BSE imaging techniques for quantifying alpha/beta titanium alloy microstructure. From the work it was determined that optical microscopy of a properly etched surface yields a statistically equivalent quantitative measurement of primary alpha volume fraction compared to the measurement on as polished surfaces using SEM BSE microscopy. It was further observed that a quantitative measurement performed optically is valid if the region is a representative region of the entire specimen and does not contain any suspect etching artifacts. These findings also showed that the two different techniques to collect a micrograph yield equivalent results, not that a single micrograph is sufficient to measure the volume fraction of a sample. Thus, an appropriate number of representative micrographs are still necessary to yield statistically relevant measurements [53].

3.6 Grain Size Analysis

Grain size measurement is complex due to a number of factors. Firstly, the size of the grains across the microstructure is not constant, thus on a cross-section we observe a range of sizes. Secondly, the sectioning plane cuts through the grains randomly and therefore an average grain size must be measured to represent the microstructure.

Thirdly, in most cases grain sizes can be represented as a distribution around a central mean. In the vast majority of cases, experimenters merely determine the mean value of the planar grain size, rather than the distribution. There are cases where the grain size distribution is not normal but bimodal, or "duplex." Also, grain shapes can be influenced by processing procedures, for example they can be flattened and/or elongated by a deformation process. Different product shapes, and processing procedures can produce a variety of non-equiaxed grain shapes. This then influences the ability to measure the grain size[54].

In this research the line intercept approach for measuring grain size was used (shown in Figures 3.7-3.9). In this method, lines are superimposed over the image at a known magnification (see Figure 3.9 below). A magnification of 20µm was used throughout for the purpose of capturing a reasonable amount of surface area per micrograph in each specimen observed. To determine the number of lines that should be superimposed over each image, a profile had to be generated (see figure 3.7 on facing page showing line intercept profiles of TMP CP Titanium and Ti-6Al-4V specimens that were sintered at 1200^0C and 1300^0C respectively), where the true line length is divided by the number of grains intercepted by the line. This gives an average of the length within the intercepted grains; the average grain length was then plotted against the number of superimposed lines. The profile shows that 10 lines should be superimposed over each image. Using less than 10 lines could affect the reliability of the measured average grain length and using more would add no value to the accuracy of the result.

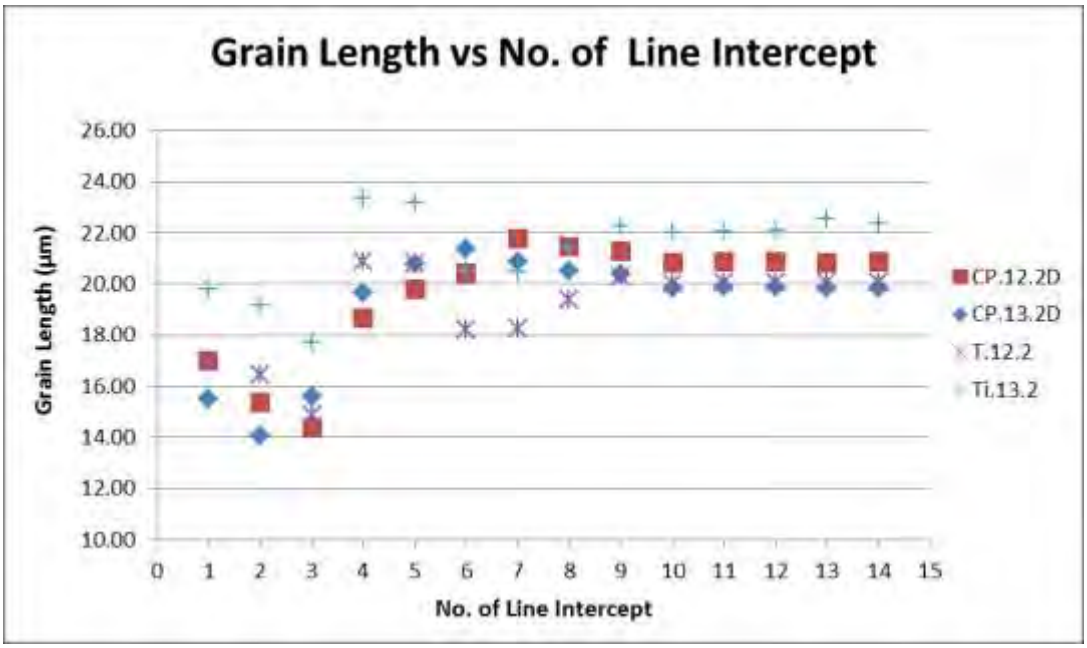

Figure 3.7: Profile showing Grain Length vs No. of Line Intercepts required to accurately determine the number of lines that should be superimposed on each microstructural image.

After having determined the number of lines per field of view that are necessary for a reliable assessment, it was essential to also determine the number of fields of view necessary to give a reasonably good average grain size. A profile was generated (see figure

3.8 below) by taking images randomly across the specimens to ensure that there is no bias on the part of the experimenter, either conscious or unconscious. Randomization gives allowance to assume independence between observations. The generated profile shows that 4 fields of view were sufficient in ensuring that the average grain size is measured effectively across the specimen.

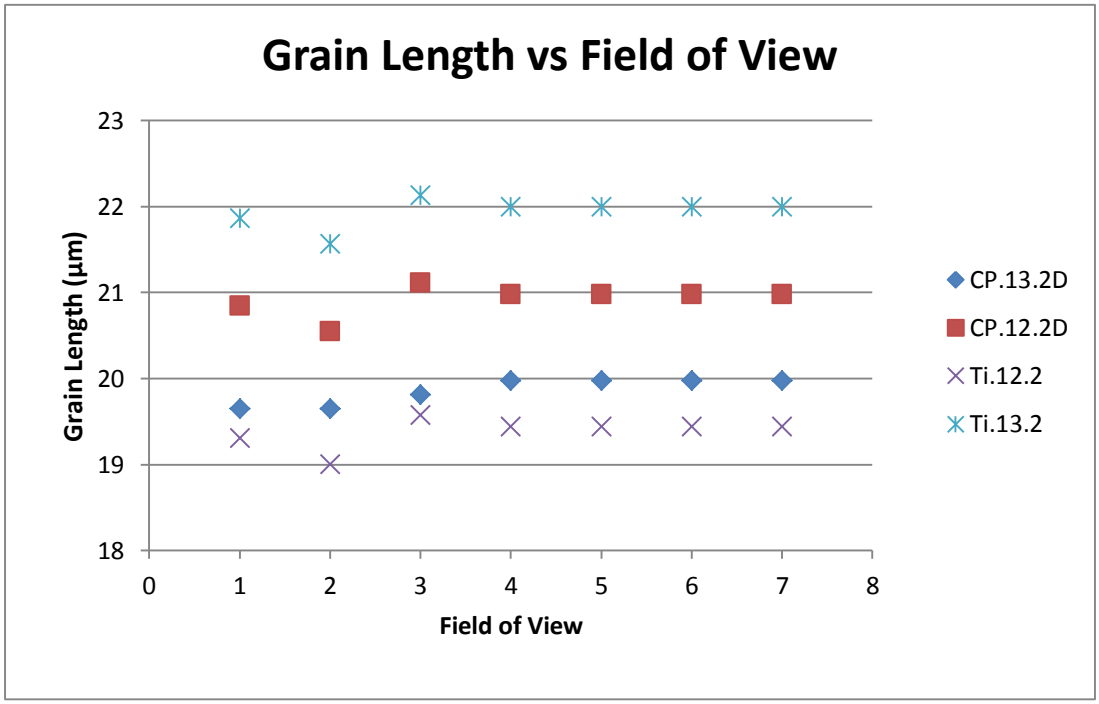

Figure 3.8: Profile showing the number of fields of view required from each specimen to reliably determine an accurate average grain length of the specimen.

The intercept method was conducted with the aid of Matlab Tool Line Cut Program [55]. The sizes of grains on a micrograph were analyzed with the line intercept method arranged in a user-friendly Graphic User Interphase (GUI). This tool allows us to measure both single phase and two phase microstructures. For a single phase microstructure each grain boundary is manually denoted where it intercepts the line as shown in the Figure 3.9 (a) below. With a two phase microstructure both the starting and end point of each grain where it intercepts the line are also manually denoted as shown in igure 3.9 (b).

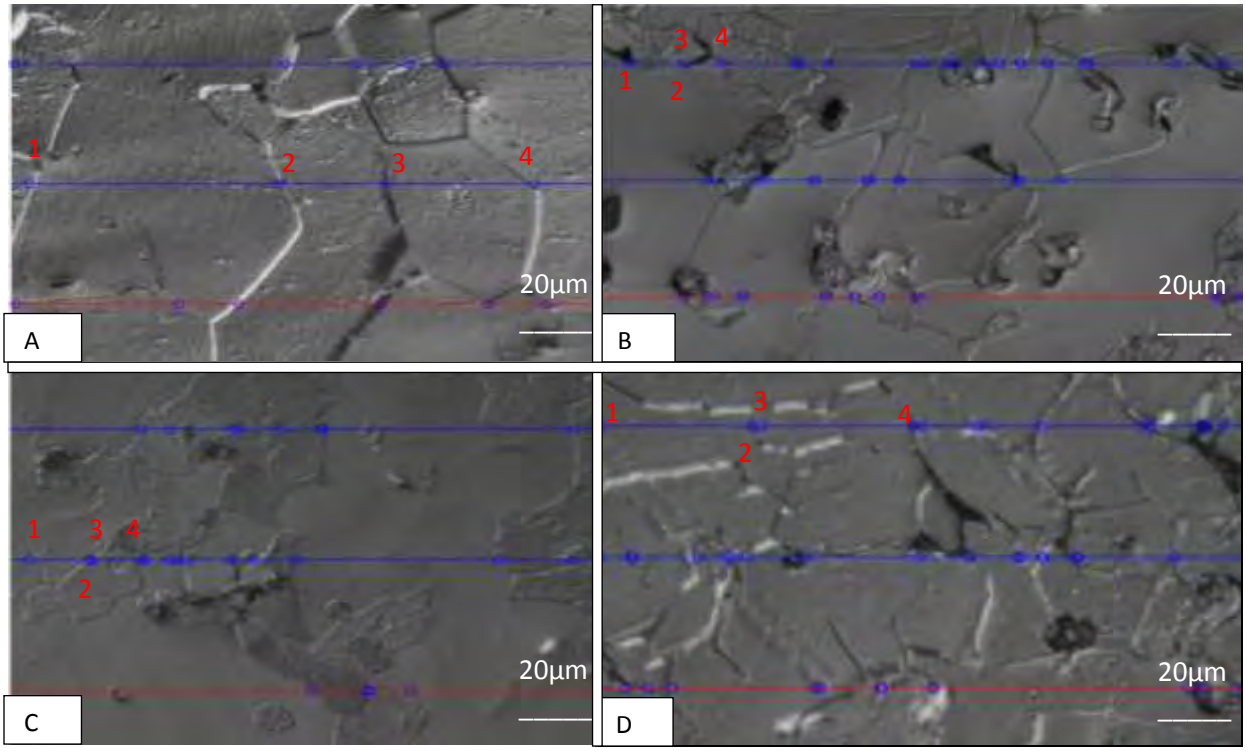

Figure 3.9: Image showing line intercept method for calculating grain size. (a) CP.13.2D specimen, example of a single phase with line intersecting grain boundaries, with 2 marks on each grain (left and right). (b, c, d) Shows microstructures with two phases, therefore each grain boundary is marked individually; this is done manually to select appropriate grains. These microstructures are those of Ti.11.4, Ti.12.1 and Ti.13.1 respectively.

CP-Ti microstructures have more uniform and equiaxed morphology, whereas Ti-6Al-4V has both equiaxed and lamella like morphologies depending on the initial sintering conditions. Due to the anisotropic nature of the Ti-6Al-4V microstructure and to further verify the average grain length, the intercept method is applied to the same images rotated at 60^0, 120^0, 240^0 and 300^0 to avoid inaccurate measurement (see Figure3.10 below) of average grain size. Rotating these images gives allows for the measurement of the diameter and length of the grains. An interpolation of the mean grain size of the rotated images was conducted and compared to the average grain size of the non-rotated image. This assisted in verifying that the average grain length can be measured at 0^0 angle with confidence that the average grain length was not misinterpreted due to anisotropic nature of the microstructure and to ensure that both the diameter and length of each grain was taken into account. It can therefore be concluded from the result that anisotropy does not affect average grain size.

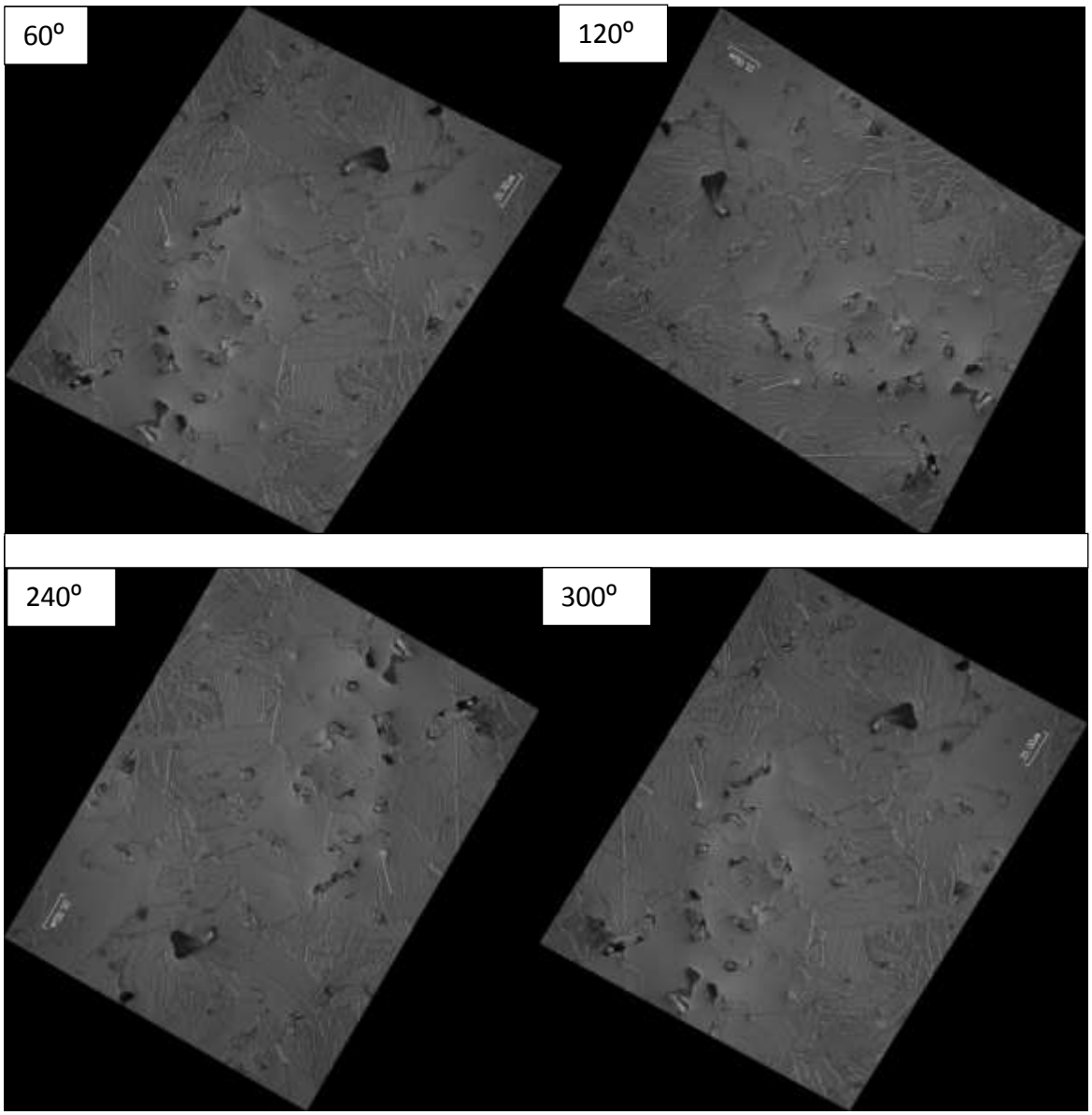

Figure 3.10: Ti-6Al-4V specimens rotated at 60^0, 120^0, 240^0 and 300^0. (Ti.11.4)

3.7 Hot Deformation Methodology

Thermo-mechanical processing (TMP) was performed by either hot uniaxial deformation of sintered cylindrical specimens or hot PSC deformation of rectangular specimens at a constant deformation temperature followed by annealing of the specimens. The methodology used for these experiments is detailed here:

3.7.1 Cylindrical Specimen Preparation

Cylindrical specimens were deformed using the Gleeble 3800 thermomechanical simulation system under uniaxial compression condition using the "ISO-T" cylindrical compression anvils. This system heats up the specimen by direct resistance heating; it then monitors the temperature of the specimen using a thermocouple that is spot welded to the outside of the specimen. A space of 5 wire diameters apart between the thermocouples should be used in the same cross sectional plane in the center of the specimen midway between contact faces of the cylinder.

In order to achieve a quality weld, the surface where the thermocouples were to be welded was lightly ground by hand using an 800 SiC grinding paper. A weld voltage of 36V was used for the welding process and a ceramic sheath was placed on one of the thermocouple wires to prevent the two wires from touching, which would result in a short circuit. A type K (chromel-alumel) thermocouple was used for all the tests as the deformation temperatures used here were below 1000°C.

The ends of the cylindrical specimens were surface ground after sintering and from the as-sintered state prior to deformation to ensure the parallelism and good surface finish of the two contact faces. In an attempt to alleviate the specimen-anvil friction and prevent welding of the specimen to the compression anvil, graphite strip and 0.10mm thick tantalum foil was used to create a "sandwich" of graphite strip-tantalum foil-graphite strip which was stuck to the contact faces of the cylindrical deformation specimen using a drop of conductive glue made from equal parts carpet glue and carbon powder (see Figure 3.11). Table 3.3 below gives a detailed description of the uniaxial deformation parameters used.

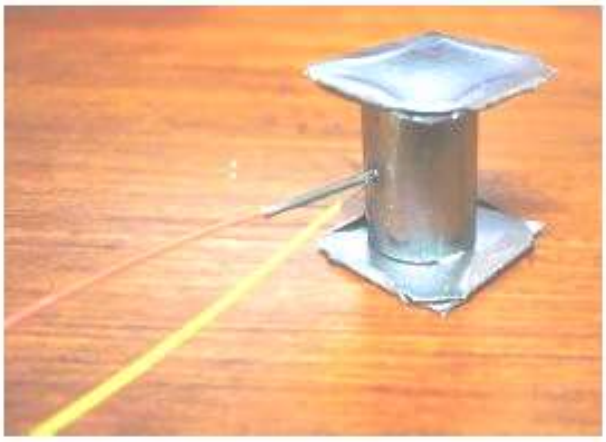

Figure 3.11: Showing cylindrical compression specimen with "sandwich" stuck to the specimen ends and type K thermocouple welded in place with a ceramic sheath over the yellow thermocouple wire. Courtesy of Nicholas Clinning [56].

Table 3.4: Description of Uniaxial Deformation Parameters

Deformation Parameters	Description of Condition
Vacuum Atmosphere	The deformations were carried out at high vacuum of greater than 10 x 10^{-3} torr throughout the test to avoid any oxidation. This vacuum was established before heating of the specimens was started.
Compression Strain	All of the cylindrical specimens were deformed to half of their original height, resulting in a nominal axial true strain of 0.69.
Strain Rate	All the cylindrical specimens were deformed at a strain rate of $1s^{-1}$.
Temperature Profiles	A single deformation temperature of 800°C was used for all cylindrical specimens. The heating rate to these temperatures was kept at a constant 300°C/min to obtain thermal equilibrium and microstructural homogeneity. Once the deformation temperature was obtained, the specimen was maintained at this temperature for a dwell time of 5 minutes to ensure thermal equilibrium throughout the specimen and allow time for microstructural homogeneity.

Following deformation the specimens were furnace cooled. An average cooling rate of 100°C/sec was maintained.

A graphical representation of this Hot Deformation program is given in figure 3.12

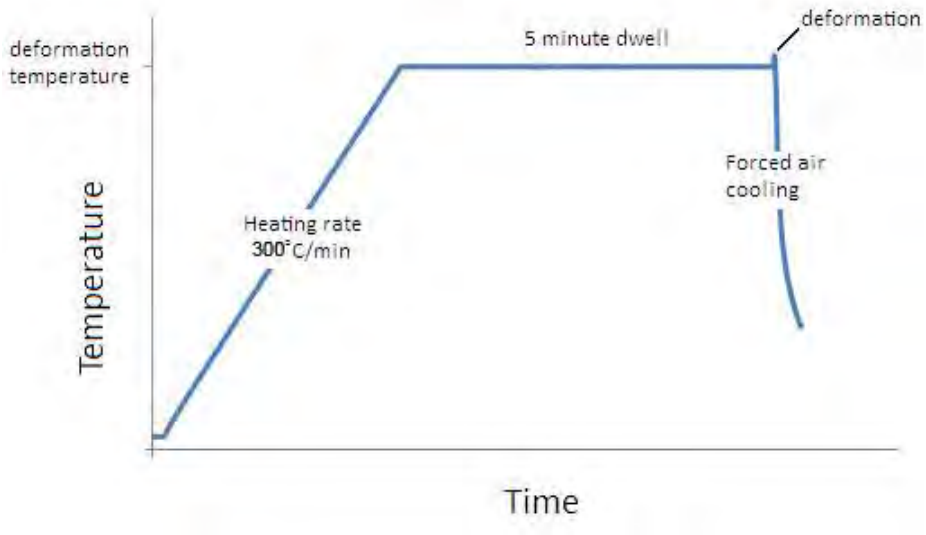

Figure 3.12: Graphical representation of the process used for the hot uniaxial deformation of the cylindrical specimens on Gleeble 3800.

3.7.2 Rectangular Specimen Preparation

Rectangular specimens were deformed using the Gleeble 3800 thermo-mechanical simulation system under 0.8 strain to maintain half height reduction while the same strain rate condition imposed on the uniaxial specimen was maintained. As a result of the rectangular specimen geometry, these specimens were deformed using the anvils normally deployed for plane strain compression (PSC) testing. The aim was to deform the rectangular specimens in such a way that the actual final three-point bend specimens could be machined from the deformation zone. The width of the contact face of these anvils is 10mm and the length (42mm) is comfortably longer than that of the rectangular specimen. The thermocouple was spot welded to the "end" of the rectangular specimen, with the two wires in the same plane (parallel to the deformation surfaces) equidistant from each of the specimen's contact faces. The same thermocouple welding procedure was used as per the uniaxial (cylindrical) test specimens.

In preparation for hot deformation; a tantalum foil was stuck to contact surfaces and a type K thermocouple welded in place with the ceramic sheath over the yellow thermocouple wire is shown in figure 3.13 below.

Figure 3.13*: Photograph showing a rectangular specimen prepared for deformation. Courtesy of *Nicholas Clinning [56]

The deformation parameters used when conducting PSC test are tabled below (See Table 3.5).

Table 3.5: Description of PSC Parameters

PSC Parameters	Description of Condition
Vacuum Atmosphere	The deformations were carried out at a high vacuum of greater than 1 x 10^{-4} torr throughout the test to avoid any oxidation. This vacuum was established before any heating of the specimen had started.
Compression Strain	The rectangular specimens were deformed to a true strain of 0.8 in PSC.
Strain Rate	The PSC deformation was carried out at a strain rate of $1s^{-1}$.
Temperature Profiles	A single deformation temperature of 800°C was used for PSC deformation. The TMP process was kept as close to that used for the uniaxial deformation of the cylindrical specimens as possible. The heating rate to the deformation temperatures was kept at a constant 5°C/min. Once the deformation temperature was obtained, a dwell time of 5 minutes at the deformation temperature was used. Following the deformation the specimen was furnace cooled in the same manner as the cylindrical specimens subjected to uniaxial compression.

3.8 Annealing Treatment

Following deformation, the samples (cylindrical and rectangular) deformed at 800°C were annealed. The specimens were annealed to continue, statically, any metadynamic recrystallization that had initiated during the deformation and subsequent cooling and to initiate new recrystallization.

The annealing cycle was as follows:

The samples were heated at 5°C/min to 870°C. They were then held at 870°C for 1 hour. The samples were then cooled from 870°C to 600°C at a rate of 3°C/min. From 600°C the samples were allowed to cool to room temperature at a rate greater than 5°C/min. These treatments were conducted in a Horizontal Elite 12/50/400 furnace, fitted with quartz tube and a vacuum system maintaining a vacuum greater than 5×10^{-5} torr.

3.9 Mechanical Testing of Material

In order to evaluate the mechanical properties resulting from the TMP of the porous as-sintered BE material, mechanical testing of the processed material was required. The limited amount of material available due to the size of rectangular specimens that underwent PSC made it impossible to conduct standard tensile tests, as a result only two mechanical test methods could be used i.e. hardness tests and three-point-bend tests.

3.9.1 Hardness Testing

Hardness tests were performed on all specimens using the Zwick Roell ZHV macro hardness tester shown in Figure 3.14. Twelve hardness measurements were taken from each specimen as shown in Figure 3.15. The same approach was used for As-sintered (AS) specimens and Uniaxially deformed specimens. To verify that there is no variation in properties between cylindrical and rectangular specimens, hardness tests were conducted on some of the rectangular specimens randomly to verify results obtained on cylindrical specimens.

Figure 3.14: Zwick Roell ZHV hardness tester in UCT Centre for Materials Engineering.

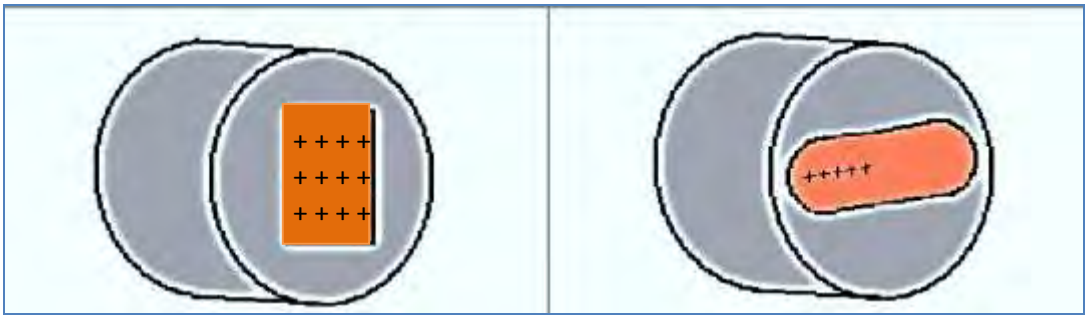

Figure 3.15 a): Image of axial section of AS specimen with hardness indentation from the middle of the specimen. b) : Image showing section of the barreled specimen as a result of hot deformation on cylindrical specimen with hardness indents made across the deformation plane. [52]

3.9.2 Three-Point-Bend Tests

Creating the Three-Point-Bending Specimens

A three-point-bend specimen needed to be created from the deformed and subsequently annealed rectangular specimens. To achieve this, the "bulging ends" (see Figure 3.16) on either side of the material that was in contact with the PSC platen was machined off until a rectangle was achieved. The sides of this rectangle that were the contact faces during the PSC deformation, were surface ground to achieve the three-point-bend specimen nominal thickness of 3.00 mm (see Figure 3.17 on the facing page). Care was taken to remove equal material from both the contact faces in order to remove any material where the deformation was influenced by the specimen-platen interface.

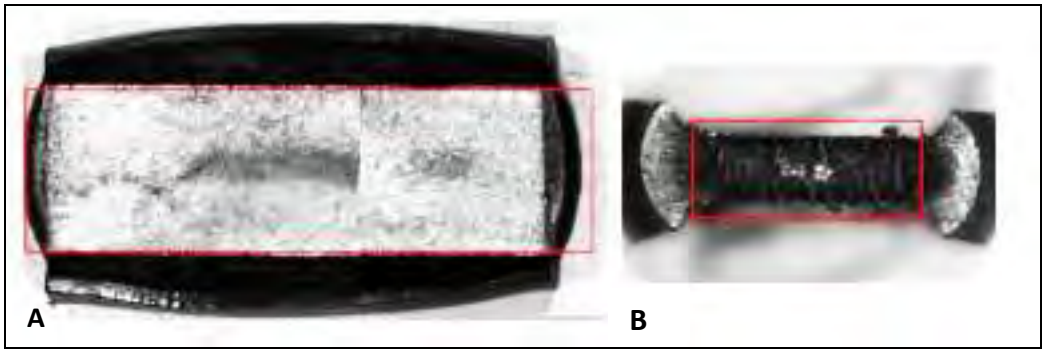

Figure 3.16 a) Plan View of Deformed Specimen. b) Cross-section of deformed specimen. (Courtesy of Nicholas Clinning).

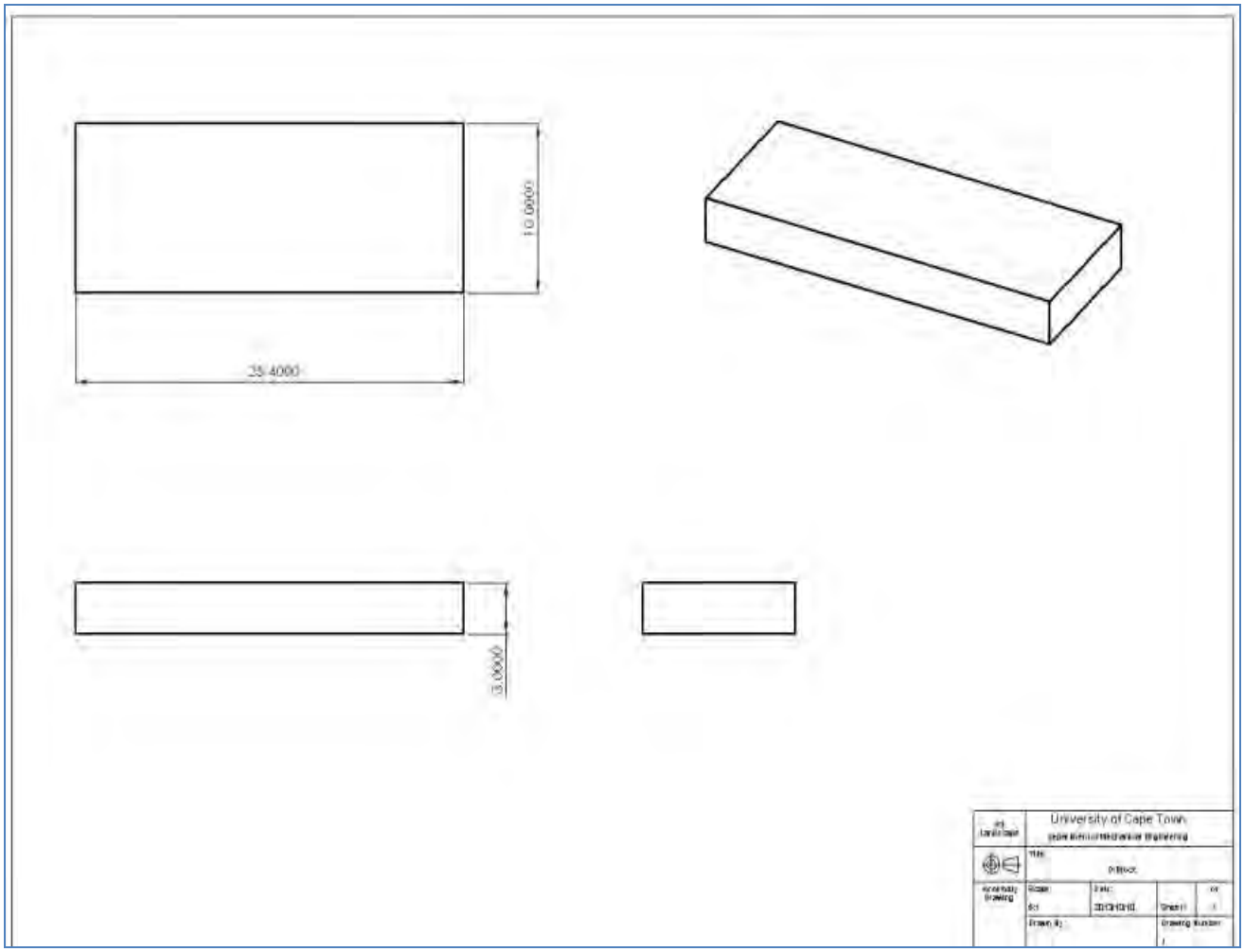

Figure 3.17: Drawing showing dimension of TRB specimens that were machined from AS rectangular bars and TMP specimens

The MPIF standard 41 [18] for determining the transverse rupture strength of PM materials, where the tooling for creating the rectangular specimens used in this research is detailed, involves breaking these rectangular specimens in a three-point-bend arrangement as shown in Figure 3.18.

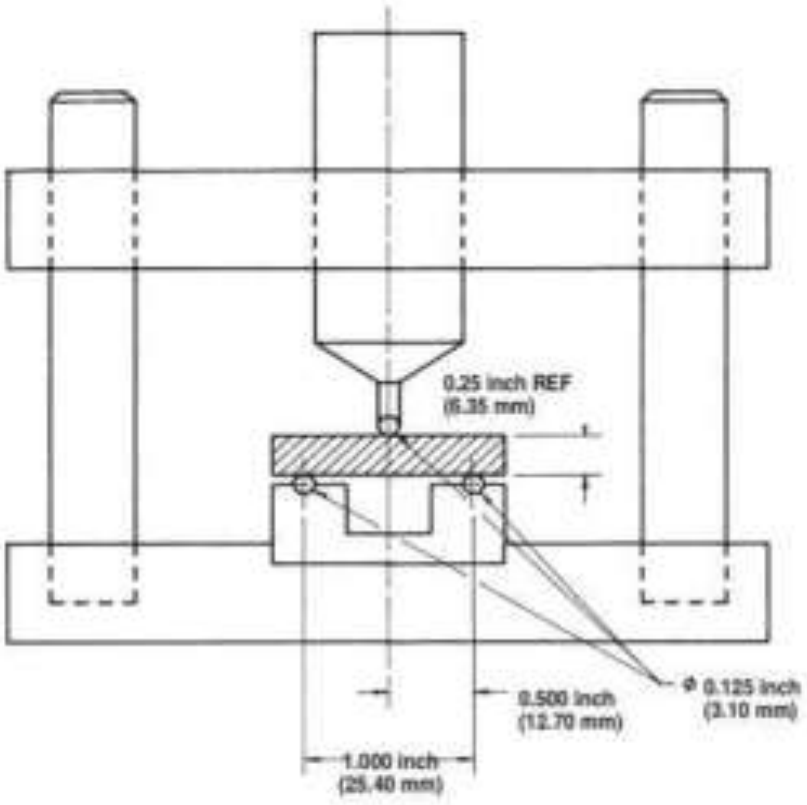

Figure 3.18: Transverse rupture test fixture used to determine the transverse strength of BE materials by loading them in the three-point-bending. [18]

The transverse rupture strength is then calculated from the following equation:

$$TRS = 3PL/2t^2w$$

Transverse rupture strength is calculated in MPa where P is the breaking force in N, L is the distance between supporting rods (mm), t is the thickness of the TRB (mm) and w is the width of the TRB (mm). The equation is the stress in the outermost material as calculated by simple bending theory.

The standard states that this test is only applicable for PM materials of negligible ductility (presumably so that bending theory is still applicable). Although it was hoped that the specimens would demonstrate some ductility, the results of a previous study using elemental powders (as opposed to Ti powder + master alloy) showed brittle behavior. [42]

Material in the as-sintered condition and TMP processed condition was evaluated using this rig. For all the specimens subjected to this transverse rapture strength evaluation a

nominal specimen geometry of width 9.70mm and thickness of 2.80mm was used to avoid any effects resulting from differing specimen geometries. A pre-load of 20N and a cross head speed of 2mm/min were employed during testing. A photograph of the three-point-bending rig and test specimen is shown in figure 3.19 below. The testing was carried out on a Zwick 1484 universal testing frame equipped with a 200kN load cell.

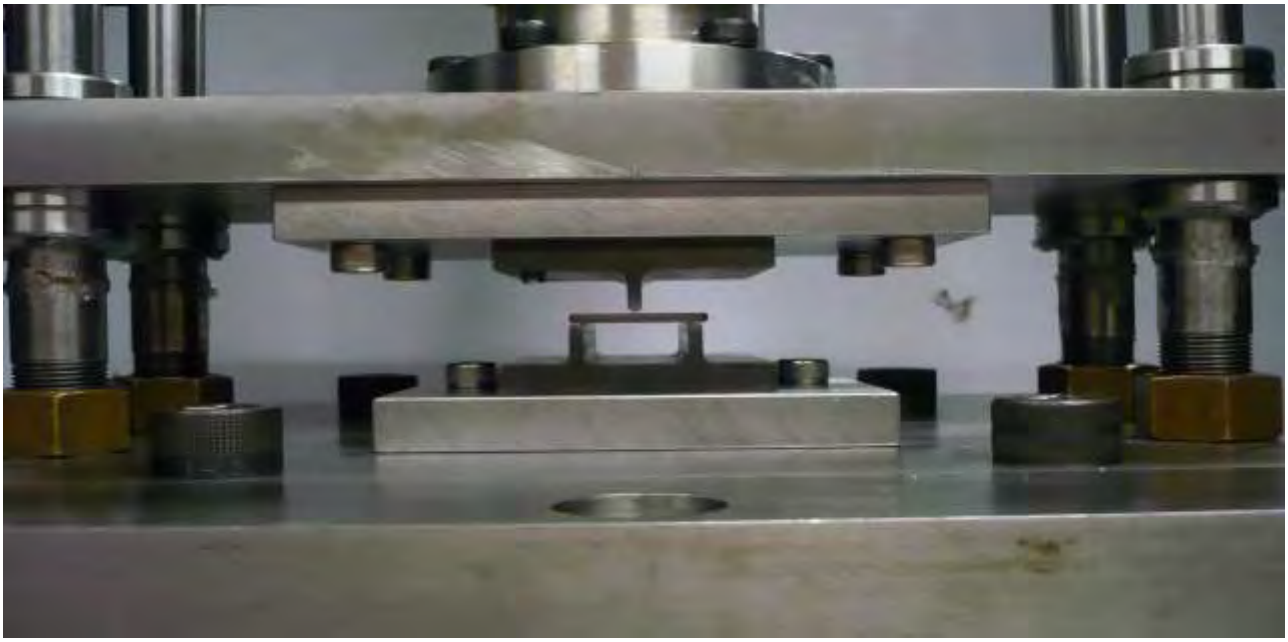

Figure 3.19: Photograph showing the three-point-bend rig with test specimen in place used to measure the mechanical properties of the material in this study. Courtesy of Nicholas Clinning (University of Cape Town - 2012) [56].

4. Results and Discussion: Density, Microstructure, Grain Size & Hardness

4.1. Density

4.1.1. Sintered Density Results

Figure 4.1 below shows the relative density profile of CP-Ti and Ti-6Al-4V specimens treated under different conditions. As per the expectation it can be seen that an increase in the sintering conditions i.e. increasing sintering temperature and/or sintering time results in an increase in density.

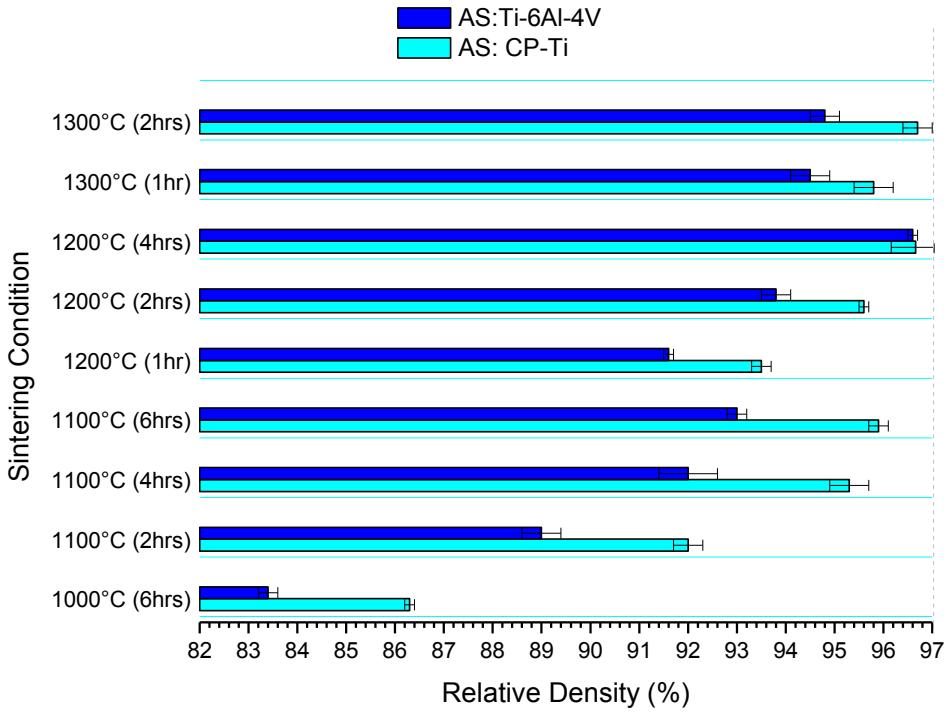

Figure 4.1: Relative Density Profiles of CP-Ti and Ti-6Al-4V Specimens Sintered Under Different Conditions

It is further observed from the profile that across all conditions tested, CP-Ti has comparatively higher densities than Ti-6Al-4V; however specimens sintered at 1200^0C for 4hrs are the exception. Ti-6Al-4V and CP-Ti specimens sintered at 1200^0C for 4hrs have similar densities. Also the specimens sintered at 1200^0C (4hrs) show the highest density output while specimens sintered at 1000^0C for 6hrs show the lowest density output.

To further investigate the density-time/temperature relationship figures 4.2 and 4.3 were plotted. Figure 4.2 show specimens sintered under same temperature groups (STG) where sintering temperature is held constant at 1100^0C and 1200^0C while sintering time varied.

Specimens were only sintered for 2hrs, 4hrs and 6hrs for STG1100^{0}C classification and 1hr, 2hrs, and 4hrs for STG 1200^{0}C. The data points are joined by dotted lines to show general behavior of the specimens with time and do not suggest that across all points on the plot the density value is related to the corresponding sintering time.

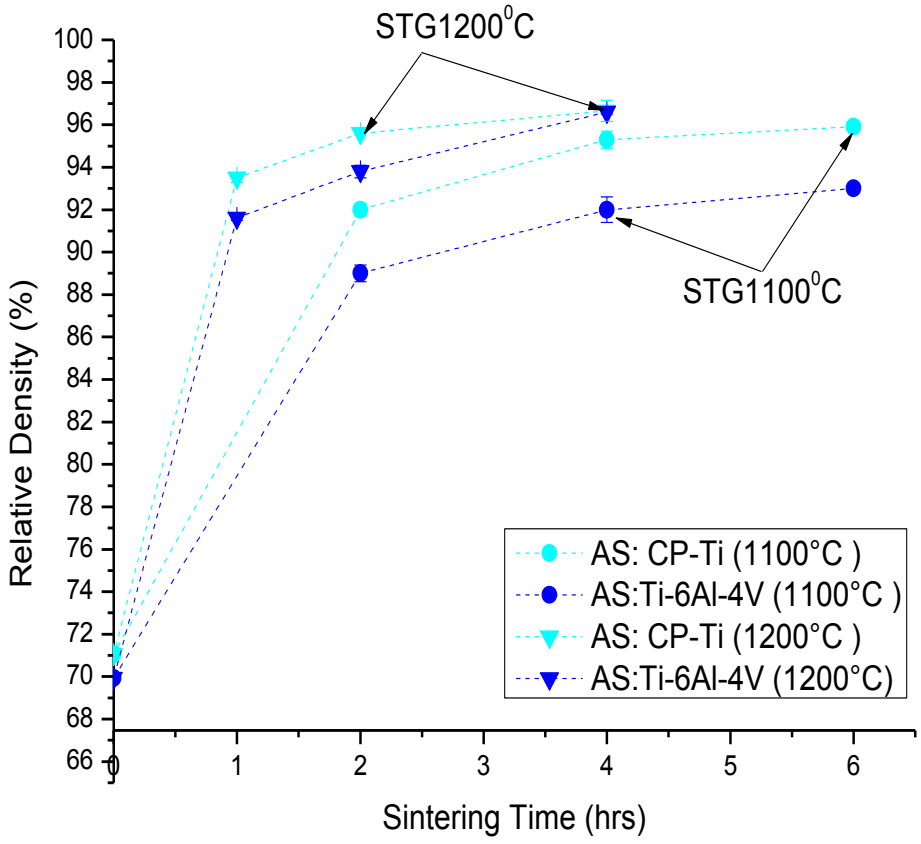

Figure 4.2: Density- Time Profiles of Specimens Sintered Under STG 1100^{0}C and 1200^{0}C

It can be seen that CP-Ti and Ti-6Al-4V specimens have similar density results at time zero (i.e. green density). Specimens sintered at 1200^{0}C expectedly have higher densities than those sintered at 1100^{0}C. The density/ time plot for STG 1200^{0}C specimens' rises sharply compared to that of STG 1100^{0}C specimens. Also the plot for CP-Ti is marginally steeper than that of Ti-6Al-4V in both STG 1100^{0}C and STG 1200^{0}C systems.

All the plots on Figure 4.2 tend towards saturation and the difference between relative density of CP-Ti and Ti-6Al-4V decreases as sintering time increases. This observation is significantly evident in STG 1200^{0}C with CP-Ti and Ti-6Al-4V eventually intersecting.

It is also observed that in the STG1100^{0}C classification, the density difference between CP-Ti and Ti-6Al-4V is relatively more pronounced than in STG1200^{0}C.

Figures 4.3 below shows density behaviors of specimens sintered under a sintering *time* groups (StG) where sintering time is held constant at 2hrs while sintering temperature varied.

A similar observation as identified in Figure 4.2 was made in that it can be seen that a saturation point is approached as sintering temperature is increased. CP-Ti and Ti-6Al-4V started at similar green densities and the difference in density increased with increasing sintering time. At temperatures above 1100^{0}C the difference in density between what is seen to decrease with increasing sintering temperature. CP-Ti has a marginally steeper plot than Ti-6Al-4V as previously observed in figure 4.2.

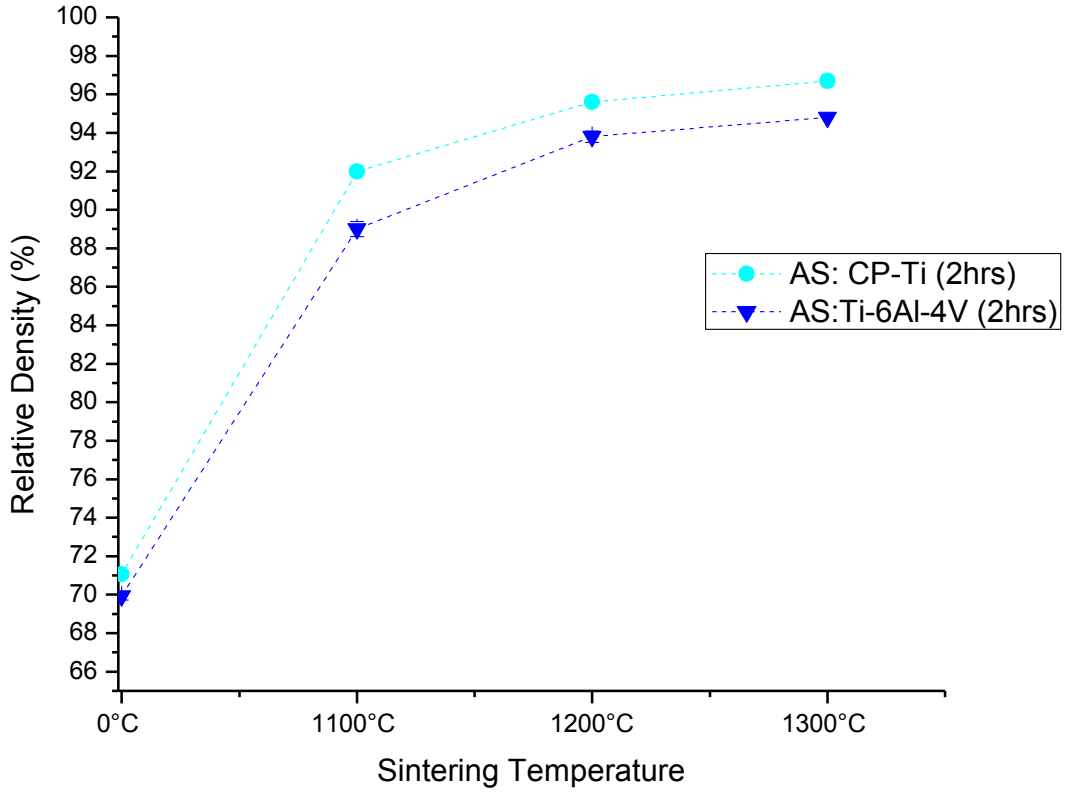

Figure 4.3: Density-Temperature Profiles of Specimens Treated under StG 2.

4.1.2. Discussion of Sintered Density Results

The compaction pressure of 450MPa used in this work is within the specified compaction pressures shown to be adequate by Ivasishin *et al*. [4] At this compaction pressure CP-Ti and Ti-6Al-4V yield green density results of 71.06% and 69.93% respectively.

CP-Ti and Ti-6Al-4V specimens compacted at 450MPa were sintered under various conditions and density results were then compared. It is known that the process of sintering influences the chemical and microstructural homogeneity of the compacted specimens resulting in improved material properties

The result observed in Figure 4.1 shows that an elevation in sintering conditions leads to an increasw relative density, which is a well understood powder metallurgy behavior. However it was interesting to observe that in all cases but one, CP-Ti had higher sintered density than Ti-6Al-4V. This is interesting because it was expected that Ti-6Al-4V having a high chemical concentration gradient than CP-Ti and also adequate particle size composition of CP-Ti (74µm) and Al-V master alloy (63µm) for packing during compaction, Ti-6Al-4V specimens would have higher relative density returns [57].

The difference in relative density of CP-Ti and Ti-6Al-4V is seen to decrease as sintering conditions improve. This position is strengthened by the observation made where CP-Ti and Ti-6Al-4V specimens sintered at 1200^0C for 4hrs have similar densities. In STG 1100^0C the difference in density between CP-Ti and Ti-6Al-4V decreases with increasing sintering time; however this difference is seen to decrease more slowly than specimens sintered under STG 1200^0C. This suggests that the rate of densification is higher for specimens sintered at elevated temperatures, which was expected. For specimens sintered under these two classifications to have the same relative density outputs, STG 1100^0C specimens would have to be sintered for far longer periods. This happens because sintering is motivated by capillary forces or surface tension forces which attempt to reduce the total surface area and consequently the total energy of the system. The forces actuate mass flow which tends to enlarge contact areas between adjacent particles and decrease the pore volume [58]. The mass of powder contains extra energy which can be released when the powder compact is converted into a solid body. The actuation of mass flow is also subject to the period the compact is exposed to a particular temperature condition. At low

temperatures, short exposure to heat results in insufficient time and energy for sufficient mass transport to take place effectively.

The results observed in both figure 4.2 and 4.3 show that CP-Ti diffuses much quicker than Ti-6Al-4V. The behavior could be justified by the fact that CP-Ti is a single component system and is subject to self-diffusion as a major material transport mechanism which is a consequence of chemical potential gradient resulting from the surface tension and capillary forces between particles [17]. Material transport occurs mainly by surface transport (through diffusion) and grain boundary transportation. Whereas in a multicomponent system the chemical concentration gradient is the primary mechanism for sintering (diffusion), in addition to self-diffusion that is caused by surface tension and capillary forces. Furthermore the sintering time and temperature have a significant effect on properties and integrity of the final product.

To confirm that sintering temperature influences densification in the same way as sintering time, Figure 4.3 shows similar behavior that was observed in Figure 4.2. These specimens were sintered under various temperature conditions but sintering time was held constant.

Figure 4.4 below can be used in defining and understanding density results in relation to the different sintering stages achieved by each specimen. Figure 4.4 shows the different stages which are also discussed in the literature review chapter (Section 2.3.2-Sintering). It is shown here that the final stage of sintering is achieved at 93% relative density. It can therefore be suggested from Figure 4.2 that Ti-6Al-4V specimens sintered under STG1100^{0}C classification do not reach the final stage of sintering although these specimens were sintered for as long as 6hrs. However, CP-Ti specimens reach this stage after 4hrs of sintering. On the other hand both CP-Ti and Ti-6Al-4V specimens sintered under STG1200^{0}C reach the final stage of sintering after only 2hrs of sintering. This confirms that the rate at which these systems densify differs, as previously mentioned. Figure 4.3 shows that it takes a sintering temperature of 1200^{0}C for both these systems to reach the final stage of sintering, if sintering time is limited to 2hrs. Therefore the correct combination of sintering time and temperature is crucial for adequate densities to be achieved.

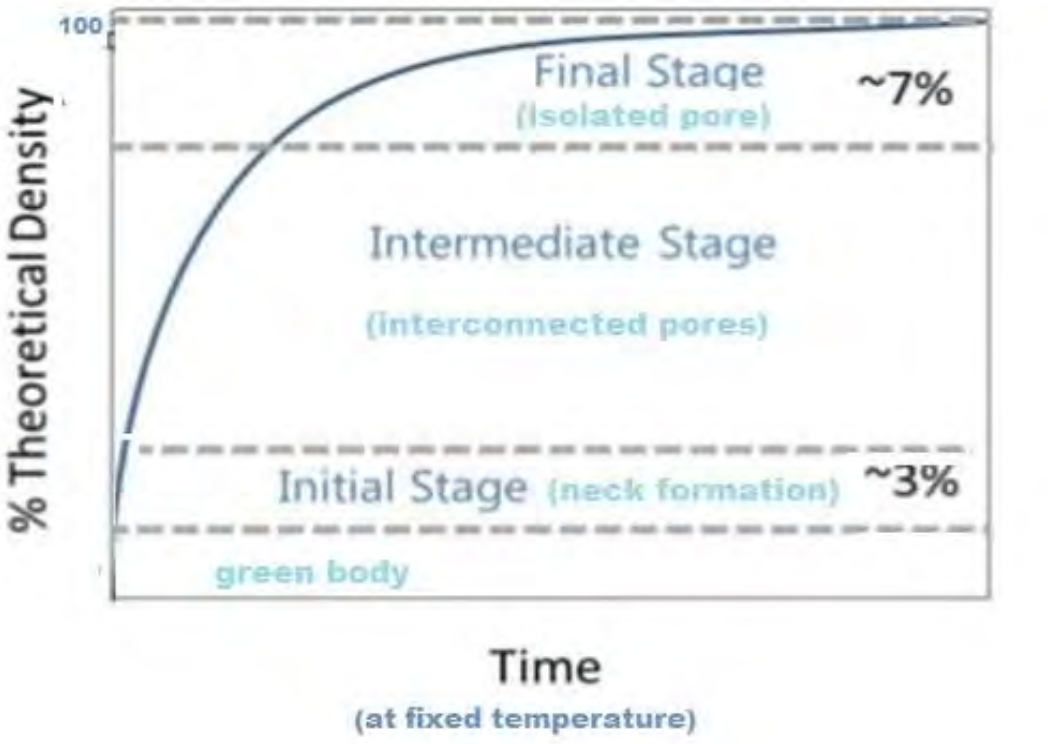

Figure 4.4: (A) Density-Time profiles of specimens showing different stages of sintering at fixed temperature [59].

Figure 4.4 also represents an ideal situation where a material is sintered to full density. The curve is seen to reach a plateau as it approaches 100% indicating full density. When Figure 4.4 is compared to the curves seen in Figure 4.2 and 4.3, it is observed that the latter do not reach 100% (full) density. Even though the data is limited, it is clear from the curves that full density cannot be achieved. In an attempt to achieve full density an additional step to the manufacturing process becomes necessary, which leads into Section 4.1.3 and 4.1.4 that respectively shows results and discussion of Thermo-Mechanical-Processing (TMP) as an additional step.

Figure 4.2 shows that with increasing sintering time, full density is being approached as the curves are not at full plateau. This is true for all cases but not for Ti.11.2 specimens. Here it can be seen that the curve has completely flattened. This observation suggests that Ti.11.2 specimens can never reach full density no matter how long the sintering period is. Theoretically, this cannot be true because if the specimens are sintered for an infinitely long period of time, full density should be achieved unless there is an inhibiting factor that is involved. Ivasishin *et al*. [51] show that the time needed for homogeneous redistribution

of the alloying elements in the matrix during alloy synthesis depends not only on diffusion mobility of alloying elements, but also on the type of alloying elements, their synergistic influence and phase composition. Ivasishin *et al*. used DICTRA™ software to model the diffusion mechanism of master alloys with varied chemical compositions such as 13Al-85V, 31Al-67V and 59Al-39V, + 2% of Ti in all cases. Ivashishin *et al*. found that chemical composition evolution occurs in different ways, depending on initial master alloy composition. For low aluminium content (13%), alloying elements freely move from master alloy to titanium matrix, and β/α interphase boundary comparatively fast migrates. Higher aluminium content (31 and especially 59%) in the master alloy results in slowing the diffusion redistribution of elements. For 13 and 31% of aluminium reaching of equilibrium state (one-phase β condition) takes about 37, 000 and 200, 000 seconds respectively, while for aluminium content of 59% equilibrium state (α+β condition) is set after 10^6s exposure. Thus 60Al-40V master alloy composition is not optimal. Meaning that a consideration to reduce aluminium content in master alloy to provide faster homogenization should be made but it would require at least two master alloys to attain desirable Ti-6Al-4V composition. Thus from Ivasishin *et al*. it can be gathered that generally, if sintering temperature is below some threshold, the harmful effect of residual porosity prevails over the positive effect of fine grains. Further decrease in sintering temperature leads to preservation of chemical inhomogeneity of material, which cannot be avoided even with longer exposure times [51].

4.1.3. Density Results Post Thermo-Mechanical-Processing (TMP)

Thermo-Mechanical-Processing

Hot deformation was carried out at 800^0C to 0.8 strain for rectangular specimens and 0.69 strain for uniaxial specimens. The specimens were then annealed at 870 ^{0}C for 1 hour. The introduction of TMP as a final step to the treatment process was done with the intention to improve density and mechanical properties of CP-Ti and Ti-6Al-4V specimens and promote recrystallization during the post deformation anneal. Shown in Figure 4.5 below are flow stress vs strain curves of rectangular CP-Ti and Ti-6Al-4V specimens that were initially sintered at various conditions.

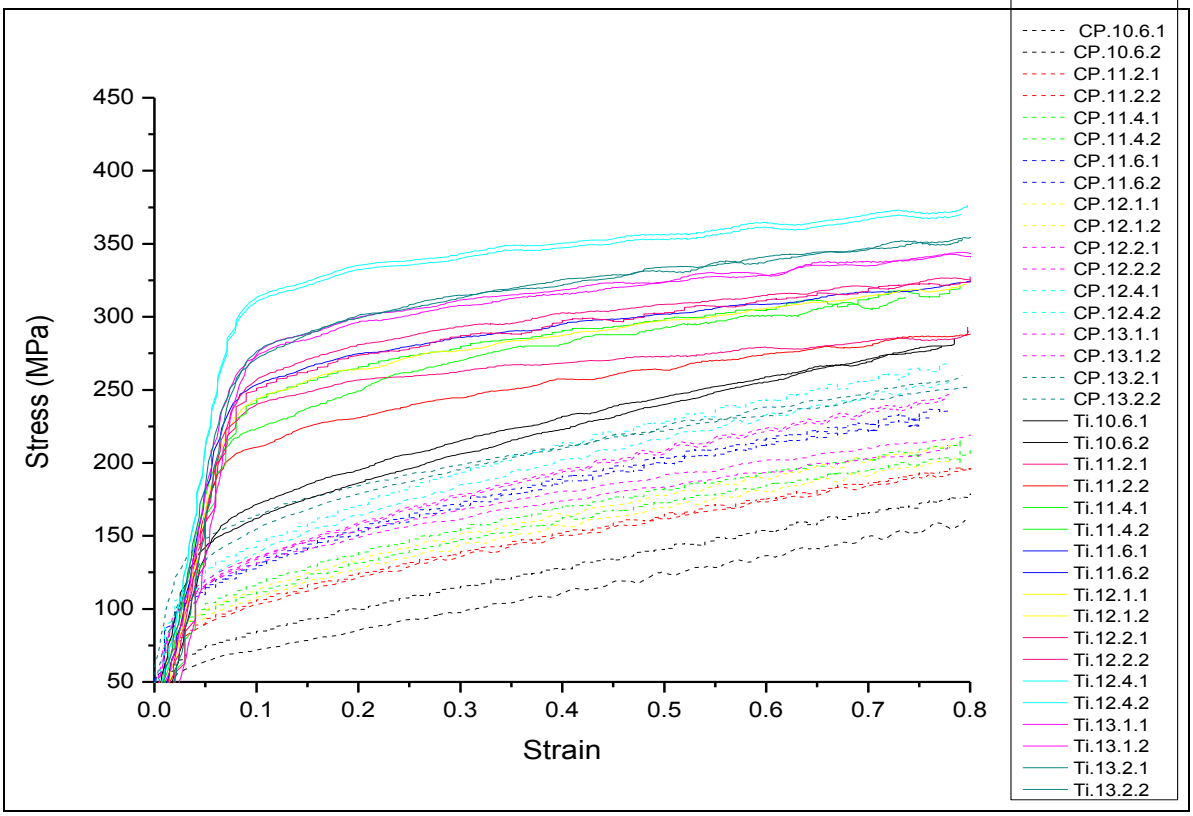

Figure 4.5: Flow Stress Curve of Rectangular Specimens Initially Sintered at Various Conditions and Deformed at 800^{0}C to 0.8 Strain. The legend indicates the sintering time/temperature condition.

It can be seen from figure 4.5 that in all cases as expected, Ti-6Al-4V specimens have higher stress values than their CP-Ti counterpart. The highest stress value (stress at 0.8 strain) for Ti-6Al-4V is that of Ti.12.4 which is just below 350MPa. The same observation is made for CP-Ti where CP.12.4 has the highest stress values of 230MPa in its batch and CP.13.2 specimens with flow stress of 225MPa having relatively close stress values to the former. The flow stress curve for Ti.11.2 specimens flattens at a lower strain than the other specimens. A similar observation is made with Ti.12.4 however the latter achieves higher stress than the former.

Density Post TMP

Figure 4.6 below shows the relative density profile of TMP CP-Ti and Ti-6Al-4V specimens. It can be seen in this profile that in all cases but one, Ti-6Al-4V consistently has higher density than CP-Ti specimens which contrasts the result observed in figure 4.1 for densities of specimens in the as-sintered state. CP-Ti specimens sintered at 1100^{0}C for 2hrs have higher density than the same condition of Ti-6Al-4V.

Post TMP it is observed that Ti-6Al-4V specimens initially sintered at 1200^0C for 4hrs show the highest density output (99%). This observation is consistent with the observation made in Figure 4.6. Contrary to Figure 4.1, Figure 4.6 shows that CP-Ti and Ti-6Al-4V specimens sintered at 1200^0C for 4hrs have inequivalent densities and in this case Ti.12.4 has higher density than CP.12.4.

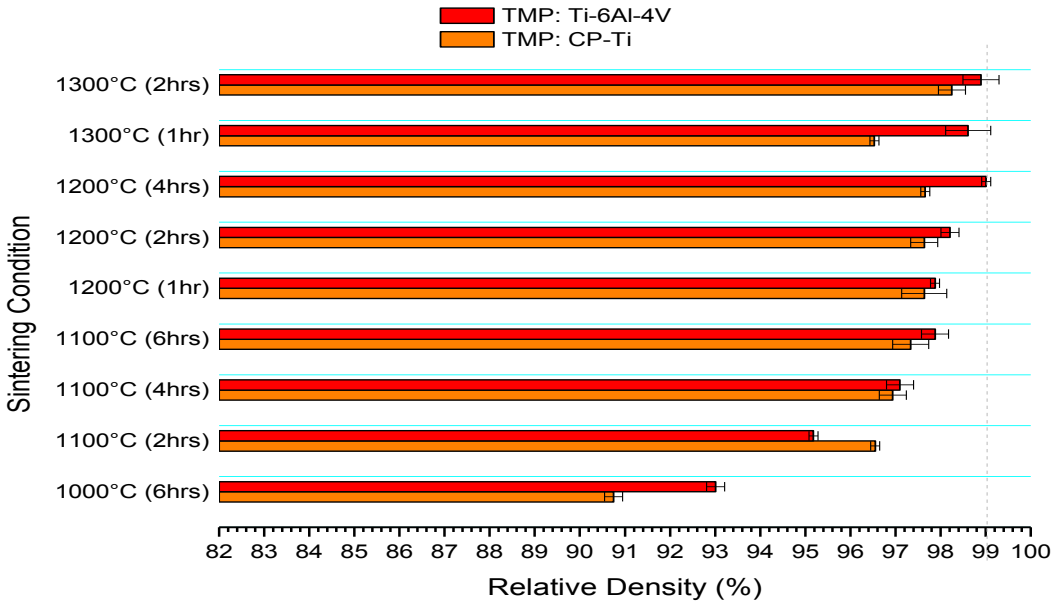

Figure 4.6: Relative Density Profiles of CP-Ti and Ti-6Al-4V Specimens Initially Sintered Under Different Conditions and TMP at 800^{0}C.

It is also observed that CP-Ti specimens that were initially sintered at 1300^0C for 2hrs have the highest relative density in its batch post deformation.

4.1.4. Discussion of Density Results Post TMP

It is generally known that a material with high porosity would have lower hardness (see section 5- hardness results) than material with near full density. This therefore suggests that both hardness and porosity of material play a significant role in densification by TMP. It was expected that Ti-6Al-4V would have higher flow stress than CP-Ti as a result of solid solution strengthening that occurs during sintering.

For a fully dense material displacement during compression is fully accommodated by plastic deformation and for a porous material displacement is partly accommodated by pore closure (collapse) and partly by plastic deformation. Since pore closure occurs at a lower flow stress than homogeneous plastic deformation, the pore closure will always occur in preference to plastic deformation to accommodate displacement.

Figure 4.5 shows that Ti-6Al-4V stress levels are higher and as a result there is more emphasis on pore closure, meaning the pores are relatively much softer than the metal. Due to enhanced effect of deformation on pore closure, Ti-6Al-4V specimens' density consequently surpasses that of CP-Ti specimen post deformation. It is also shown in Figure 4.6 that Ti.11.2 specimens are the only specimens where CP-Ti has higher densities than Ti-6Al-4V post sintering. Ti.11.2 flow stress curve reaches the same stress level as Ti.10.6. Considering that Ti.11.2 specimens were exposed to relatively low temperature for shorter periods they may be susceptible to relatively larger pores than Ti.10.6 specimens. It can be surmised in the case of Ti.11.2 specimens porosity coupled with larger pores result in pore closure being the primary preference in accommodating displacement at lower strains and as strain increases the pores become harder and consequently plastic deformation takes over and accommodates the displacement while extensive porosity persists which justifies Ti.11.2 having lower density than CP.11.2.

4.2. Microstructure

4.2.1. Microstructure Results

From figures 4.7-4.9 it can be observed there isn't strong evidence regarding the relationship between sintering conditions and porosity. The micrographs shown in the above mentioned figures represent a very small area of each specimen. The selection process may have been biased of the target area as the selection was solely based on human judgement which would in turn affect the precision of the result in determining degree of porosity present in each condition assessed.

However even though the observations on the micrographs alone may not be particularly convincing due to the selection process, the micrographs show to a small degree that generally an increase in sintering time and temperature results in reduced porosity which is consistent with the density results obtained.

It was also generally observed that pores in CP-Ti are rounded and angular in Ti-6Al-4V. It can be appreciated that when TMP was introduced as a final step to the manufacturing process, TMP resulted in further pore reduction and this result is consistent with the outcome in section 4.1.4 where an improvement in density was observed as a result of TMP.

Post TMP it can be seen that Ti.11.2D specimens have retained pores, which are severely reduced in size but appear to be in large quantities and are populated in one area in a linear orientation.

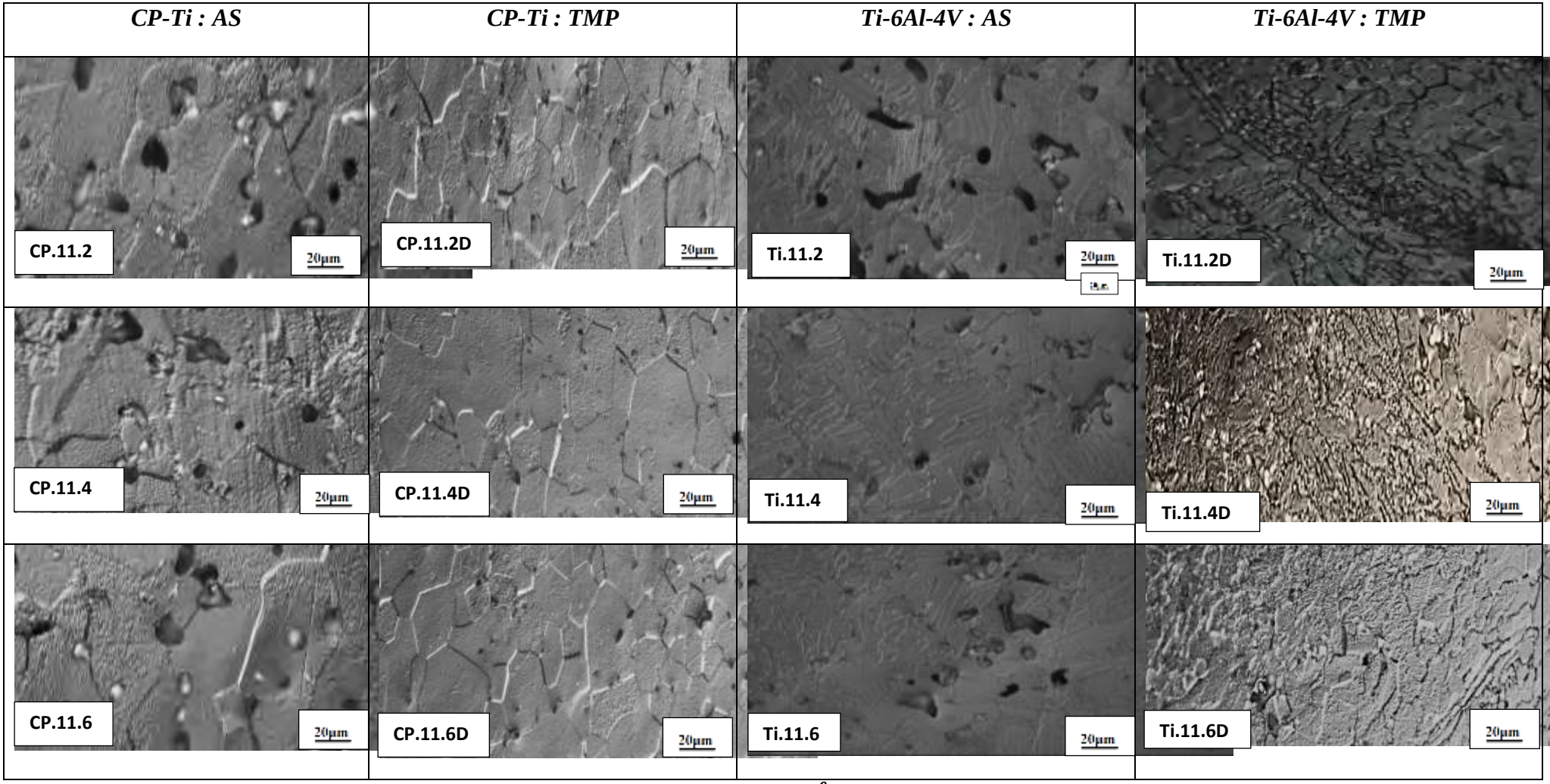

Figure 4.7: Microstructures of CP-Ti and Ti-6Al-4V Specimens Sintered at 1100^{0}C. AS specimens are positioned on the left hand side and TMP on the right hand side of each system. Specimens were sintered for 2, 4 and 6 hrs respectively.

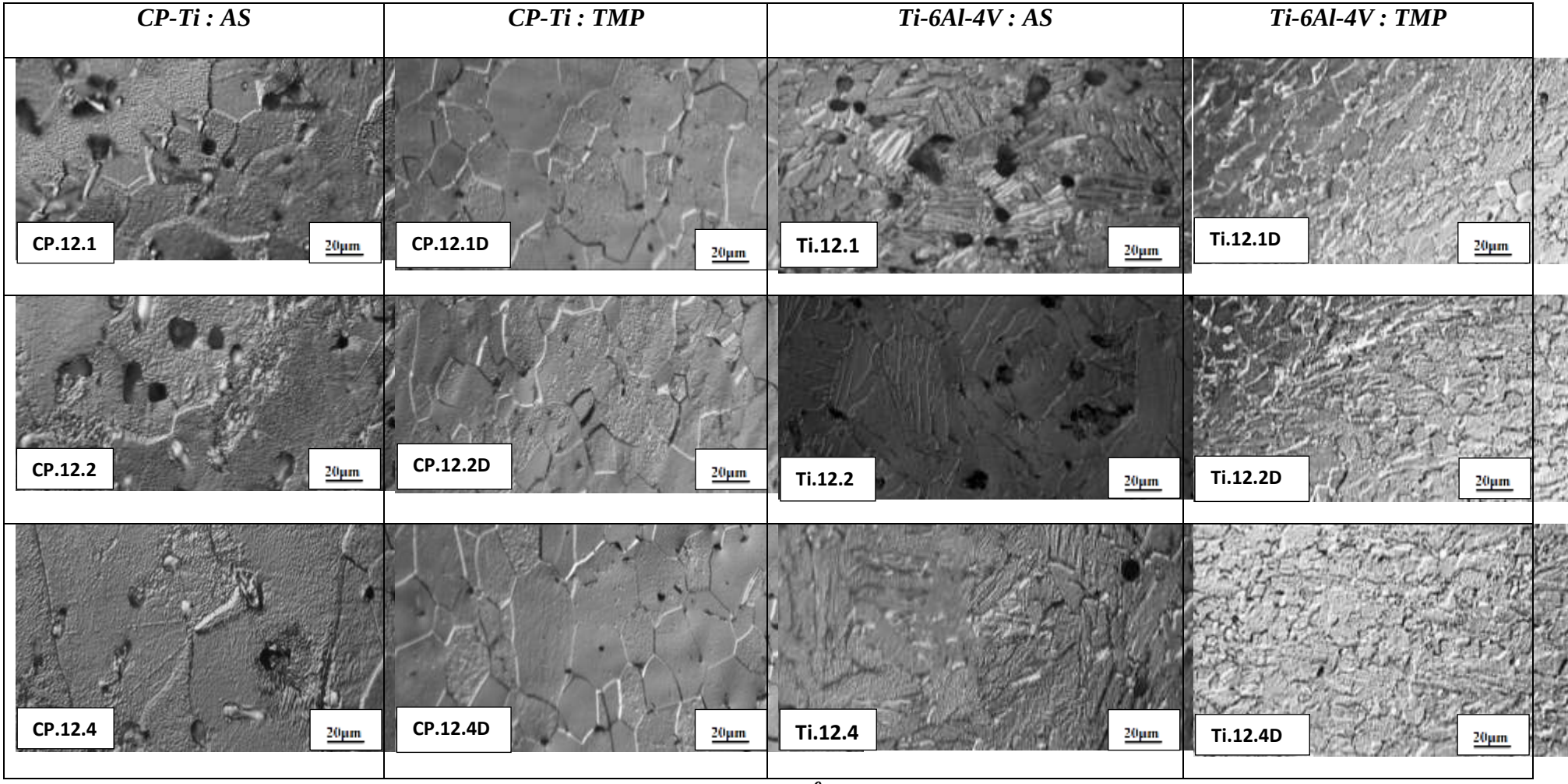

Figure 4.8: Microstructures of CP-Ti andTi-6Al-4V Specimens Sintered at 1200^{0}C. AS specimens are positioned on the left hand side and TMP on the right hand side of each system. Specimens were sintered for 1, 2 and 4 hrs respectively.

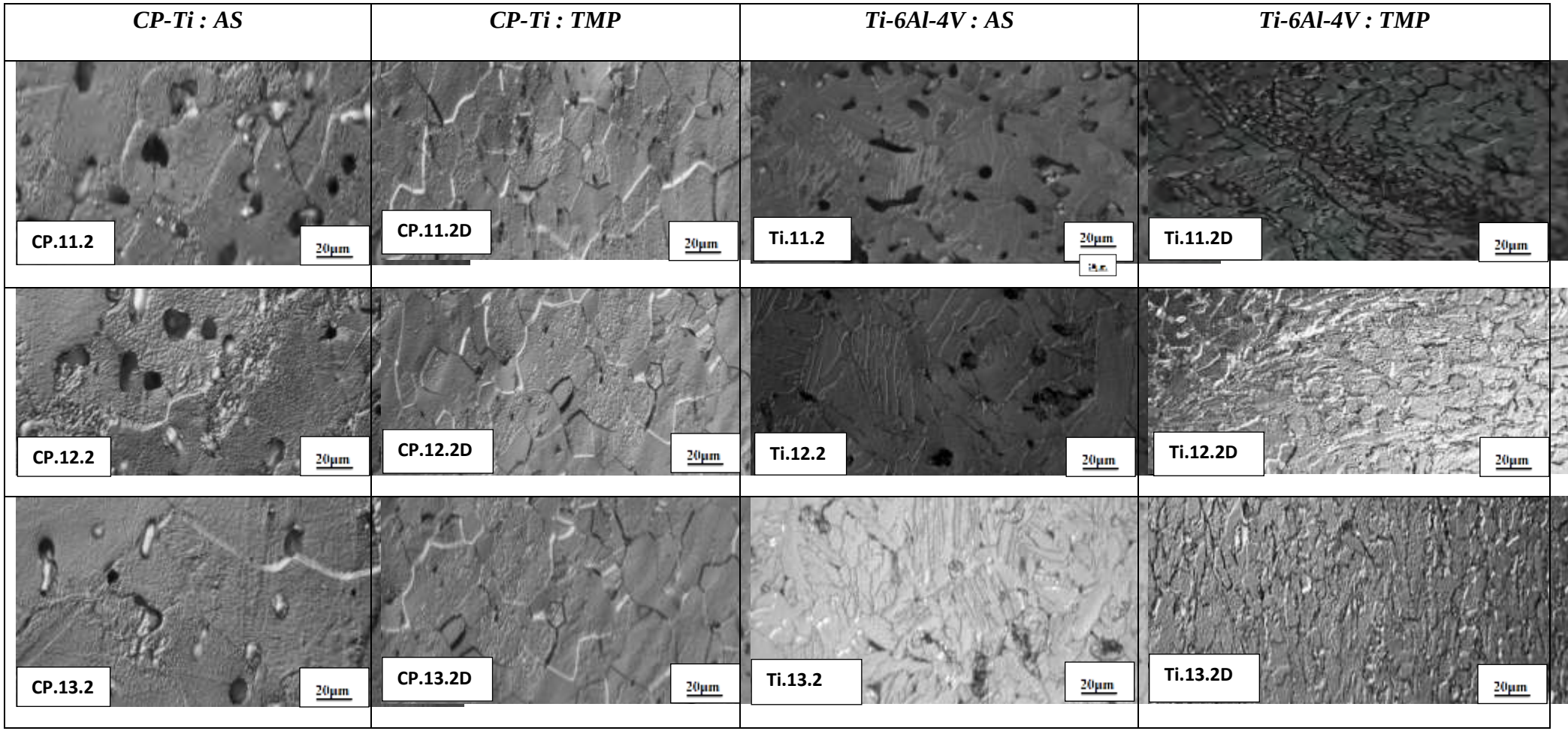

Figure 4.9: Microstructures of CP-Ti andTi-6Al-4V Specimens Sintered for 2hrs. AS specimens are positioned on the left hand side and TMP on the right hand side of each system. Specimens were sintered at 1100^{0}C, 1200^{0}C, 1300^{0}C respectively.

4.2.2. Discussion of Microstructure Results

Depending on temperature, time and processing history, different microstructure, porosity and mechanical properties result. Porosity cannot be completely eliminated by using only the traditional press and sinter method because voids are retained, thus full density is not attained. Porosity may consist either of a network of interconnected pores or of closed holes. Generally, if the density of the material is less than 80% of its theoretical density the pores are interconnected [3, 17, 61, 63].

Earlier it was established that Ti-6Al-4V specimens in the as-sintered state exhibit lower density than CP-Ti specimens. This was suggested to be due to CP-Ti being a single component system resulting in faster diffusion rates than the multicomponent Ti-6Al-4V specimens. When paying attention to the micrographs in Figure 4.7-4.9 and comparing CP-Ti to Ti-6Al-4V, it is observed that CP-Ti specimens have relatively round pores which become smaller in size with sintering temperature and time. On the other hand Ti-6Al-4V specimens have irregularly shaped pores which are thought to be a signature of packing history during compaction and the diffusion mechanisms that take place during sintering. Nevertheless the Ti-6Al-4V specimen pores also get smaller and rounded with increasing sintering conditions.

Post TMP it can be appreciated that visible porosity reduces to a significant degree in both systems. This is consequent to the applied stress that occurs during deformation. It is also seen that the small and rounded pores in TMP CP-Ti specimens are mostly found in the intra-granular space as opposed to being randomly located on the as-sintered specimens. These pores migrate from the grain boundaries to the inner grain consequent to the applied stress during deformation and are further reduced by annealing. This observation could not be clearly identified in Ti-6Al-4V specimens. The pores in Ti-6Al-4V generally appear to be as large as the grains also overlapping them for the AS specimens and post TMP they are reduced significantly and further reduced consequence to recrystallization that takes place during annealing.

4.3. Grain Size Analysis

4.3.1. Grain Size Results

Figure 4.10 shows the grain size profile of CP-Ti and Ti-6Al-4V in AS and TMP state. Here it is observed that Ti-6Al-4V AS specimens have smaller grains compared to CP-Ti AS specimens. Showing consistency with density results, CP.12.4 and Ti.12.4 specimens have the largest average grain sizes of 65 ± 10µm and 27 ± 2µm respectively when individually compared its respective CP-Ti and Ti-6Al-4V associates. CP.13.2 and Ti.13.2 have the second largest grains after CP.12.4 and Ti.12.4 specimens. In the AS state it was observed that in both systems grain growth generally increases with sintering temperature and time although there is considerable overlap in error bars which reflect large grain size range.

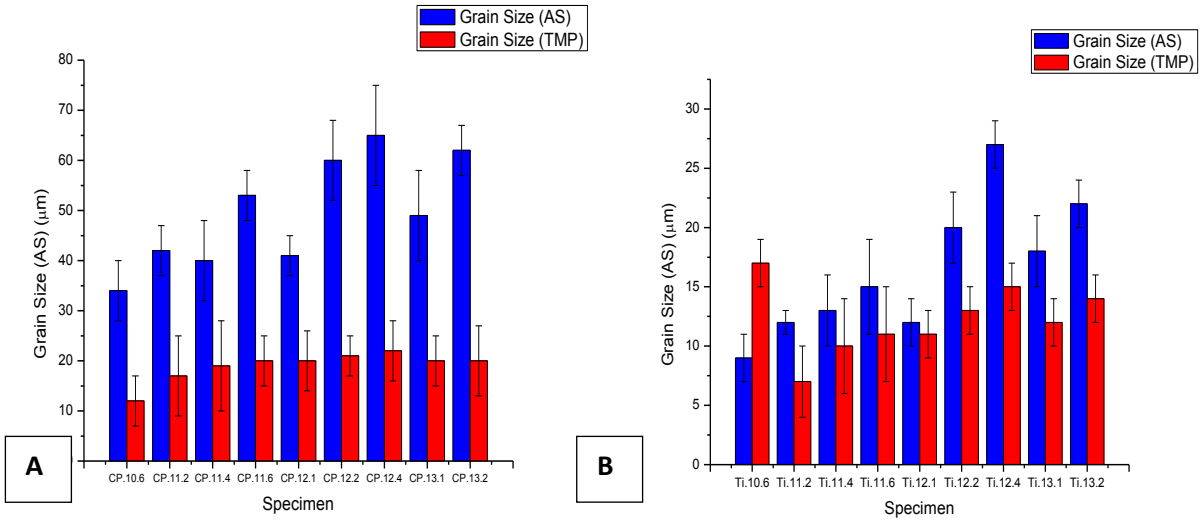

Figure 4.10: Grain Size Profile of CP-Ti and Ti-6Al-4V in AS and TMP conditions. (a) Shows CP-Ti grain size profile, (b) Shows Ti-6Al-4V grain size profile

Post TMP it is observed that there is a reduction in grain size for both CP-Ti and Ti-6Al-4V specimens. TMP results in the reduction in size of CP-Ti grains, showing that on average there is a 70% grain size reduction and while Ti-6Al-4V experience an average of 40% reduction in grain size. Ti.10.6D specimens are observed to have higher average grain size than the AS counterpart.

4.3.2. Discussion of Grain Size Results

The grain size results show that the CP-Ti specimens have larger grains than Ti-6Al-4V specimens, this was expected because the grain growth of Ti-6Al-4V is dependent primarily on homogenization and diffusion requirements resulting in the growth of lamellae grains which arise from the Widmanstatten transformation and this process is coupled with reduction of porosity while CP-Ti does not accommodate for homogenization therefore

grain growth in CP-Ti specimens consequently occurs readily with a significant reduction in porosity and for that reason grain sizes of CP-Ti and Ti-6Al-4V cannot certainly be compared.

However it can be generally noted that the influence of sintering temperature and time have the same effect in both systems. An increase in sintering temperature/time results in increasing grain size.

The results expectedly show that TMP causes grain refinement. However results show that Ti.10.6 specimens do not comply with this expectation. The grain size of the TMP Ti.10.6 specimen does not fall within the average grain size reduction range of 40% that was observed in other specimens, rather an increase in grain size post TMP was observed. Thus this result can be considered as an experimental outlier.

Based on the density results, microstructure and grain size results it is clear that CP-Ti and Ti-6Al-4V have different diffusion mechanisms due to the different starting powder compositions. Due to the difference in the diffusion mechanisms between CP-Ti and Ti-6Al-4V, AS CP-Ti undergoes a less complex diffusion process than AS Ti-6Al-4V which results in the AS CP-Ti specimens yielding higher density outputs and consequently larger grains than Ti-6Al-4V specimens. The impact of grains size refinement by TMP is greater on CP-Ti specimens with 70% reduction in grain size while TMP promoted to a significant degree the densification of Ti-6Al-4V specimens resulting in them having higher densities than CP-Ti specimens.

4.4. Hardness

4.4.1. Hardness Results

Figure 4.11 shows hardness profile for AS and TMP CP-Ti and Ti-6Al-4V specimens. It was observed from this figure that AS Ti-6Al-4V specimens are generally harder than AS CP-Ti. However, specimens sintered at 1000^0C (6hrs), 1100^0C (2hrs), 1300^0C (1hr) and 1300^0C (2hrs) do not comply due to the overlapping error bars. It can also be observed that hardness in both CP-Ti and Ti-6Al-4V increases with sintering time and temperature.

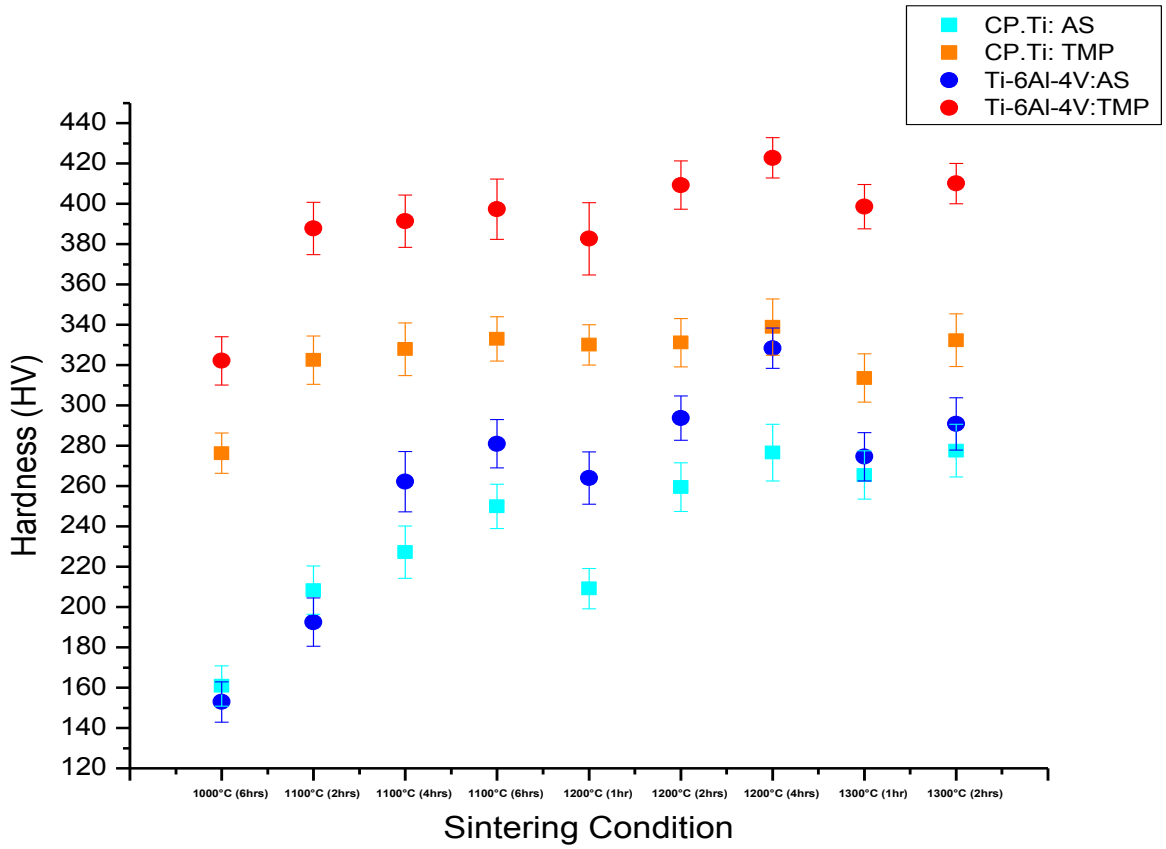

Figure 4.11: Hardness Profile for AS and TMP CP-Ti and Ti-6Al-4V Specimens.

Post deformation it was observed that Ti-6Al-4V specimens are significantly harder than CP-Ti across the board. CP-Ti hardness averages at 320HV post deformation while Ti-6Al-4V specimens have a hardness range of 380HV to 420HV.

It is observed that specimens sintered at low temperature or short sintering time yield lower hardness as expected. Ti.10.6 and CP.10.6 specimens have the lowest hardness both in the AS and TMP state respectively. TMP Ti.10.6 has equivalent hardness almost the full range of TMP CP-Ti specimens while TMP CP.10.6 has equivalent hardness to AS Ti.11.6 specimens.

Influence of Grain Size on Hardness

Figure 4.12 (a) and (b) below shows the relationship between hardness and grain size. It should be noted that CP-Ti specimens with hardness below 300HV are as-sintered specimens and specimens above this hardness value are TMP specimens. Similarly with Ti-6Al-4V specimens, the specimens below 350HV are AS specimens and specimens above are TMP specimens. In CP-Ti it can be observed that AS specimens have larger grain sizes and as a result lower hardness than TMP specimens. While in Ti-6Al-4V this relationship is seen not to be very strong.

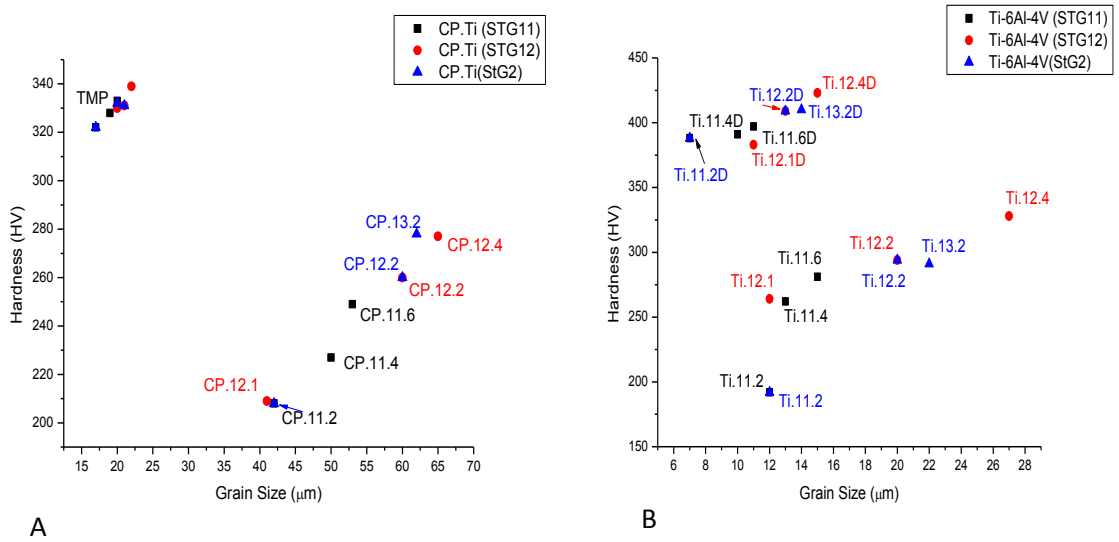

Figure 4.12: Showing hardness and grain size relationship for (a) CP-Ti Specimens (b) Ti-6Al-4V Specimens. Only STG 1100^{0}C, STG 1200^{0}C and StG2 specimens were considered.

When respectively looking at AS and TMP groups, it is observed that specimens with larger grains exhibit higher hardness. At face value it could be assumed that an increase in grain size results in an increase in hardness.

4.4.2. Discussion of Hardness Results

In powder metallurgy it is generally known that porosity affects hardness of sintered material. Fully dense materials are expected to have higher hardness than porous material of the same kind. For that reason if porosity alone influenced hardness, the AS Ti-6Al-4V specimens would have had poorer hardness yields than AS CP-Ti specimens' consequent to them having lower relative densities than the latter.

It is evident from figure 4.11 that in most cases Ti-6Al-4V specimens have higher hardness values than CP-Ti. Ti-6Al-4V specimens have a different composition to CP-Ti therefore a

difference in hardness would be expected. Solid solution strengthening contributes to Ti-6Al-4V having higher hardness than CP-Ti specimens suggesting that Ti-6Al-4V specimens have a harder metal surface. However in cases where there is a higher degree of residual porosity present, in the AS Ti-6Al-4V specimens' hardness is compromised. In essence this is a play off between higher solid solution strengthen in Ti-6Al-4V and higher density in CP-Ti.

Grain size results show that Ti-6Al-4V specimens have smaller grains than CP-Ti specimens thus if the Hall-Petch Equation (see below) is taken into consideration, it makes sense that Ti-6Al-4V specimens have higher hardness yields if hardness is considered to be related to yield strength. In non-equiaxed grains the measure of grain size is the size of the crystallographically coherent block, which may be the packet size or block size, if packet is subdivided. This allows the use of Hall-Petch as this equation generally caters for equiaxed grains.

$$\sigma_y = \sigma_0 + \frac{K}{\sqrt{d}}$$

Hall-Petch Relationship

Where σ_y is yield strength, K is a constant and d is the mean grain size,

Figure 4.12 (a) and (b) individually show that at each of the different processing platforms (AS or TMP) an increase in grain size results in an increase in hardness which is not in line with the Hall-Petch Equation. Therefore increase in hardness is thought to be due to the reduced porosity that occurs as consequence to the improvement in initial sintering conditions.

In CP-Ti specimens when the two processing routes are compared together it is seen that TMP specimen grains are much more refined than AS specimen and as a result higher hardness yields became evident post TMP. In Ti-6Al-4V the percentage reduction in grain size is as low as 40%, suggesting that grain refinement does not play a major role in improving hardness in these specimens, rather pore reduction is the major contributor.

It can thus be concluded that the primary role of TMP in CP-Ti is to refine grains while in Ti-6Al-4V specimens it is to reduce porosity and grain refinement become a secondary upshot. Thus it can be suggested that CP-Ti specimens' hardness is improved by grain refinement while in Ti-6Al-4V pore reduction is a major contributor to hardness keeping in

mind that the impact of solid solution strengthening on hardness is greater than that of grain size.

Another explanation would be that CP-Ti pores are harder than the actual metal which results in plastic deformation being the net result of TMP as opposed to pore closure. The CP-Ti pore strength may be attributed to their round nature thus reducing stress points around the pores, while Ti-6Al-4V pores are irregular shaped and as such have high stress points compared to rounded pores.

The round nature of the CP-Ti pores may be a contributing factor to why CP-Ti specimens cannot easily achieve full density post TMP.

5. Mechanical Properties

5.1. Fracture Results

Three-Point-Bend tests were performed to determine the fracture toughness and fracture mechanism of CP-Ti and Ti-6Al-4V. From the hardness results it became evident that increasing sintering does aid in reduction of porosity and as a result increases hardness. From this point going forward specimens with a sintering time of 2 hours will be evaluated. This is done to determine the minimum temperature with acceptable mechanical strength and thus specimens sintered at 1100°C, 1200°C and 1300°C were investigated. Also specimens sintered at 1000°C were incorporated to determine the impact of low sintering temperatures on mechanical properties while sintering time is extended to 6 hours.

The specimens were machined down to achieve a nominal thickness of 2.80mm with the aim of shaving off the highly porous outer edges. However for the purposes of complying with MPIF Standard 41 for determining bending strength of powder metallurgy material there was a limitation on how much the specimen dimensions could be reduced.

Figure 5.1 below shows bending stress curves and fracture surface SEM images of Ti.10.6 and Ti.10.6D specimens while figure 5.2 shows just the fracture surfaces of Ti.10.6 and Ti.10.6D specimens.

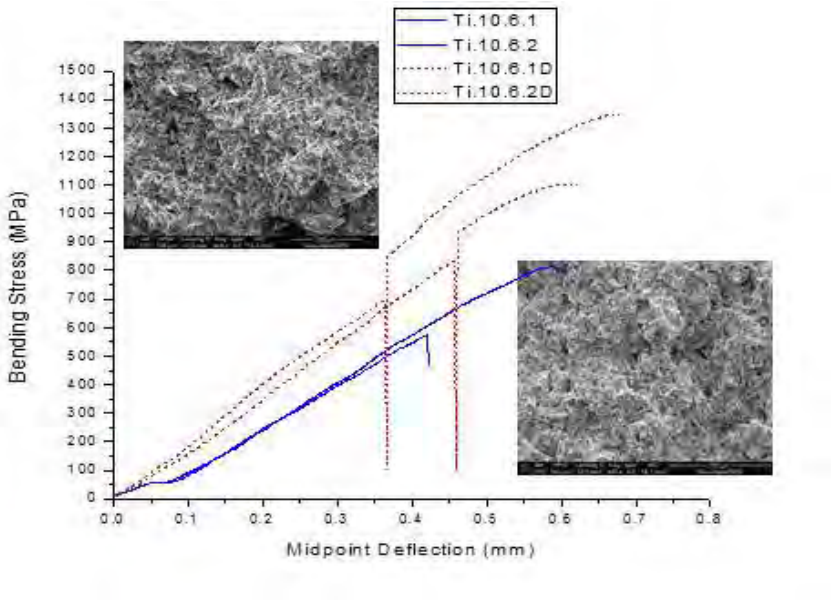

Figure 5.1: Fracture Curves and fracture surface SEM images of Ti.10.6 and Ti.10.6D specimens. Top left images are for AS specimens and bottom right images are for TMP specimen.

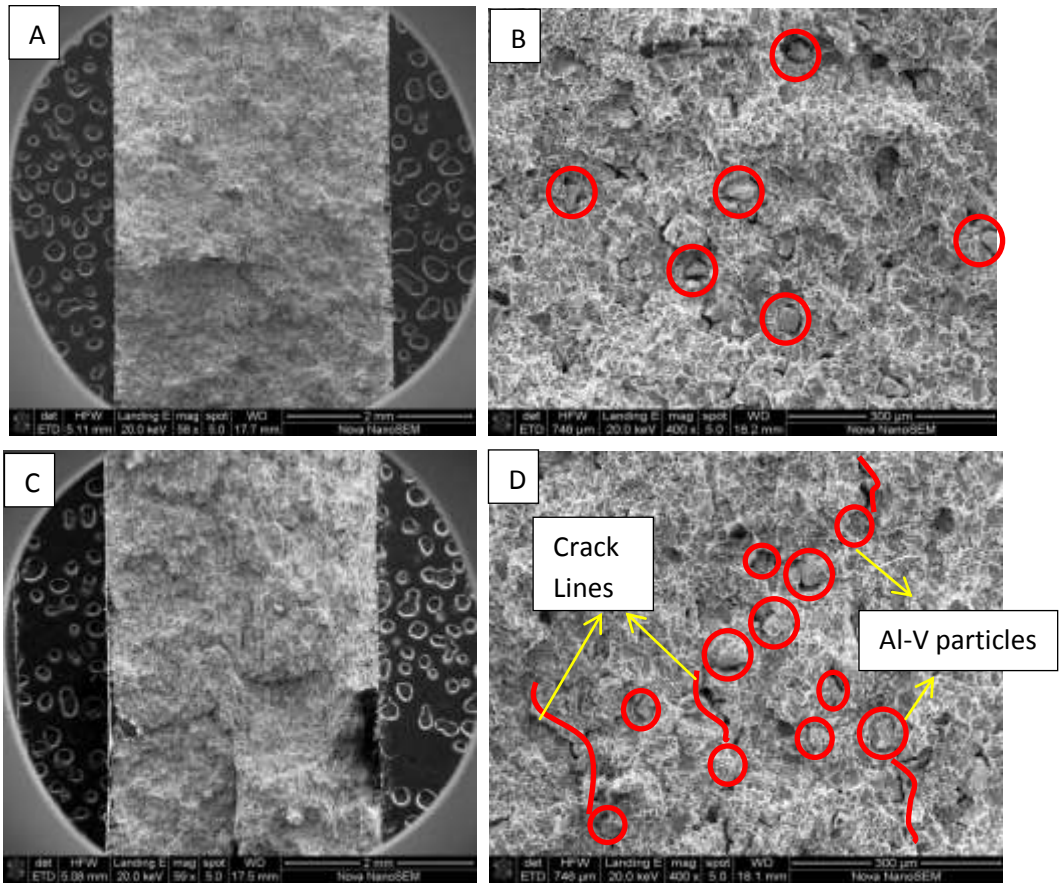

Figure 5.2: (A & C) Respectively shows fractured AS and TMP Ti.6.10 specimens mounted on conductive carbon tape, (B) Fracture surface of AS specimen, (D) Fracture surface of TMP specimen.

It is evident from Figure 5.1 that the deformed specimens have higher bending stress than the AS specimens. However the TMP specimens appear to fail twice. The first failure point occurs between 0.35 and 0.45mm midpoint deflection. The strength picks up again which suggests that the material had not completely failed. The material then finally fails completely between 0.7 and 0.8mm midpoint deflection.

Figure 5.2 shows the fracture surfaces of both the AS and TMP specimens. It can be seen from figure 5.2 (a & c) that AS specimens have a relatively flat fracture surface than the TMP specimens. In Figure 5.2 (b) which shows the fracture surface of the AS Ti.10.6 specimen, non-diffused Al-V particles (see also Figure 5.3) circled in red were observed. These non-diffused Al-V particles are far apart from one another and are delimited by irregular voids; the same voids are also restricted by the adequately diffused Ti-6Al-4V metal matrix. In contrast the TMP specimen fracture surface presented in Figure 5.2 (d) shows that at the same magnification, more non-diffused Al-V particles are observed and are in close proximity to one another. In TMP specimens the voids start near non-diffused

Al-V particles and extend further into the metal matrix looking more like cracks. The extended voids "cracks" are denoted in red as show in figure 5.2 (d)

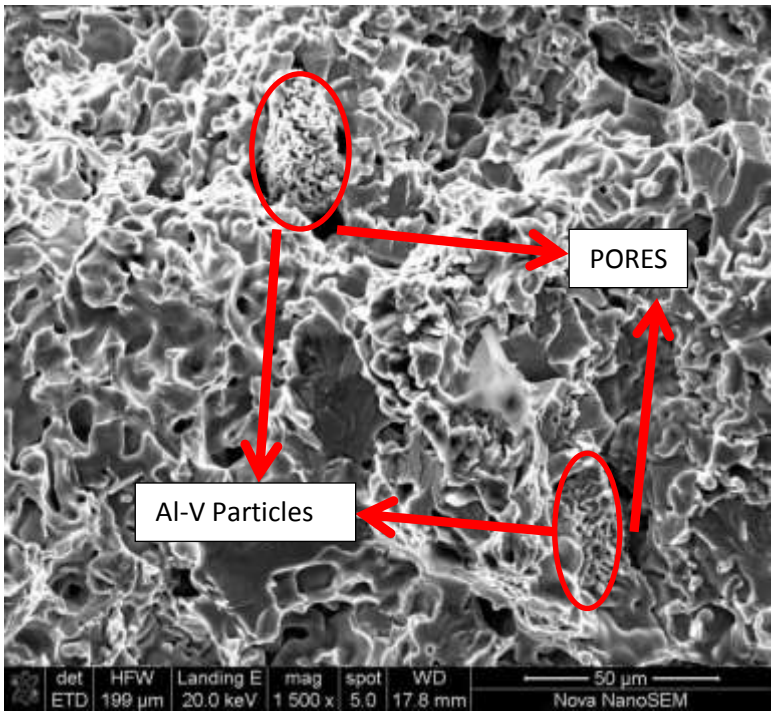

Figure 5.3: Showing high resolution SEM image of Ti.10.6 specimen with non- diffused Al-V particles circled in red.

On the other hand CP-Ti specimens as seen in figure 5.4 on the facing page show normal failure in all cases. TMP specimens expectedly have higher bending stress than the AS specimens. It was also observed that no non-diffused Al-V particles were present in the Ti-6Al-4V SEM images in both the AS and TMP states.

Figure 5.5 shows the fracture surface of the AS and TMP CP.10.6 specimens. It can be seen in this figure that the fracture surfaces of AS CP-Ti specimens have lots of pores and oblong hollow openings (dimples) while the TMP specimens show shallow-wide openings with striations and some visible pores.

Figure 5.6 shows fracture curves along with fracture surface SEM images of StG 2 specimens arranged in the same order as described in Figure 5.1 and 5.4. It was observed that in all cases TMP specimens had higher bending stress than their AS counterparts.

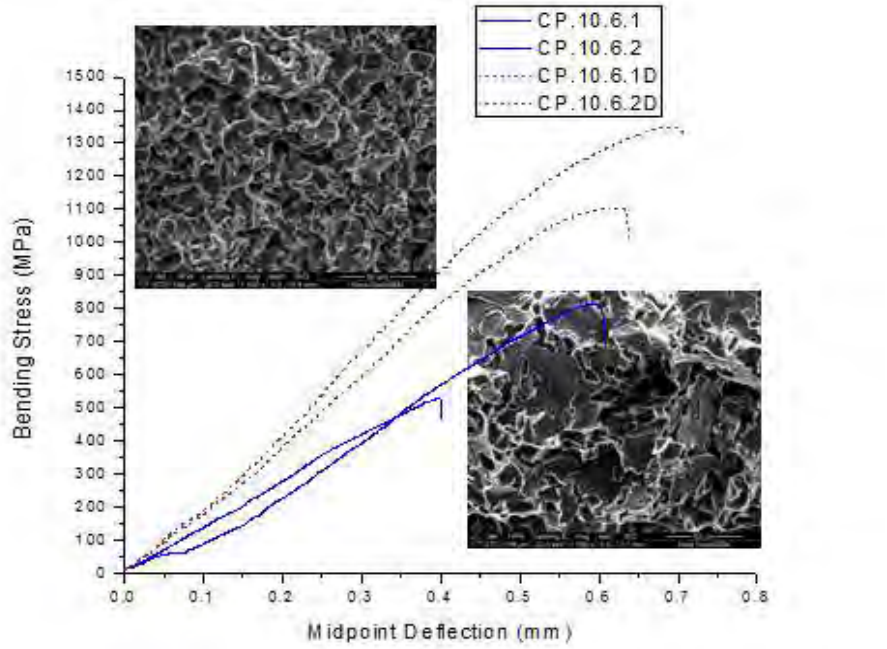

Figure 5.4: Fracture curves and fracture surface SEM images of CP.10.6 and CP.10.6D specimen. Top left images of AS specimens and bottom right images are of TMP specimen.

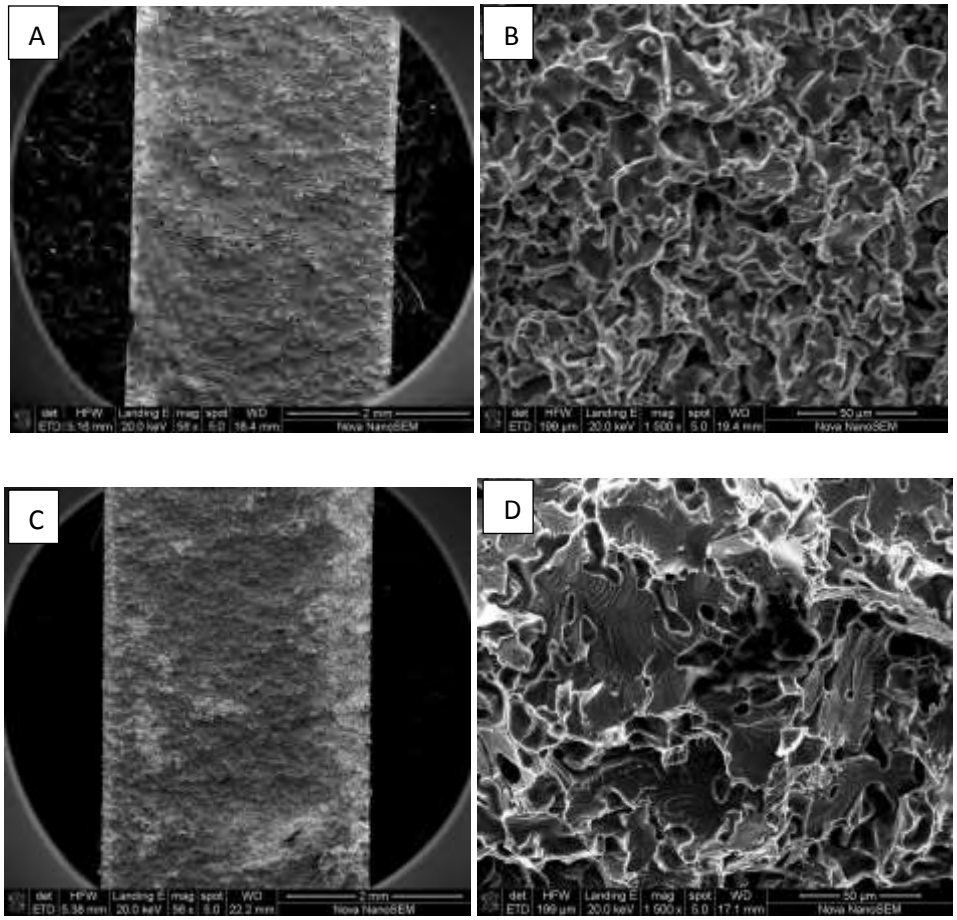

Figure 5.5: (A & C) Respectively shows fractured AS and TMP CP.10.6. specimens mounted on conductive carbon tape, (B) Fracture surface of AS specimen, (D) Fracture surface of TMP specimen.

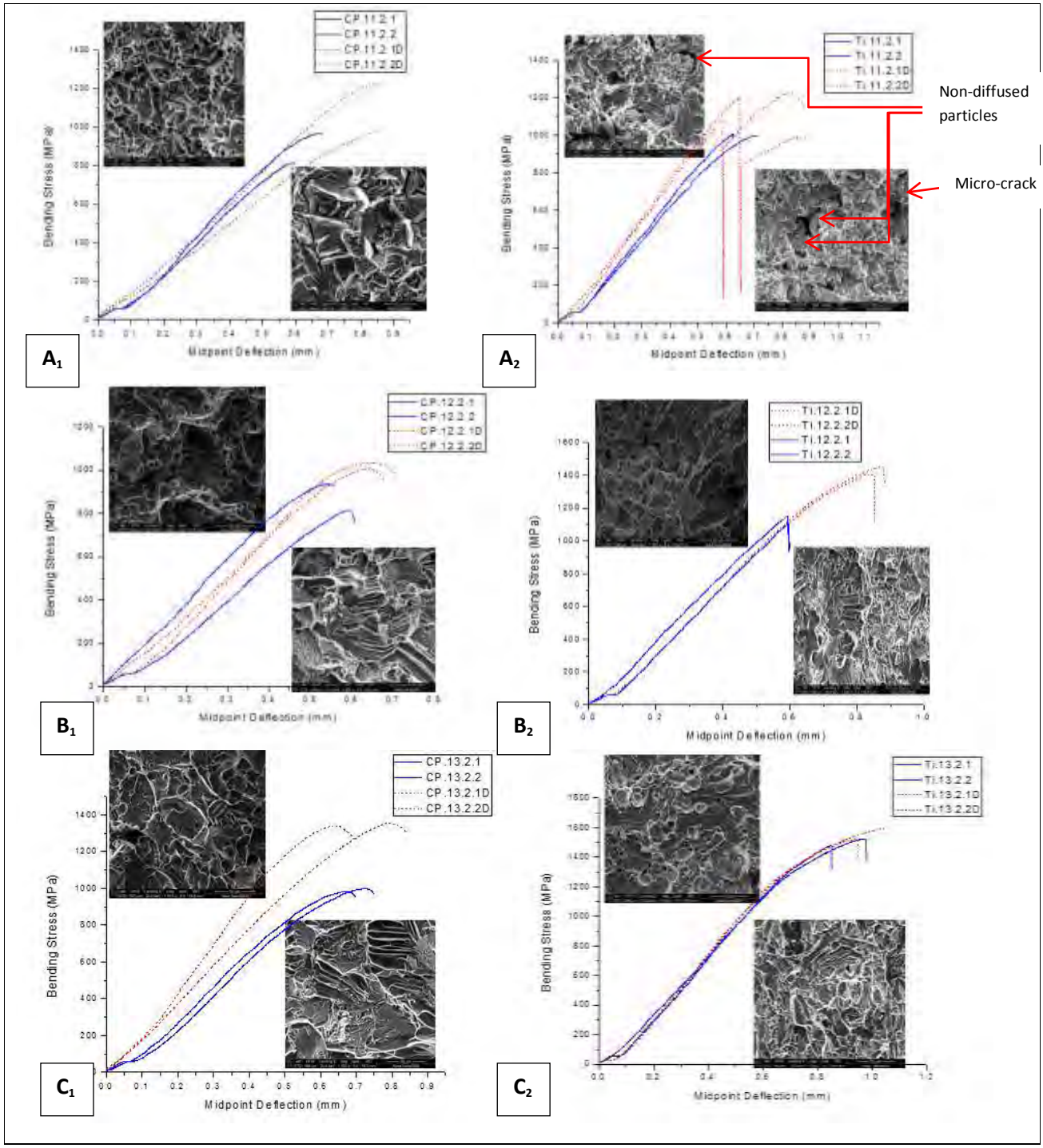

Figure 5.6: Fracture curves and fracture surface images of StG 2 specimens of both CP- Ti and Ti-6Al-4V systems. (X_1) CP-Ti Specimens, (X_2) Ti-6Al-4V Specimens. Top left images are images of AS specimens and bottom right images are those of TMP specimens.

Figure 5.6 (A_2) which represents bending stress curves for Ti.11.2 and Ti.11.2D, shows that the failure behavior of Ti.11.2D is similar to that of Ti.6.10D specimens. Both AS and TMP Ti.12.2 specimens have non-diffused Al-V particles present in their matrix. The bending stress curves show that Ti-6Al-4V undergoes brittle failure while CP-Ti shows slight ductility (i.e. the decrease in stress load after peak load is less sharp).

It can be seen that in each system the shear facets increases with increasing initial sintering temperature. The scales are more prominent in the denser materials. Shear facets are generally associated with brittle fracture indicative of a hard material that resists plastic deformation. Less visible pores are present on the fracture surfaces of the TMP specimens as sintering temperature is increased.

5.2. Crack Path Study

To better understand the how the material failed, a study of internal crack distribution of the three-point-bend specimens was conducted. This analysis was done on both the fracture surface and on the side that was loaded in tension during the three point bend test as shown in Figure 5.7 (b) below. These specimens were carefully polished using the conventional titanium polishing method shown in the methodology; however these specimens were polished down several times to get to the level where pores and cracks are clearly visible.

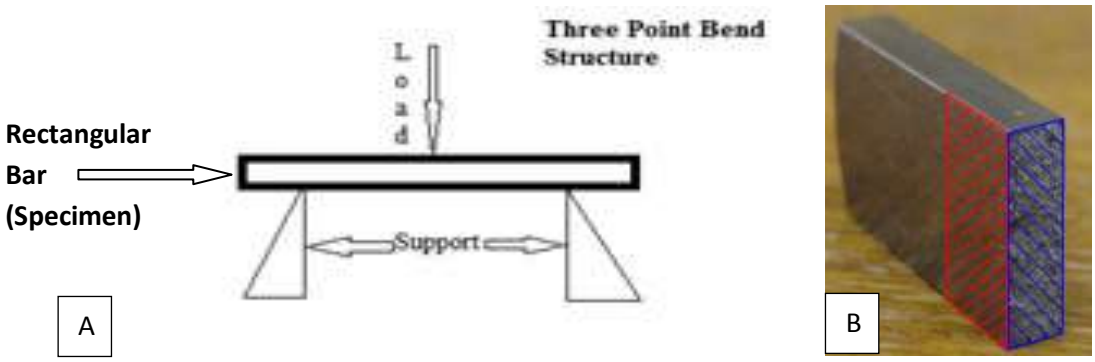

Figure 5.7: (a) Showing the three- point- bend structure, load direction, support and rectangular bar. (b) Photograph showing the two surfaces that were prepared for light microscopy in order to investigate the fracture of the three-point specimens. The surface shown by red cross-hatching is the sub-surface perpendicular to fracture plane and the surface shown in blue cross-hatching is the sub-surface parallel to fracture plane. (Figure 5.7 (b) Courtesy of Nicholas Clinning)

Figure 5.8 below shows sub-surface parallel to fracture plane of AS CP-Ti and TMP CP-Ti specimens (inclusive of specimens sintered at 1000^0C). CP-Ti specimens had porosity which was visible on all specimens; however no cracks were observed. Porosity was seen to be reduced post TMP.

Figure 5.9 shows polished fracture surfaces of Ti-6Al-4V, and whilst severe porosity is visible for specimens sintered at 1000^0C (6hrs) and 1100^0C (2hrs), the porosity decreases as the sintering temperature conditions were improved. Post deformation cracks on the

surface of Ti-6Al-4V specimens sintered at 1000^0C (6hrs) and 1100^0C (2hrs) were observed.

No further cracks were observed with specimens that were treated at higher initial sintering temperatures. Interestingly an observation is made on Ti.12.2D specimens where pores are clearly being sealed (pore curing) resulting in reduced porosity or this could be a polishing artefact where smearing occurs giving the illusion of reduced porosity.

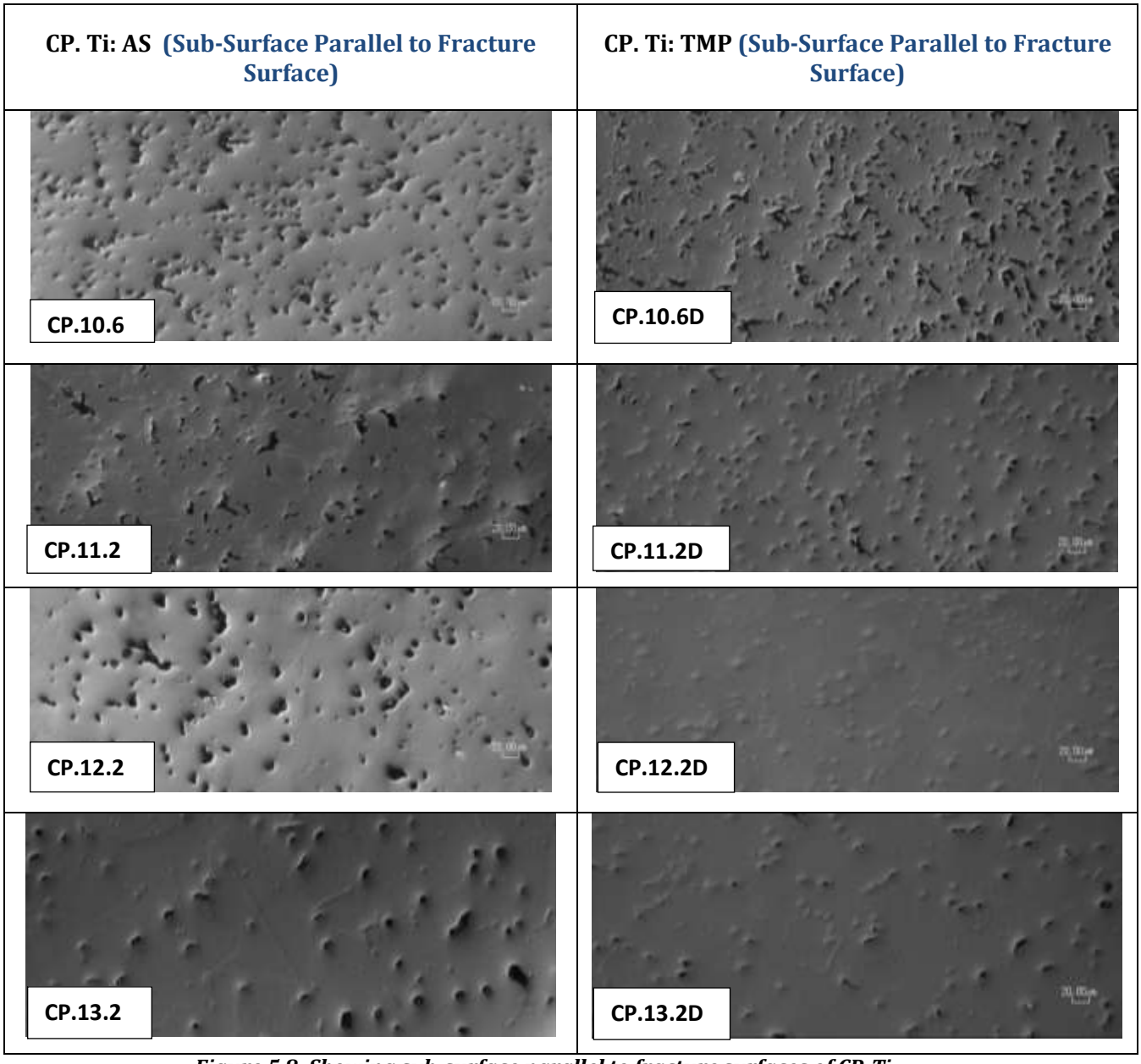

Figure 5.8: Showing sub-surface parallel to fracture surfaces of CP-Ti.

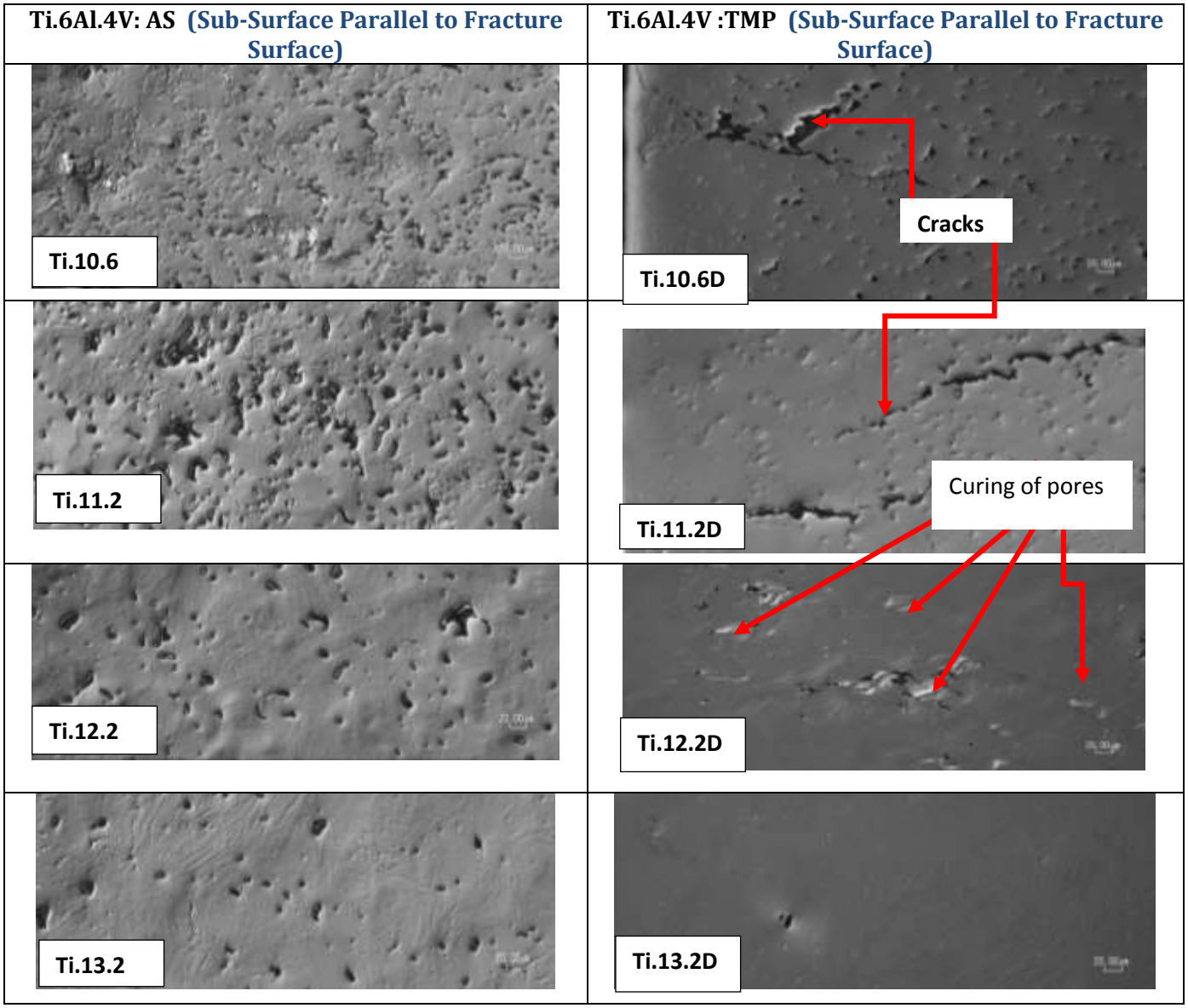

Figure 5.9: Showing sub-surface parallel to fracture surfaces of Ti-6Al-4V.

Figure 5.10 on the facing page shows images taken on the subsurface perpendicular to the fracture surfaces of the specimens. Only Ti-6Al-4V specimens were investigated in this instance as there was no evidence of crack formation in CP-Ti specimens on the sub-surface parallel to the fracture surface. It was further observed that Ti.10.6D and Ti.11.2D showed cracks as expected. It can be seen here that these cracks are formed as a result of pore inter-connectedness. Therefore Ti.10.6D and Ti.11.2D are subject to crack formation which results from the non-diffused particles and interconnected pores observed.

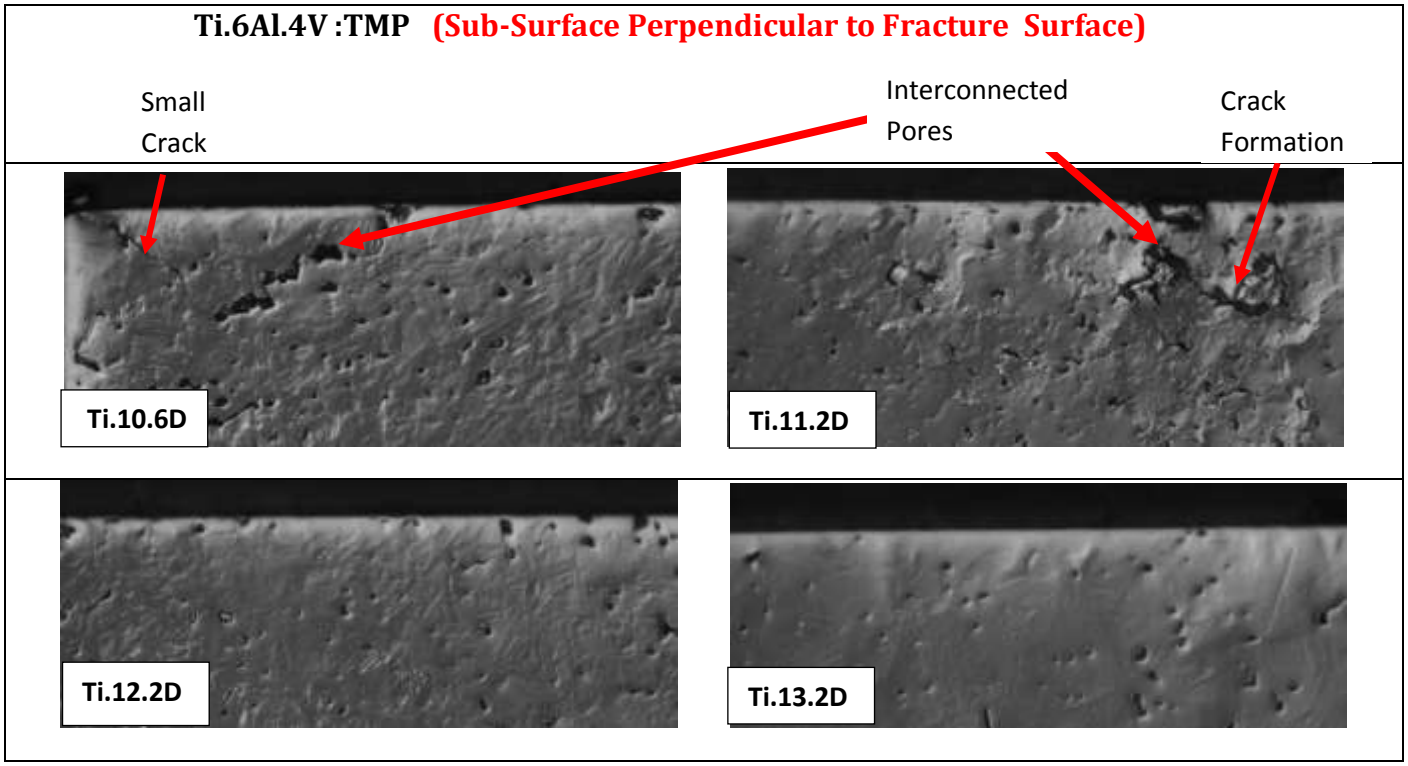

Figure 5.10: Showing sub-surface perpendicular to fracture surface of Ti-6Al-4V specimens.

5.3. Influence of Grain Size and Sintering Temperature on Fracture Strength

It was discussed in Chapter 4 how sintering time and temperature affects density, as well as microstructural and hardness properties of CP-Ti and Ti-6Al-4V systems. This section aims to assess how grain size and sintering temperature affects the strength of these materials.

Table 5.1 and Figure 5.11 below illustrates the data and profiles of the relationship between grain size, sintering temperature and the strength of both CP-Ti and Ti-6Al-4V systems in the AS and TMP states respectively.

The profiles revealed that after TMP there was significant reduction in grain size of the CP-Ti specimens which consequently led to improved strength. When the Ti-6Al-4V specimens were assessed, a similar observation was made.

Figure 5.11 (a) shows that increasing sintering temperature results in an increase in the strength of both materials. AS Ti-6Al-4V is stronger than AS CP-Ti and similarly TMP has higher strength than CP-Ti. AS Ti.11.2 specimens have lower strength than TMP CP.11.2 specimens. TMP generally increases the strength of the AS specimens.

Table 5. 1: Grain Size and Peak Stress (PS) values of AS and TMP CP-Ti and Ti-6Al-4V Specimens in StG2.

SPECIMEN	Ti-6Al-4V (AS)		Ti-6Al-4V (TMP)		CP-Ti (AS)		CP-Ti (TMP)	
	Grain Size	PS	Grain Size	PS	Grain Size	PS	Grain Size	PS
	μm	*MPa*	*μm*	*MPa*	*μm*	*MPa*	*μm*	*MPa*
X.11.2	12	986	7	1140	42	825	17	1090
X.12.2	20	1175	13	1445	60	850	21	1145
X.13.2	22	1425	14	1545	62	995	20	1315

Figure 5.11(b) indicates that for a particular material, the increase in peak stress cannot be explained by reduction in grain size. This result was also observed in Chapter 4.4.1 (hardness results). It is also evident that specimens with grossly larger grains (AS-CP-Ti) have severely lower strength compared to the specimens with smaller grains such as the AS Ti-6Al-4V notwithstanding that Ti-6Al-4V is also strengthened by alloying.

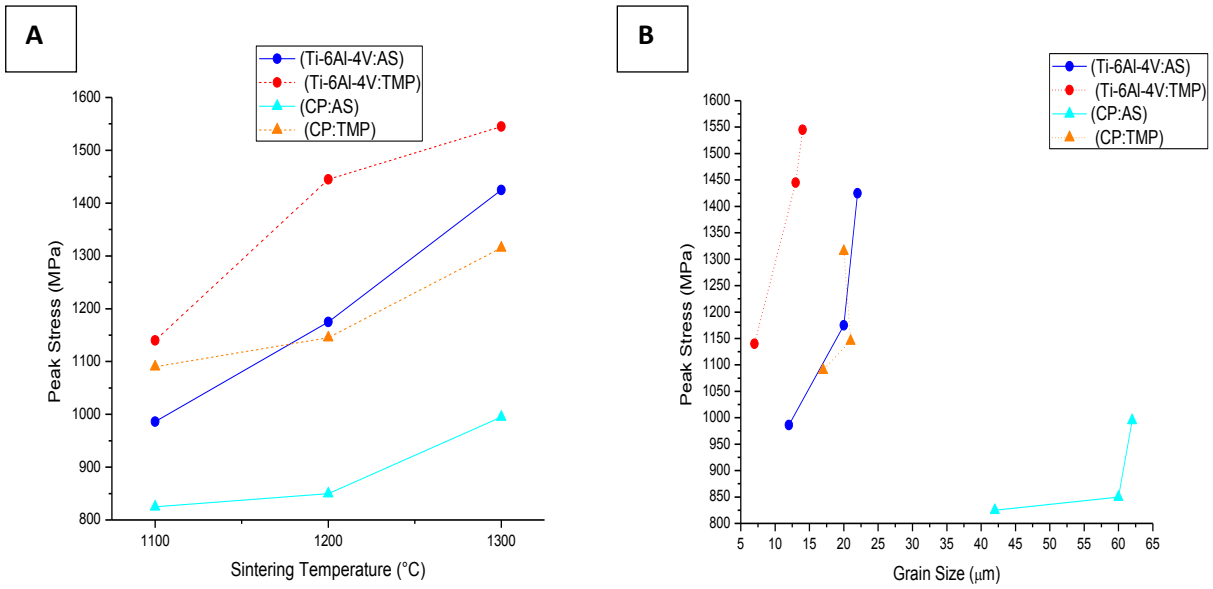

Figure 5.11: Profiles showing (a) Sintering Temperature and Strength of AS and TMP Specimens (b) Strength with respect to a change in grain size.

5.4. Discussion of Mechanical Property Results

As shown in Chapter 5.1 Ti-6Al-4V specimens which were initially sintered at low sintering temperature and later subjected to three-point-bending test resulted in catastrophic failure compared to specimens initially sintered at higher sintering temperatures. Specimens that were initially sintered at lower temperature (1100^0C and 1000^0C) and subsequently TMP treated showed unsatisfactory results, with the presence of non-diffused Al-V particles in the matrix Ti.10.6D and Ti.11.2D. These particles contribute to the unexpected failure characteristics. Even though the non-diffused particles were also present in the AS Ti.10.6 and Ti.11.2 specimens the manner in which they were dispersed on the specimens did not compromise their integrity.

In Chapter 4.1, it was seen that CP-Ti specimens have higher density than Ti-6Al-4V across the board. The difference in density was more prominent for specimens sintered at lower temperatures and decreased as sintering temperature and time increased so much so that CP-Ti and Ti-6Al-4V specimens sintered at 1200^0C for 4 hours had comparable densities. In this section it was established that a decrease in sintering temperature leads to preservation of chemical inhomogeneity of material, which cannot be avoided even with longer time exposure. In Chapter 4.1, Figure 4.2 it was shown that STG 1100^0C specimens can take very long to reach full density as the profile curve seemed to plateau at less than 93% relative density, also Ivasishin *et al*. [51] showed that 59-Al-39V master alloy would take up to 10^6 s exposure at these temperatures for the master alloy to move into the titanium matrix. This then further confirms that these non-diffused Al-V particles found on the fracture surface of specimens sintered at low initial sintering temperatures are more than likely to be non-diffused Al-V particles from the master alloy powder.

The non-diffused Al-V particles in AS Ti-6Al-4V specimens are far apart from each other suggesting that Ti and Al-V master alloy powders were originally adequately blended. These Al-V particles are associated with voids which in most cases separate the Al-V particles from the metal matrix. Because of the highly dispersed non-diffused Al-V particles the strength and failure mechanism appear to be normal. During TMP there is more porosity near/on the surface because less plastic deformation occurs in these regions due to the "dead zone" effect created by high friction at specimen/anvil interface an example of this is shown in Figure 5.12 on the facing page. Here the pores become interconnected and also the non-diffused Al-V particles are in close proximity to each other. Porosity is greater near the surface due to the "dead zone" effect during compression testing (high friction), in

other words, plastic strain is partitioned towards the center of the specimen and hence much less pore collapse occurs at the edges. It should also be noted that part of the surface is machined away prior three-point-bend testing. Due to the specimen size limitation not all the concentrated porosity could be removed.

During specimen loading the cracks develop easily along the areas with concentrated porosity however when the denser regions are reached a greater force becomes essential to overcome the denser regions due to the successive pinning of the cracks, explaining the false failure observed in Ti.10.6D and Ti.11.2D specimens. Evidence of these cracks is shown in Figure 5.2(d), Figure 5.9 and Figure 5.10 (T.10.6D and Ti.11.2D). Because it would be difficult to measure the crack mechanism post the first failure point and also the unpredictable nature of this failure as it occurs at slightly different positions if midpoint deflection is considered then at the first failure point the material is considered to have failed even though it has not failed completely. In a real life application such a failure would lead to catastrophic events.

Figure 5.9 Ti.12.2 further shows that in cases where the specimens do not have severe porosity, TMP closes (cures) the pores resulting in less porosity in the dead zone.

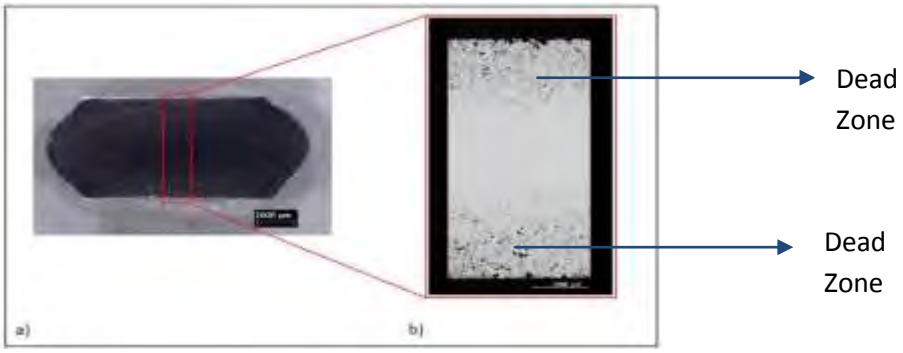

Figure 5.12: Showing porous edges of TMP specimen (curtesy of Nicholas Clinning) [56]

It was observed that even though AS Ti-6Al-4V specimens generally have higher porosity than CP-Ti specimens they had the higher yield strength than the former. This is due to Ti-6Al-4V being inherently stronger than CP-Ti as a consequence of solid solution strengthening. Fracture curves for CP.10.6 (Figure 5.4) shows inconsistent results with the two test specimens showing considerable difference in the Peak Stress which further extends to CP.10.6D specimens. This observation was made with Ti-6Al-4V in Figure 5.1. The servere degree of porosity affected the integrity of the results thus making them

inconsistent. It can be seen however that the results become more consistent (see Figure 5.6) as the initial sintering conditions improve; indicating that porosity also affects the consistency of the results. This may have something to do with the manner in which mainly the pores and/or non-diffused Al-V particles are orientated in the specimens during loading. Also one can argue that the sample size was not adequate statistically, therefore more test specimens should have been produced per test condition. However due to limited time for this work only a few specimens could be produced that two specimens per test condition were investigated and the average result taken.

If the average of two specimens is taken as a rule of thumb then CP.10.6 has higher Peak Stress than Ti.10.6 and this can generally be attributed to density and homogenization requirements of Ti-6Al-4V.

In this chapter it has become evident that sintering temperature is crucial in optimizing strength of powder metallurgy material. Figure 5.11 (a) shows that the higher the sintering temperature, the higher the strength output which similarly this feeds in to the TMP treated specimens. It is known that higher sintering temperatures promote grain growth and grain growth affects material strength as per the Hall-Petch equation. Figure 5.11(b) contradicts this relationship as it is seen that an increase in grain size seems to be correlated to an increase in Peak Stress. This observation is in line with what was observed with grain size vs hardness results in Figure 4.12. We can thus conclude from both results that the primary benefit of TMP is not grain refinement but pore reduction and grain size refinement plays a secondary role as it is a consequence of the deformation process.

Based on the results obtained in this section, it can be generally observed that the initial sintering temperature and TMP are the major factors which influence mechanical properties in both CP-Ti and Ti-6Al-4V. The results show that increasing sintering temperature results in denser material with less pores intersecting with the surface coupled with greater material strength, while poorer sintering conditions affect the integrity of the material with greater incidence of porosity intersection with surface post TMP.

The cost benefits of using lower sintering temperatures do not outweigh the structural integrity of the final product. Therefore it can be concluded that the ideal (minimum) sintering temperature that can be used to ensure high strength - high density outcomes is 1200^0C.

6. Comparing Al-V master alloy to Elemental Al and V alloy

Compared to work done by Clinning [56], the use of a Master Alloy instead of Al and V elemental powders does yield some benefits in material properties. Specimens sintered at 1200^0C for 2hrs and deformed at 800^0C were compared and are shown in Table 6.1 below.

Table 6.1: Comparing Al-V Master Alloy to Al and V Elemental Powders.

Properties	**AS: Elemental Al-V Alloy***	**AS: Al-V Master Alloy***	**TMP: Elemental Al-V Alloy**	**TMP: Al-V Master Alloy**
Density	88%	93.5%	98%	98%
Average Grain Size	No data	20µm	13µm	10µm
Hardness	269HV	294HV	419HV	409HV
Peak Stress	890MPa	1175 MPa	700MPa	1445MPa
Crack formation/Porosity	Servere cracking	Retained porosity	Servere cracking	Curing pores

*Blue represents work done by Clinning [56].

*Red represents this work.

On table 6.1, the noteworthy differences between the Al-V elemental and master alloy composition is observed with their initial sintered densities and fracture strength. It should however be noted that the sintered density difference could also be associated with the different compaction pressure used. Clinning's specimens were compacted at 375MPa compared to the 450MPa used in this work.

Clinning experienced a decrease in fracture strength which was attributed to embrittlement of the final product as a result of using elemental Al and V. While this work also shows that the use of the Al-V master alloy results in a brittle final product, there was considerable strength gain post TMP when Al-V master alloy is used. This then suggests that there must have been another reason for the reduced strength in Clinning's work and this might have something to do with the diffusion mechanism that the elemental Al and V undertakes which could be different from that of the Al-V master alloy. Clinning suggested that it was the melting of the Al powder which led to

large pores that resulted in the compromised strength properties of the elemental Al and V alloy.

The formation of cracks on Clinning's specimens gives clues that the diffusion mechanism could be indeed cause of the poor strength result. In this work cracks were observed only in cases where there was inadequate diffusion which resulted in inhomogeneous non-diffused Al-V particles existing on the specimen matrix thus leading to excessive and closely structured pores which upon loading initiate the cracks.

7. Conclusions

- Green densities were similar for the CP-Ti and Ti-6Al-4V alloy.
- AS densities for the two metal types evolved differently, with Ti-6Al-4V reflecting lower densities than CP-Ti. It can thus be concluded that Ti-6Al-4V required additional energy for densification and chemical homogenization.
- After TMP, the Ti-6Al-4V specimens generally showed higher density than the CP-Ti specimens. It can thus be concluded the impact of TMP is primarily pore reduction in Ti-6Al-4V, while it predominantly promotes grain refinement through plastic deformation in CP-Ti.
- The peak stress values during three-point-bending tests are strongly influenced by the process condition. AS specimens sintered at higher temperatures yield higher peak stress values while specimens sintered at low temperatures showed lower peak stress. TMP treated specimens show significantly improved peaked stress which were also influenced by the initial sintering conditions. CP-Ti showed lower peak stress values than Ti-6Al-4V which is due to solid solution strengthening of the alloy metal.
- This work shows that Ti-6Al-4V specimens sintered at 1200^0C for 2hrs and subsequently TMP yielded higher density, hardness properties and also show significantly refined grains compared to specimens sintered at 1200^0C for 4hrs without any subsequent deformation step. Therefore, under carefully controlled conditions Partial Sintering + Hot Deformation Processing can be used as an alternative to Cold Compaction + Sintering process.
- Post TMP, specimens originally sintered at relatively low temperatures negatively affects mechanical properties of Ti-6Al-4V specimens, these yield non-diffused Al-V powder particles which attract porosity and result in failure by crack propagation upon load.
- Therefore, the cost benefits of using excessively low sintering temperatures results in compromised final product. Therefore, it can be concluded that the ideal (minimum) sintering temperature that can be used to ensure high strength - high density outcomes is 1200^0C (2hrs).

- In Al-V master alloy TMP improves mechanical properties compared to the Al and V elemental alloy which is affected negatively due to the different diffusion mechanisms involved so much so that in the elemental Al and V alloy the aluminium melts before the beta-transus temperature resulting in large pores consequently compromising its mechanical properties.

8. Future Work and Recommendations

As a result of the current research and finding, the author suggests the following:

- Any further work conducted on BE Ti-6Al-4V should be proceeded with the use of TiH_2 as the major powder constituent as it is thought that this will assist in achieving better sintered densities.

- If CP-Ti is used as the major constituent any further work should be done with Al-V particles size ranging from 30-40μm in size. This may result in much quicker diffusion and prevent the presence of non-diffused powder particles in the final product where low sintering temperatures are used.

- Also the mechanical properties of specimens treated at 1200^0C (1hr) should be investigated as they showed very promising density results which were comparable to specimens sintered at the same temperature for 2hrs.

9. Bibliography

[1] W. Gregor, "Titanium and Titanium Alloys," *Kirk-Othmer Encycl. Chem. Technol.*, vol. 3, 2007.

[2] G. Lutjering, J. C. Williams, and A. Gysler, "Microstructure and Mechanical Properties of Titanium Alloys," *Tech. Univ. Hamburg-Harburg, Hamburg, Ger.*, 2012.

[3] F. H. S. Froes, "Developments in Titanium P / M," *Inst. Mater. Adv. Process.*, vol. University, no. ID 83844–3026, 1980.

[4] O. M. Ivasishin, D. G. Savvakin, F. Froes, V. C. Mokson, and K. A. Bondareva, "Sintered Metals and Alloys," vol. 41, no. 426, pp. 382–390, 2002.

[5] S. Peterson and R. Knutsen, "Investigation of the hot deformation of sintered compacts produced from direct reduction powder," *Cent. Mater. Eng.*, 2010.

[6] F. Froes, S. Mashl, V. Moxson, V. Duz, and J. Hebeinsben, "The Technologies of titanium powder metallurgy," *Joutnal Mater.*, 2004.

[7] F. Thummler and R.Oberacker, "An introduction to powder metallurgy.," *Inst. Mater. Ser. Powder Metall.*, 1993.

[8] R. German, *Powder Metallurgy Science*, Second edi. Princeton, 1994.

[9] R. McGeary, "Mechanical Packing of Spherical Particles," *J. Am. Ceram. Soc.*, vol. 44, no. 10, pp. 513–522, 1962.

[10] Y. Boonyongmaneerat, "Mechanical properties of partially sintered materials," *Mater. Sci. Eng. A*, vol. 452–453, no. October 2006, pp. 773–780, 2007.

[11] "Design Advantages of Porous Metals," *Porous Metal Design Guidebook, Metal Powder Industries Federation, 105 Road East, Princeton, NJ08540 USA*. 2012.

[12] P. C. Angelo and R. Subramanian, "Powder Metallurgy, Science, Technology and Applications," *PHI Learn. –Private Limited, Connaught Circus, New Delhi, India.*, pp. 87–125, 2008.

[13] W. Chen, Y. Yamamoto, and W. H. Peter, "Investigation of pressing and sintering processes of CP-Ti powder made by Armstrong Process," *Key Eng. Mater.*, vol. 436, pp. 123–130, 2010.

[14] D. Elyon, F. H. Froes, and S. Abkowitz, "Titanium Powder Metallurgy Alloys and Composites," *ASM Handb. Powder Met. Technol. Appl.*, vol. 07, pp. 874–883, 1998.

[15] D. Gordon, *Powder Metallurgy: The Process and Its Products*, 2nd ed. Shrewsbury: European Powder Metallurgy Association, 1992.

[16] Z. Esen and E. T. Bor, "Characterization of loose powder sintered porous titanium and Ti6Al4V alloy," vol. 33, pp. 207–219, 2009.

[17] R. G. Narayanan, “Powder metallurgy – basics & applications,” 2011.

[18] M. Standard and T. Methods, *Standard Test Methods for Metal Powders and Powder Metallurgy Products 2010 Edition Standard Test Methods for Metal Powders and Powder Metallurgy Products*. 2010.

[19] Z. Gronostajski, P. Bandoła, and T. Skubiszewski, “Influence of cold and hot pressing on densification behaviour of titanium alloy powder Ti6Al4V,” vol. IX, no. 2, 2009.

[20] S. Nemat-Nasser, W. G. Guo, and J. Y. Cheng, “Mechanical properties and deformation mechanisms of a commercially pure titanium,” *Acta Mater.*, vol. 47, no. 13, pp. 3705–3720, Oct. 1999.

[21] M. Ashby, “A First Report on Sintering Diagrams,” *Acta Metall.*, vol. 22, 1974.

[22] X. Xu and P. Nash, “Sintering Mechanism of Armstrong Prealloyed Ti-6Al-4V Powders,” *Mater. Sci. Eng.*, no. A 607, pp. 409–416, 2014.

[23] Y. Mishin and C. Herzig, “Grain boundary diffusion: recent progress and future research,” *Mater. Sci. Eng.*, no. A 260, pp. 55–71, 1999.

[24] F. Swinkels and M. Ashby, “A second report on sintering diagrams,” *Acta Metall.*, no. 29, pp. 259–281, 1981.

[25] S. L. Kang, *Sintering, Densification, Grain Growth & Microstructure*, no. 52(15). 2004.

[26] X. Xu, K. Araci, and P. Nash, “Cost Effective Press and Sinter of Titanium and Ti-6Al-4V Powder for Low Cost Components in Vehicle Applications,” *Thomas Zwitter*, vol. Webster-Ho, no. 003, 2010.

[27] L. Bolzoni, P. G. Esteban, E. M. Ruiz-Navas, and E. Gordo, “Mechanical Behaviour of Pressed and Sintered Titanium Alloys Obtained from Prealloyed and Blended Elemental Powders,” *J. Mech. Behav. Biomed. Mater.*, pp. 29–38, 2012.

[28] G. Shi-bo, X. Qu, and X. Xe, “Influence of Sintering Temperature on Mechanical Properties of Ti-6Al-4V Compacts by Metal Injection Molding,” *Mater. Sci. forum*, vol. 475–479, pp. 2639–2642, 2005.

[29] J.R.Davis, Ed., “Mechanical Testing,” in *Metals Handbook*, Ninth Edit., ASM, 1985.

[30] L. Bolzoni, E. M. Ruiz-Navas, E. Neubauer, and E. Gordo, “Inductive hot-pressing of titanium and titanium alloy powders,” *Mater. Chem. Phys.*, vol. 131, no. 3, pp. 672–679, Jan. 2012.

[31] K. Kubiak, “Technological Plasticity of Hot Deformed Two-Phase Titanium Alloy(in Polish),” *Rzesz. Univ. Technol.*, 2004.

[32] R. Ding, Z. X. Guo, and A. Wilson, “Microstructural evolution of Ti-6Al-4V Alloy During Thermomachenical Processing,” *Mater. Sci. Eng.*, vol. A327, pp. 233–245, 2002.

[33] J. Sieniawski and M. Motyka, "Superplasticity in Titanium Alloys," *J. Achiev. Mater. Manuf. Eng.*, vol. 24, no. 1, pp. 123–130, 2007.

[34] M. Motyka and J. Sieniawski, "Influence of Thermomachincal Process Conditions on Superplastic Behaviour of Ti-6Al-4V Titanium Alloy," *Adv. Mater. Sci. Technol.*, vol. 28, no. 31–43, 2004.

[35] J. Davis and Editor, "Metal Handbook," *Mech. Test.*, vol. 8, no. 9th edition, 1985.

[36] DSI, "Gleeble System Application Notes," 2011.

[37] A. Duckham and R. Knutsen, "Asymetric flow during plane strain compression testing of aluminium alloys," *Mater. Sci. Eng.*, vol. 256, no. 1, pp. 220–226, 1998.

[38] J. Kliber, S. Aksenov, and R. Fabik, "Numerical Study of deformation characteristics in plane strain compression tests (psct) volume certified following microstructure.," *Metalurgija/Metallurgy*, vol. 48, no. 4, pp. 257–261, 2009.

[39] A. D. Rietman, "Numerical Analysis of Inhomogeneous deformatio in plane strain compression," *Univ. Twente*, 1999.

[40] J. Beynon and C. Sellars, "Strain distribution patterns during place strain compression," *J. Test. Eval.*, vol. 13, no. 1, pp. 28–38, 1985.

[41] F.J. Humphreys and M. Hatherly, "Recrystallisation and related annealing phenomena," *Elsevier Sci. Ltd.*, 1995.

[42] G.Greetham, "'Component Manufacture by Uniaxial Pressing'. The A to Z of Materials," *Powder Metallurgy*. 2013.

[43] P. Cotteril and P. Moud, "Recrystallization and grain growth in metals," *Surrey Universtiy Press*, p. Chapter 9, 1976.

[44] M. Hashayi, H. Yoshimura, M. Ishii, and M. Harada, "Recrystallisation behaviour of commercially pure titanium during hot rolling," *Nippon Steel Tech. Rep.*, no. 62, 1994.

[45] T. Furuhura, B. Poorganji, H. Abe, and T. Maki, "Dynamic Recovery and Recrystallisation in titanium alloys by hot deformation," *JOM J. Miner. Met. Mater. Soc.*, vol. 59, no. 1, pp. 64–67, 2007.

[46] M.J. Tan and X.J. Zhu, *Microstructure evolution of CP-Titanium during high temperature deformation*, Vol 28, Is. Archives of Materials Science and Engineering, 2007.

[47] P. Ari-Gur and S. Semiatin, "Evolution of microstructure, macrotexture and microtexture during hot rolling of Ti-6A1-4V," *Mater. Sci. Eng.*, vol. A2575, p. 118, 1998.

[48] F. Humphrey, B. Priestner, and F. Pragnell, "New Technologies," *Solid State Mater. Sci.*, vol. 5, no. 15, 2001.

[49] P. Sirlilar and P. Srichandr, “Grain Refinement of alpha and beta phase Ti-6Al-4V alloy by thermomechanical treatment,” *Div. Mater. Technol. Sch. Energy Mater.*, vol. M13.

[50] H. Bosman and D. Blaine, “Influence of Powder Particle Size Distribution on the Properties of Press-and-Sintered Titanium and Ti-6Al-4V Preforms,” *Adv. Mater. Res.*, vol. 1019, no. 225–230, 2014.

[51] O. Ivasishin, D. Eylon, V. Bondarchuk, and D. Savvakin, “Diffusion during Powder Metallurgy Synthesis of Titanium Alloys,” *Defect Diffus. Forum*, vol. 277, no. 177–185, 2008.

[52] G. Fernandez and V. Gerardo, “Constitutive relations to model the hot flow of commercial purity copper – 2 Experimental Procedure,” *TDX- Tesis Doctorals en Xarxa*. 2004.

[53] J. Miller, “A Comparison of Optical and SEM BSE Imaging Techniques for Quantifying ALPHA-BETA Titanium Alloy Microstructures,” *Mater. Manuf. Dir. Air Force Res. Labarotary*, no. AFRL-ML-WP-TP-2006–432, 2006.

[54] G. G. E. Seward, S. Celotto, D. J. Prior, J. Wheeler, and R. C. Pond, “In situ SEM-EBSD observations of the hcp to bcc phase transformation in commercially pure titanium,” *Acta Mater.*, vol. 52, no. 4, pp. 821–832, Feb. 2004.

[55] Mathworks, “Particle and Grain Size Analysis with line intersection method.” .

[56] N. Clinning and R. Knutsen, “Evolution and Mechanical Properites of Porous Blended Elemental Ti-6Al-4V Subjected to Thermomechanical Processing, Centre for Materials Engineering,” *Univeristy Cape T.*, vol. 1, no. 1, 2012.

[57] J. Xiaoping and Z. Chao, “A New Rapid Tooling Process,” *Manuf. Futur. Concepts-Technologies-Visions*, p. 908, 2006.

[58] R. L. Coble, “Sintering Crystalline Solids. I. Intermediate and Final State Diffusion Models,” *Gen. Electr. Res. Lab. Schenectady, New York*, 1960.

[59] S. Khang, *Sintering Densification Growth and Microstructure*. Burlington MA: Elsevier Butterworth-Heinemann, 2005.

[60] Y. Liu, L. F. Chen, H. P. Tang, C. T. Liu, B. Liu, and B. Y. Huang, “Design of powder metallurgy titanium alloys and composites,” *Mater. Sci. Eng. A*, vol. 418, no. 1–2, pp. 25–35, Feb. 2006.

[61] Y. Xue, L. H. Lang, G. L. Bu, and L. Li, “Densification modeling of titanium alloy powder during hot isostatic pressing,” *Sci. Sinter.*, vol. 43, no. 3, pp. 247–260, 2011.

[62] R. Coble, “Sintering Crystalline Solids. I. Intermediate and Final State Diffusion Models,” *Gen. Electr. Res. Lab. Schenectady, New York*, 1960.

10. Appendix 1

Found in this appendix are the MPIF standards used to conduct this research.

MPIF Standard 41

METAL POWDER INDUSTRIES FEDERATION

Method for

Determination of Transverse Rupture Strength of Powder Metallurgy (PM) Materials

MPIF Standard 41

Issued 1951, Revised 1962, 1973, 1991, 1998, 2000, 2008

(Formerly included in Standard 13)

STANDARD 41

1. SCOPE

1.1 This standard covers the apparatus, test specimen and procedures for determining the bending strength or transverse rupture strength of powder metallurgy materials.

1.2 The test as described and specified herein is applicable only to materials of negligible ductility. If applied to materials showing noticeable plastic deformation (exceeds 0.02 inch [0.5 mm] permanent deflection), the maximum load may not be equal to the break load, which could lead to misinterpretation of results. For such materials the tensile strength test should be used.

1.3 *This standard may involve hazardous materials, operations and equipment. This standard does not purport to address all of the potential safety problems associated with its use. It is the responsibility of the user of this standard to establish appropriate safety and health practices, and to determine the applicability of regulatory limitations prior to use.*

2. APPARATUS

2.1 Gauges capable of measuring from 0 to 1.000 inch (0 to 25 mm) to the nearest 0.001 inch (0.025 mm).

2.2 A transverse strength fixture as shown in Figure 2.

2.3 A universal testing machine readable to within 0.1% of full scale reading. Use the lowest testing range that can provide a measurable result.

NOTE 1—Names of manufacturers of this apparatus are listed in General Information IV.

3. TEST SPECIMEN

3.1 The specimens may be pressed in the die shown in Fig. 1 and shall be free from visible laminations and other flaws.

3.2 The die may be prepared as a solid die with dimensions as shown in Fig. 1. The uniformity of the "green" specimens ejected from the die may be determined by measuring the thickness with a gauge and by weighing. The mass of any specimen in a given lot shall not vary more than ± 1.5 % from the mean.

shown in Fig. 3. Parallelism shall not exceed 0.003 inch (0.076 mm).

4. PROCEDURE

4.1 The specimen shall be prepared in accordance with MPIF Standard 60.

4.2 Transverse rupture strength.

4.2.1 Measure the width and thickness of the specimen to the nearest 0.001 inch (0.025 mm). After measuring, break the specimens in the testing fixture as shown in Fig. 2. In this fixture the specimen is supported by, and perpendicular to, two hardened steel (or carbide) rods 0.125 inch (3.10 mm) in diameter whose centers are 1.000 inch (25.40 mm) apart. Another hardened steel (or carbide) rod 0.125 inch (3.1 mm) in diameter presses upon the upper face of the test piece, central to the span. Test the specimen in the fixture in a universal testing machine. Apply the load at the rate of not more than 0.2 inch per minute (5 mm/min) travel of the bed of the testing machine, and note the load at which the specimen breaks.

5. CALCULATIONS

5.1 Calculate the transverse rupture strength as follows:

$$TRS = \frac{3PL}{2t^2w}$$

where:

TRS = transverse rupture strength in 10^3 psi or MPa

P = break load lbf (N) (as determined)

L = the distance between the supporting rods 1.000 inch (25.40 mm)

t = the thickness of the piece in inches (mm)

w = the width of the piece in inches (mm).

6. REPORT

6.1 Report the transverse rupture strength as the average of a minimum of 5 tests to the nearest 10^3 psi or 10

6.1 The following supplementary information may also be reported for clarification:

6.2.1 Identification of powder, brand, grade, lot number.

6.2.2 Chemical composition of powder mix used if other than elemental powders being tested.

6.2.3 Type, brand and percent of lubricant.

6.2.4 Density, green and sintered.

6.2.5 Sintering temperature.

6.2.6 Sintering time.

6.2.7 Furnace atmosphere.

6.2.8 Final total carbon content where applicable.

6.2.9 Other processing information as required.

7. PRECISION

7.1 The repeatability (r) and reproducibility (R) measurements were determined (1995) according to ASTM E 691 Practice for Conducting an Interlaboratory Test Program to Determine the Precision of Test Methods and are listed below for six materials and a range of transverse rupture strength values. On the basis of test error alone, the difference in absolute value of two test results obtained in the same laboratory will be expected to exceed (r) only 5% of the time. If such a difference is found to be larger than (r), there is reason to question one or both results. Similarly, the difference in two test results obtained in different laboratories will be expected to exceed (R) only 5% of the time. If the difference is found to be larger than (R), there is reason to question one or both measurements.

APPENDIX

A1. COMPARABLE STANDARDS.
ASTM B 528
ISO 3325

Table 1. Precision of Transverse Rupture Strength

MATERIAL	DENSITY g/cm³	APPARENT HARDNESS	TRS psi	# LABS	(r) psi	(R) psi
F-0005-15	6.22	37 HRB	63,000	19	4,600	7,900
FC-0205-30	6.21	43 HRB	66,500	16	5,600	11,300
F-0005-25	6.91	40 HRB	71,000	12	3,500	14,000
FN-0208-35	6.85	27 HRB	122,500	19	6,000	11,600
FL-4405-40	7.04	75 HRB	129,500	16	7,000	13,300
FC-0208-50	6.89	81 HRB	144,000	12	12,500	21,000
FC-0208-65HT	6.45	31 HRC	138,500	22	15,400	28,900
F-0008-65HT	6.68	35 HRC	148,500	16	22,000	31,700
FLC-4608-70HT	6.89	33 HRC	174,000	14	28,500	41,500
FN-0205-105HT	6.93	31 HRC	191,500	14	25,700	40,500
FC-0205-90HT	7.05	41 HRC	236,000	16	28,100	42,400
FLN-4205-140HT	7.12	41 HRC	251,500	22	32,700	46,900
FLN2-4405-160HT	7.04	38 HRC	246,000	35	21,500	31,200

The (r) and (R) values were determined from the testing of three (3) transverse rupture test specimens by each participating laboratory.

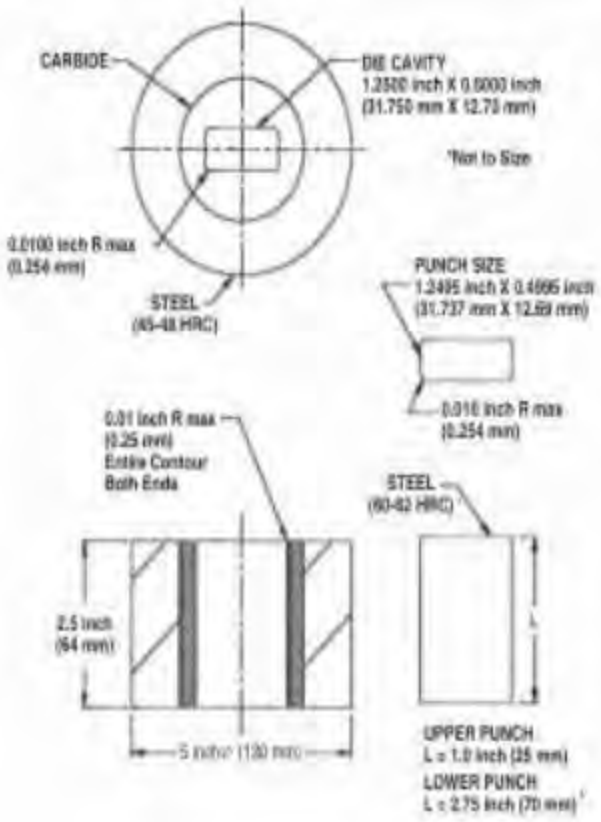

FIGURE 1: Example of Tooling to Produce a Rectangular Test Specimen.

Note: The dimensions for the cavity shall be 0.500 ± 0.004 inch wide (12.70 ± 0.10 mm) by 1.250 ± 0.004 inch long (31.75 ± 0.10 mm). The mating parts should be fitted and lapped to a 4 micro inch (N3) finish or better, to dimensions of 0.0005 inch (0.0130 mm) to 0.0010 inch (0.0250 mm) smaller than the die cavity in each dimension. The dimensions given in the drawing typify the die cavity and punch within the stated tolerance at the nominal width and length. The outer ring may be AISI H-11 hardened to 45-48 HRC. The punches may be AISI A-2 or A-7 hardened to 60-62 HRC. The die insert should be die grade tungsten carbide. The shrinkage between the carbide insert and the die case typically is 0.0015-0.0025 inches per inch (0.0380-0.0635 mm per 25 mm).

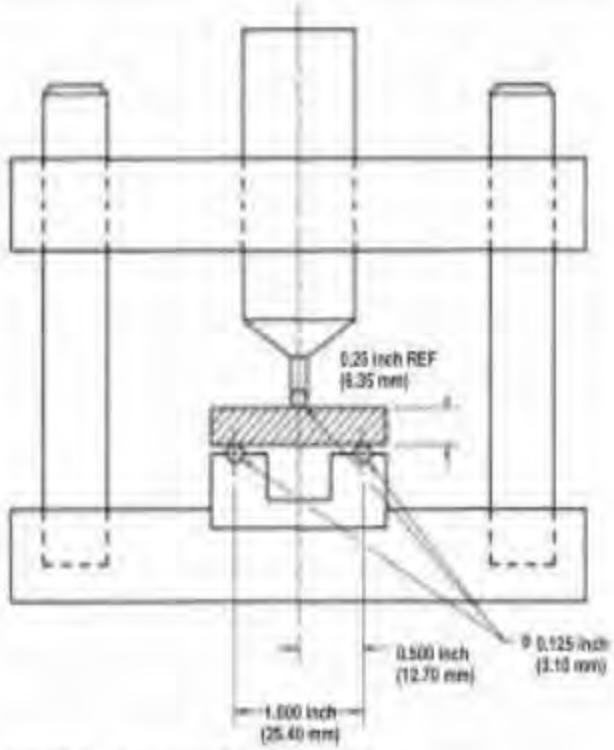

FIGURE 2: Transverse Rupture Test Fixture

Tolerance on all dimensions to be ± 0.001 inch (0.0250 mm).
Hardness on 0.125 inch Ø (3.10 mm) pins to be 60 HRC minimum.

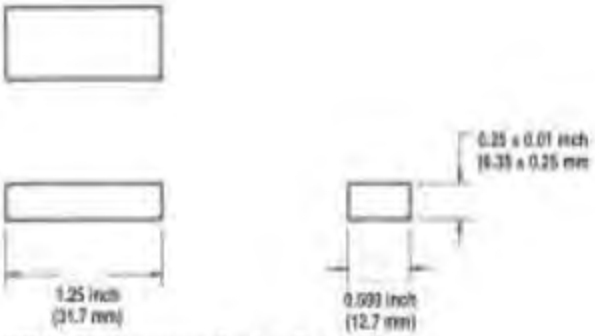

FIGURE 3: Transverse Rupture Test Specimen

MPIF Standard 54

METAL POWDER INDUSTRIES FEDERATION

Method for

Determination of Density of Impermeable Powder Metallurgy (PM) Materials

MPIF Standard 54
issued 2006

STANDARD 54

1. SCOPE

1.1 This standard describes a procedure for determining the density of powder metallurgy (PM) materials and cemented carbides containing less than two percent porosity. The method is based on the principle of water displacement.

NOTE 1—A test specimen that gains mass when immersed in water indicates the specimen contains surface-connected porosity. Unsealed surface porosity will absorb water and cause density values higher than the true value. If this problem occurs, this method is not applicable and Standard 42 should be used instead.

1.2 The values stated in SI units are to be regarded as standard. Values in parentheses are for information only.

1.3 *This standard does not purport to address all of the safety problems, if any, associated with its use. It is the responsibility of the user of this standard to establish appropriate safety and health practices and determine the applicability of regulatory limitations prior to use.*

2. APPARATUS

2.1 Balance – A precision single pan balance that will permit readings within 0.01% of the test specimen mass. The balance shall be supported in a manner to eliminate mechanical vibrations and be shielded from air drafts.

2.2 Weighing Liquid - Distilled or deionized water to which 0.05 to 0.1 volume percent of a wetting agent has been added to reduce the effects of surface tension.

NOTE 2—Degassing the water by evacuation, boiling or ultrasonic agitation helps to prevent air bubbles from collecting on the test specimen and specimen support when immersed in water.

2.3 Water Container - A glass beaker or other suitable transparent container should be used to contain the water.

NOTE 3—A transparent container makes it easier to see air bubbles adhering to the test specimen and specimen support when immersed in water.

NOTE 4—For the most precise density determination, the water container should be of a size such that the level of the water does not rise more than 2.5 mm (0.10 inch) when the test specimen is lowered into the water.

2.4 Test Specimen Support for Weighing in Water - Two typical arrangements are shown in Figure 1. The suspension wire may be twisted around the test specimen or the test specimen may be supported in a wire basket that is attached to the suspension wire. For either arrangement, a single corrosion resistant wire, e.g. austenitic stainless steel, copper, or nichrome shall be used for the basket and suspension wire. The maximum recommended diameter of suspension wire to be used for various mass ranges is:

Mass, g	Wire Diameter, mm (inch)
less than 50	0.12 (0.005)
50 to less than 200	0.25 (0.010)
200 to less than 600	0.40 (0.015)
600 and greater	0.50 (0.020)

NOTE 5—For the most precise density determinations it is important that the mass and volume of all supporting wires immersed in water be minimized.

2.5 Thermometer – A thermometer with an accuracy of 0.2 °C (0.5 °F) to measure the temperature of the water.

3. TEST SPECIMEN

3.1 A complete part or a section of a part may be used for the test specimen. For the highest precision, the test specimen shall have a minimum mass of 5.0 g. If less precision can be tolerated, several test specimens may be used to reach the minimum mass, provided each test specimen has a mass of not less than 1.0 g.

NOTE 6—For metal injection molded (MIM) parts of less than 1.0 g several parts may be used to reach the minimum mass.

3.2 All test specimen surfaces shall be thoroughly cleaned of all adhering foreign materials such as dirt, grease, oil, oxide scale, metal powders or assembly materials. For cut specimens, avoid rough surfaces to which an air bubble can adhere. A 100-grit sanding or abrasive grinding is recommended to remove all rough surfaces.

4. PROCEDURE

4.1 Weigh the test specimen in air. This is mass A. This and all subsequent weighings shall be to 0.01% of the test specimen mass, for example :

Mass, g	Balance Sensitivity, g
less than 10	0.0001
10 to less than 100	0.001
100 to less than 1,000	0.01
1,000 to less than 10,000	0.1

It is important that the test specimen, balance, water and surrounding air be at a uniform temperature when the weighing is performed.

NOTE 7—For the most precise density determination, duplicate weighings should be made for all mass determinations. The balance should be adjusted to zero prior to each weighing. Duplicate mass determinations should be averaged before calculating the density.

NOTE 8—For improved reproducibility, the balance should be calibrated periodically with a standard mass that is approximately equal to the test specimen mass.

4.2 Support the container of water over the pan of the balance using a suitable bridge as shown in Figure 2a. The container of water may also be supported below the balance for weighing larger specimens if the balance has a lower beam hook for this purpose. See Figure 2b. If this arrangement is used, it is important to shield the suspension wire between the container of water and the bottom of the balance from air drafts. Ensure that the bridge does not touch the balance pan.

4.3 Suspend the test specimen support with the test specimen from the beam hook of the balance. The water should cover any wire twists and the specimen support basket by at least 6 mm (0.25 inch) to minimize the effect of surface tension forces on the weighing. Care should be taken to ensure that the test specimen and specimen support hang freely from the balance beam hook, are free of air bubbles when immersed in the water and are at the same temperature as the water and balance. Ensure that the surface of the water is free of dust particles.

4.4 Weigh the test specimen and the specimen support immersed in water. This is mass B.

4.5 Remove the test specimen. Weigh the test specimen support immersed in water at the same depth as before. This is mass C. Ensure that the suspension support is free of air bubbles and that the suspension wire is not immersed below its normal hanging depth as a change in depth will change the measured mass.

NOTE 9—Some balances are capable of being tared. This automatically removes the necessity of reweighing the specimen support every time. In this case, tare the specimen support alone, immersed in water to the same depth as with the specimen, before weighing the specimen support and specimen immersed in water. The mass of the specimen support and specimen immersed in water is mass F, which replaces mass B minus mass C.

4.6 Measure the temperature of the water to the nearest 0.5 °C (1 °F) and record its density ρ_w, at that temperature, from Table 1.

5. CALCULATION

5.1 Calculate the density as follows :

$$\text{Density} = D = \text{Mass/Volume}$$

$$= \frac{A}{\frac{[A-(B-C)]}{\rho_w}}$$

$$= (A\rho_w)/(A-B+C) = (A\rho_w)/(A-F)$$

where :

D = density of test specimen, g/cm³

A = mass of test specimen in air, g

B = apparent mass of test specimen and specimen support in water, g

C = mass of specimen support immersed in water, g

F = mass of test specimen in water with mass of specimen support tared, g,

and

ρ_w = density of water, g/cm³

6. REPORT

6.1 Report the density rounded to the nearest 0.01 g/cm³.

7. PRECISION

The following precision data were developed using the procedures contained in ASTM B 311-86. A new interlaboratory study is planned using the procedures in a revised version of B 311. The interlaboratory study will evaluate the effect of the influence of air buoyancy on the measured density values. Calculations indicate that higher density materials such as carbides and tungsten heavy alloys may require air buoyancy to be taken into account in order to report a density value to the nearest 0.01 g/cm³.

Material Density (g/cm³)	Specimen Mass (g)	Repeatability (r)	Reproducibility (R)
4 to 8	< 5	0.04	0.05
	> 5 < 50	0.01	0.02
	> 200	0.02	0.03
> 14	> 5 < 50	0.06	0.07

7.2 The repeatability, r, and reproducibility, R, were determined at the 95% confidence level.

7.3 Duplicate results from the same laboratory should not

be considered suspect at the 95% confidence level unless they differ by more than r.

7.4 Test results from two different laboratories should not be considered suspect at the 95% confidence level unless they differ by more than R.

Table 1. Effect of Temperature on Water Density

Temperature °C	ρ_w g/cm³	Temperature °F	ρ_w g/cm³
15	0.9991	60	0.9990
15.5	0.9990	61	0.9989
16	0.9989	62	0.9988
16.5	0.9988	63	0.9987
17	0.9988	64	0.9986
17.5	0.9987	65	0.9985
18	0.9986	66	0.9984
18.5	0.9985	67	0.9983
19	0.9984	68	0.9982
19.5	0.9983	69	0.9981
20	0.9982	70	0.9980
20.5	0.9981	71	0.9978
21	0.9980	72	0.9977
21.5	0.9979	73	0.9975
22	0.9978	74	0.9974
22.5	0.9976	75	0.9973
23	0.9975	76	0.9972
23.5	0.9974	77	0.9970
24	0.9973	78	0.9969
24.5	0.9972	79	0.9967
25	0.9970	80	0.9966
25.5	0.9969	81	0.9964
26	0.9968	82	0.9963
26.5	0.9966	83	0.9961
27	0.9965	84	0.9959
27.5	0.9964	85	0.9958
28	0.9962	86	0.9956
28.5	0.9961		
29	0.9959	*Interpolated from °C data.	
29.5	0.9958		
30	0.9956		

The values of ρ_w shown are taken from, "Metrological Handbook 145, Quality Assurance for Measurements", 1990, NIST, pp. 9.10., and represent the values in air at one atmosphere pressure.

APPENDIX

A.1 COMPARABLE STANDARDS
ASTM B 311
ISO 3369

NOTE A.1—The water density table in ISO 3369 differs from the table contained in this standard.

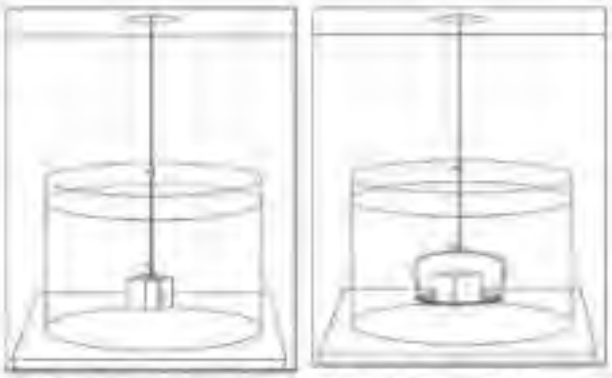

a. Twisted wire arrangement b. Basket support arrangement

FIGURE 1: Methods for Holding the Test Specimen When Weighing in Water.

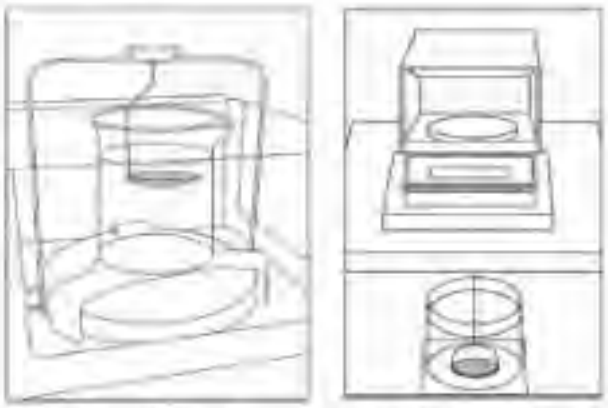

a. Beaker support above balance pan b. Weighing arrangement below the balance pan

FIGURE 2: Methods for Weighing in Water.

[1] Values reprinted, with permission, from ASTM B 962 – 99 *Standard Test Methods for Density of Compacted (Pressed) Powder Metallurgy (PM) Products Using Archimedes' Principle*, copyright ASTM International, 100 Barr Harbor Drive, West Conshohocken, PA 19428.

11. Appendix 2

TRB Specimen

Figure 7.3: a) Photographs showing two specimens, the one on the left being the standard TRB specimen and to its right a machined down three-point-bending test specimen